ON EFFICIENCY OF SPECIFIC NUCLEATION IN POLYPROPYLENE

Bc. Lenka Chvátalová

Master Thesis
2006

Tomas Bata University in Zlín
Faculty of Technology

Univerzita Tomáše Bati ve Zlíně

Fakulta technologická

Ústav inženýrství polymerů

akademický rok: 2005/2006

ZADÁNÍ DIPLOMOVÉ PRÁCE
(PROJEKTU, UMĚLECKÉHO DÍLA, UMĚLECKÉHO VÝKONU)

Jméno a příjmení: **Bc. Lenka CHVÁTALOVÁ**

Studijní program: **N 2808 Chemie a technologie materiálů**

Studijní obor: **Inženýrství polymerů**

Téma práce: **On Efficiency of Specific Nucleation in Polypropylene**

Zásady pro vypracování:

The aim of this Master thesis is to assess an efficiency of the beta-specific nucleation in polypropylenes with different molecular parameters. Several grades of commercial-available polypropylenes differing in melt-flow indexes will be modified by beta-nucleator. Induced changes in polymorphic composition of polypropylenes will be examined via polarized-light microscopy, differential scanning calorimetry and wide-angle X-ray scattering

Rozsah práce:
Rozsah příloh:
Forma zpracování diplomové práce: **tištěná/elektronická**

Seznam odborné literatury:

1. BRYDSON, J.: Plastics Materials (7th Edition), Butterworth–Heinemann, 1999

2. MAIER, C. – CALAFUT, T.: Polypropylene – The Definitive User's Guide and Databook, Plastics Design Library, 1998

3. PHILLIPS, J. P. – MEZGHANI, K.: Polypropylene, Isotactic (Polymorphism), University of Tennessee, 1996

4. KARGER – KOCSIS, J.: Polypropylene – An A–Z Reference, Kluwer Academic Publishers, 1998

5. PRIDCHARD, G.: Plastics Additives – An A–Z References, Chapman & Hall, 1998

6. CAMPBELL, D. – WHITE, J. R.: Polymer Characterization Physical Techniques, London, 1989

7. CHERMISINOFF, N. P.: Polymer Characterization – Laboratory Techniques and, Analysis, Noyes/William Andrew Publishing, 1996

8. HATAKEYAMA, T. – QUINN, F. X.: Thermal Analysis, Wiley & Sons, New York, 1994
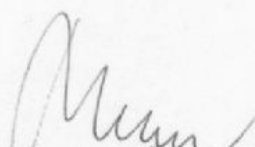
další literatura dle doporučení vedoucího diplomové práce

Vedoucí diplomové práce: **Ing. Roman Čermák, Ph.D.**
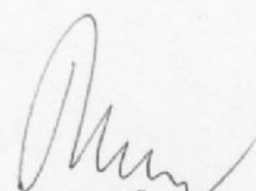   Ústav inženýrství polymerů
Datum zadání diplomové práce: **29. listopadu 2005**
Termín odevzdání diplomové práce: **12. května 2006**

Ve Zlíně dne 7. února 2006

prof. Ing. Josef Šimoník, CSc.   prof. Ing. Josef Šimoník, CSc.
děkan   *ředitel ústavu*

ABSTRACT

This master thesis deals with efficiency of the β-specific nucleation agent NJ Star NU 100 in isotactic polypropylenes Borealis differing in melt flow indexes. This study was carried out at different crystallization conditions using a differential scanning calorimetry. The crystallinity and β-form content have been determined from wide-angle X-ray scattering patterns. The structure of the samples has been examined using light microscopy.

It has been found, that the molecular structure (MFI) influences the efficiency of the nucleator only in its very low concentration. Moreover, the crystallization conditions also play an important role.

Keywords: isotactic polypropylene, polymorphism, β-form, α-form, specific nucleation, crystallization

ABSTRAKT

Diplomová práce se zabývá účinkem specifického β-nukleačního činidla NJ Star NU 100 na isotaktický polypropylen Borealis s rozdílnými indexy toku taveniny. Studie byla prováděna při různých krystalizačních podmínkách za použití diferenciální snímací kalorimetrie. Krystalický podíl a obsah β-fáze byl stanoven rentgenograficky z difrakčních spekter. Vzniklá struktura vzorků byla zkoumána pomocí optického mikroskopu.

Bylo zjištěno, že molekulární struktura (ITT) ovlivňuje účinnost nukleačního činidla pouze při jeho nízké koncentraci. Mimoto, důležitou roli hrají také krystalizační podmínky.

Klíčová slova: isotaktický polypropylen, polymorfismus, β-fáze, α-fáze, specifická nulkeace, krystalizace

Acknowledgement

My great appreciate belongs to my supervisor, Roman Čermák, for initiating and supporting this work and suggestive reminders by the master thesis creation. I am also kindly grateful to Jana Výchopňová for her precious time, help with experiments, valuable advice and language corrections. My sincere gratitude belongs to Jiřina Dohnalová for help with X-ray scattering. Finally, my thanks belong to the whole my close family for the amiable approach and patience.

I declare, I worked on this Master thesis by myself and I have mentioned all the used literature.

Zlín, May 12, 2006

_____

Lenka Chvátalová

CONTENTS

INTRODUCTION

Plastics play an important part of everyday live because they very often substitute traditional materials. This substitution has to be profitable from several points of view. The most important are the improvement of processing performance and reduction of the manufacture cost. The ease and the low energy consumption of processing and broad range of physical and chemical properties belong to the main advantages of plastics. Depending on the processing conditions the plastic product obtains not only the shape but also the supermolecular structure which markedly influences its properties [1, 2].

The supermolecular structure and thus final behaviour of the materials are strongly influenced by crystallization of polymers. Therefore, research in this field is under the growing interest. Consequently, the study of the processing-morphology-property relations of polymers has become a topic of major scientific importance during last years mainly because of intensified technological interest in this area [1, 2].

One of the most important semi-crystalline materials is isotactic polypropylene (iPP). Isotactic polypropylene is an important polymer not only from a commercial point of view, but also from the scientific perspective because of its specific morphological behavior. As a result of various crystallization conditions, iPP can crystallize in several forms denoted α, β, γ and smectic [26-36]. The most stable form among all crystal structures is α-form, being found in ordinarily melt-crystallized or solution-crystallized samples. Commercial iPP grades crystallize predominantly into α-form. On the other hand, β-form is observed only occasionally during crystallization from the melt. Its higher amounts can be obtained by crystallization in shear field, in the temperature gradients or in the presence of specific nucleating agents. β-form content has a strong influence on mechanical, optical and thermal properties of iPP. β-form compared to α-form shows higher toughness and drawability, but lower stiffness and strength. As for physical characteristics, β-form has a lower melting temperature and density. Consequently, isotactic polypropylene containing the prevailing β-form is currently classified among common polymeric materials, and for specific applications it is rated as a suitable alternative to the conventional polypropylene. The β-form of isotactic polypropylene is used for industrial pipeline construction, dielectric capacitors, paper like films, biaxially drawn microporous film and porous fibers with improved moisture adsorption [14, 34, 42].

The interrelations between structure, properties and processing of both pure and specifically nucleated iPP are a fundamental presumption for their use. The interrelations can be studied using a variety of experimental methods, such as differential scanning calorimetry, X-ray scattering, electron and light microscopy or infrared spectroscopy.

In this context, the aim of this master thesis is to determine the influence of molecular structure, in this work represents by MFI, on efficiency of nucleating agent at different crystallization conditions. The investigation of the isothermal and non-isothermal crystallization processes and melting behaviour of isotactic polypropylene Borealis with different MFI modified by various amounts of a specific β-nucleating agent NU100 is carried out using differential scanning calorimeter. Wide angle X-ray scattering is used in order to investigate relative amount of β-form in the samples. For the study of the polypropylenes morphology polarized light microscopy is used.

I. THEORETICAL BACKGROUND

1   CRYSTALLIZATION OF POLYMERS

Crystallization behaviour of semi-crystalline polymers is strongly influenced by processing conditions and molecular characteristics (e.g., molecular weight, molecular weight distribution, and stereoregularity). Consequently, understanding the effects of molecular characteristics on crystallization behaviour is the key to determine the final properties of the products [1].

When the melt of a crystalline polymer is cooled to a temperature between the glass-transition and the equilibrium melting point, the thermodynamic requirement for crystallization is fulfilled [2]. The thermodynamic description of the crystallization process, can be written

$$\Delta G = \Delta H - T \Delta S \qquad (1)$$

where ΔG is the free enthalpy (Gibbs free energy) of the crystallization, ΔH is enthalpy and ΔS entropy of crystallization. Equation (1) applies to the overall macroscopic transformation. Crystallization becomes possible as soon as ΔG assumes negative values. If the phase transition would strictly follow Equation (1), crystals grown on cooling would have to be distributed uniformly over the volume, which has reached the melting temperature T_m at which ΔG is zero [3].

For polymers, primary and secondary crystallization are usually distinguished. Primary crystallization is the transition of an amorphous molten substance into a crystalline phase. However, the structure formed during primary crystallization is in a non-equilibrium state, and thus the crystallization is not completed. This structure may be improved by   post-crystallization and recrystallization processes, which are collectively designed   secondary crystallization. The rate of primary crystallization is markedly higher than that of secondary. These two processes are generally consecutive and well separated [3].

Crystallization occurs in two stages – nucleation and growth [4].

1.1   Nucleation

Nucleation is a reversible process at which nuclei are formed by cooling the melt below the melting temperature. Nucleation can be divided into two steps - primary nucleation and secondary nucleation.

A) Primary Nucleation

Primary nucleation is the first step in crystallization. The free energy of crystallization involves the sum of:

- the free energy for formation of a stable nucleus embryo. This energy decreases with decreasing temperature below the melting temperature;

- the free energy for diffusion of molecular segments to join the growing crystal. This energy increases, creating a maximum in the nucleation rate [4].

B) Secondary Nucleation

When a folded layer on the surface of a crystal has finished growing, a new nucleus needs to form on the surface for continued growth of the crystal. Secondary nucleation requires a high undercooling because it has low temperature dependence. The secondary crystallization layers are completed by an attachment-detachment mechanism [4].

Different types of nucleation can be identified: homogenous, heterogeneous and self-nucleation.

1.1.1   Homogeneous Nucleation

Homogeneous nucleation generally does not provide consistent properties, as nuclei appear throughout the crystallization, giving a broad distribution of sizes, and hence crystallization will be controlled too much by the processing conditions [4].

Homogeneous nucleation may occur through a fringed micelle, a bundle of polymer chains with long sections remaining random, or by chain folding to reach the critical nucleus dimensions. Chain folded nuclei are more probable than fringed micelle nuclei. Homogeneous nucleation is rarely reached, and most polymers crystallize from heterogeneous nuclei [4].

1.1.2   Heterogeneous Nucleation

Heterogeneous nucleation gives crystals of consistent size, as all nuclei are present in the melt at the start of crystallization and the nucleants controls crystallization. Heterogeneous nucleation may be caused by initiator residues, impurities etc., or preferably by addition of a specialized nucleating agent. The latter is preferred as control of the system is deliberate [4].

Heterogeneous nucleation involves the creation of a nucleus on an existing foreign surface, which greatly decreases the free energy for formation on a stable nucleus embryo. This will decrease the critical nuclei size so that nuclei can form at lower undercooling [4].

Nucleation Agents

Nucleating agents are added to the polymers to improve processing characteristics, clarity and alter its mechanical properties. The addition of nucleating agents provides a large number of sites for the initiation of crystallization, so that spherulites formed are smaller and more numerous than in unnucleated polymer.

Spherulite crystallization around a nucleating agent is shown in Figure 1.1. The nucleating agent is at the centre of the spherulite, suggesting that the nucleating agent initiated crystal formation [5].
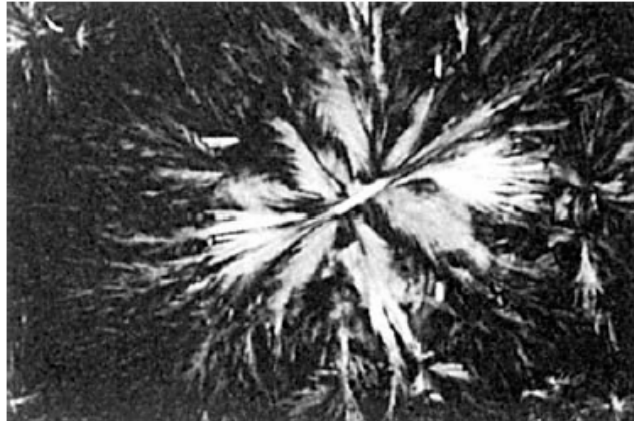
Figure 1.1 Micrograph of polypropylene spherulite
formed in the presence of a nucleating agent [5]

Clarity is enhanced due to the increased cooling rate and the decreased spherulite size, which reduces the scattering of light as it passes through the material. Smaller spherulites can reduce warpage in some applications and can provide a harder, more stain-resistant surface [5].

Nucleating agents may be melt sensitive, i.e. they melt below or near the processing temperature, or melt insensitive, i.e. they do not melt below normal processing temperatures. The melt sensitive nucleants form a physical gelation network within the polymer while the melt insensitive nucleants provide single nucleation sites within the polymer [4].

Typical nucleating agents include:

- lithium, sodium, potassium benzoate;
- sodium salts of organophosphates;
- finely divided (< 40 nm) clays, silica flour;
- Millad, bis-(3,4-dimethylbenzylidene sorbitol diacetal);
- 4-chloro-, 4-methyl- and 4-ethyl- substituted forms of dimethylbenzylidene sorbitol;
- diacetal [4].

1.2 Growth

The second stage of the crystallization is the crystallite growth. Under ideal conditions, macroscopic spherical structures (spherulites) are apparent. They grow in all directions, according to external conditions. The radius of the spherulite may represent the length dimension. High supercooling creates many small spherulites. Crystallization at higher temperatures (approaching the melting point) produces fewer spherulites (fewer nuclei) but of larger dimensions [6].

2   MORPHOLOGY OF CRYSTALLIZED POLYMERS

One important thing to determine physical and mechanical properties of any semi-crystalline polymer is morphology, which is, in turn, related directly to the crystallization behaviour [1]. In general, upon increasing the crystallinity, resistance to the attack of chemicals and solvents, as well as to hostile environments, is augmented. From the mechanical point of view, the rise of crystallinity increases rigidity and strength but at the same time decreases elongation and impact strength. The optical properties are also affected by the presence of crystallites, as the transparency decreases. Small crystallites are more favourable than larger ones for improving optical and mechanical properties of polymers [6].

The crystallites of polymers do not resemble the crystals of minerals. Depending on the processing conditions, one rather obtains very different morphologies [7]. Morphology deals with the structure of the solid state [6] and there are various types of these structures. Some common morphology observed include [8]:

- faceted single lamellas containing folded or extended chains,
- nonfaceted lamellas,
- branched (dendritic) structures,
- sheaf-like arrays of lamellar ribbons (axialites, hedrites),
- spherulitic arrays of lamellar ribbons (spherulites),
- fibrous structures, and
- epitaxial lamellar overgrowths on microfibrils.

2.1   Single Lamellas

Single lamellas (platelets) can be formed by isothermal crystallization from quiescent supercooled melt or solution of a large variety of polymer with a wide range of chain   flexibility [8].

Polymer lamellas can have a highly regular geometry, appearing to be single crystal. Lamellas with uniform size and shape can be prepared by a self-seeding technique involving simultaneous nucleation of all the lamellas and isothermal growth. Faceted lamellar geometries reported include: diamond, hexagonal, pyramidal, square and lathe shapes. Lamellas with rounded edges are also observed [8].

A schematic representation of the centre part of a polymer lamella is shown in Figure 2.1. In this picture, each straight line represents a section of a polymer chain incorporated in the crystal lattice and contains a number of repeat units; the loops shown depict the folds. Most of the folds in this figure are tight adjacent re-entrant (region 1). A few of the folds depicted in his figure are loose adjacent re-entrant (2) and some are nonadjacent re-entrant (3); some short protruding chain ends (4) are shown [8].
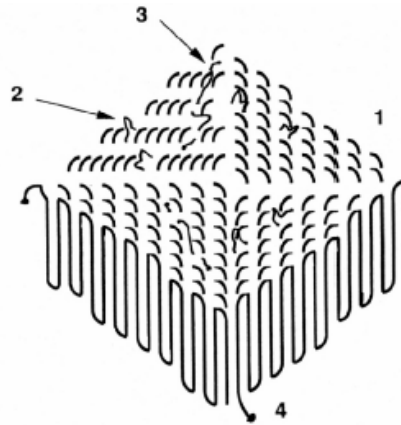
Figure 2.1 Polymer single lamella. The number identify features described in text [8]

2.2 Branched and Multilamellar Structures

Slow crystallization from semiconcentrated solutions delivers branched and multilamellar structures like networks, dendrites and hedrites. In melts and other highly viscous environments, sphere-like entities are formed that are called spherulites [7].

Dendrites

Dendrites are branched lamellas with the branches related in a definite crystallographic way to each other. Branching occurs under conditions in which crystal growth from solution is fast relative to the diffusion of polymer molecules to the crystallization site. This results in lower polymer concentration at the growth faces [8].

Hedrites

Hedrites (axialites) are stacks of centrally connected lamellas that grow from solution or melt. The lamellas are usually somewhat longer than they are wide, with growth occurring principally at the ends. During growth from solution, these lamellas can develop further connections due to the incorporation of a single chain or a group of chains in neighbouring lamellas [8].

Spherulites

When polymer samples are crystallized from the melt, spherulites are the most obvious observed structures. As the name implies, spherulites are sphere-shaped crystalline structures that form in the bulk. They are large enough to be visible with an optical microscope. They produce the appearance of a Maltese cross, when viewed through crossed polarizers. The spherulite contains both crystalline and amorphous material. Amorphous domains, called tie lines, connect zones of single crystals and are important for the toughness and plastic deformation of certain polymers. Spherulites are spherical when small enough so that each spherulite is independent of the others in the sample, and change shape when they have grown enough so that they impinge on one another. The chains are oriented in a direction that is perpendicular to the radius of the spherulite [9].

A model of the spherulite structure is illustrated in Figure 2.2. The chain direction in the bulk-crystallized lamellas is perpendicular to the broad plane of the structure, just like the dilute solution crystallized material [10].
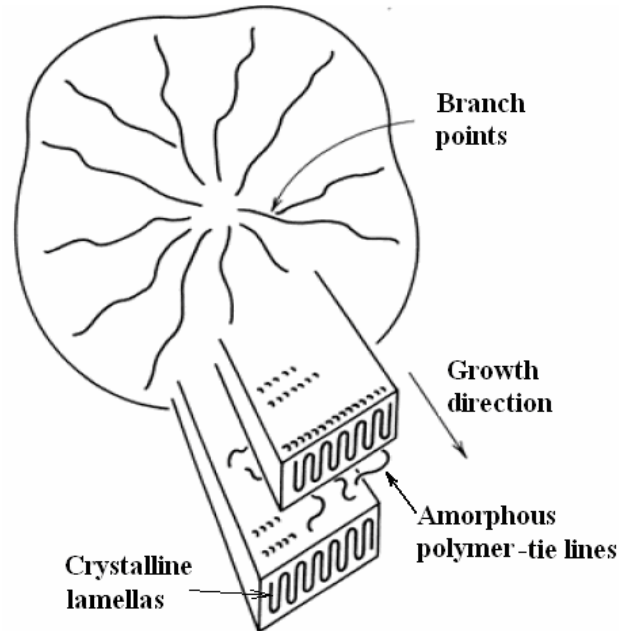

Figure 2.2 Model of spherulitic structure [10]

Spherulites exhibit radial symmetry and consist of lamellar, fibrous, or lath crystallites that grow from the centre and have chain axes tangential to the circumference of the spherulite [7].

2.3 Fibrous Structures

Fibres are long, narrow, ribbon-like structures, having a different chain orientation than that present in lamellas. In these structures, the chain orientation is mainly along the ribbon direction; it is not perpendicular to it, as found in lamellas. Fibres are usually composed of smaller units, fibrils, microfibrils and nanofibrils, oriented in the same direction [8].

2.4 Epitaxial Crystallization

Epitaxial or oriented growth of flexible chain polymer crystals on crystalline substrates can occur during crystallization from solution or melt. The substrate is cut to expose a particular crystal plane prior to polymer crystal growth. Needle-shaped growths containing folded chains and with growths oriented in certain direction, as directed by the crystallography of the substrate, are observed [8].

Epitaxial crystallization can take place in stirred solution; the lamellas, nucleated on the extended chains, are separated and easily distinguished [8].

3 POLYPROPYLENE

Polypropylene (PP) is a versatile thermoplastic material, compatible with many processing techniques and used in many different commercial applications [11]. It is an economical arterial that offers a combination of outstanding physical, chemical, mechanical, thermal and electrical properties not found in any other thermoplastic. Therefore polypropylene is one of the fastest growing classes of commodity thermoplastics.

3.1 Polymerization Reaction

Polypropylene is prepared by polymerization of propylene, a gaseous product of petroleum refining, in the presence of a catalyst under carefully controlled heat and pressure [12]. Propylene is an unsaturated hydrocarbon, containing only carbon and hydrogen atoms. Life cycle of polyolefins, such as polypropylene, is shown in Figure 3.1.
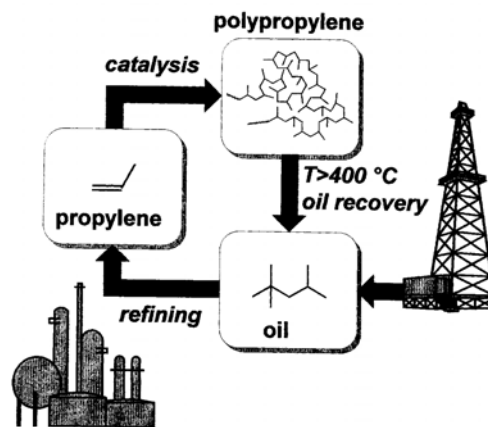
Figure 3.1 Polyolefin life cycle [12]

As early as 1869 propylene was polymerized by Berthelot by reaction with concentrated sulphuric acid. The resulting viscous oil, at room temperature, did not exhibit interesting properties for industrial application. Its industrial importance results from the appearance of crystalline high molecular weight polypropylene, which was first polymerized in 1955 by Natta from organo-metallic catalysts based on titanium and aluminium (Figure 3.2). The resulting semi-crystalline polymer has strong mechanical properties which explain its rapid industrial development [13].
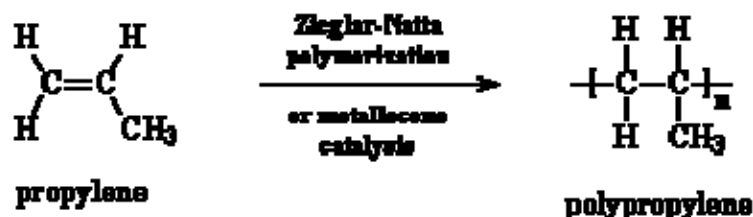

Figure 3.2 Polymerization of propylene [14]

3.2   Structure and Properties

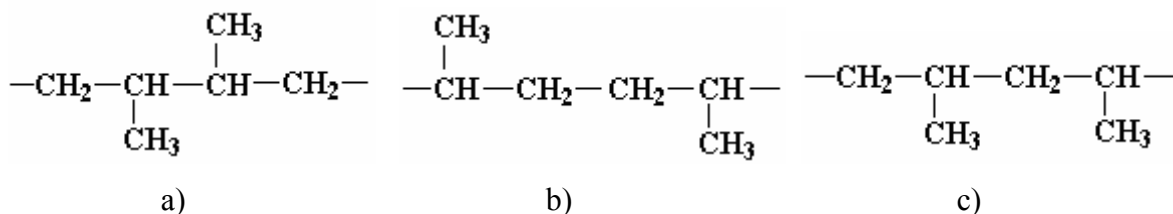Polymerization of the non-symmetrical propylene molecules leads to three possible sequences (Figure 3.3) [13].

$$-CH_2-CH-CH-CH_2- \quad \overset{CH_3}{\underset{|}{-CH}}-CH_2-CH_2-CH- \quad -CH_2-CH-CH_2-CH-$$

a)   b)   c)

Figure 3.3 Isomerism for the units positions in PP: a) tail-to-tail, b) head-to-head, c) head-to-tail [13]

The steric effect of the methyl group highly favours the head-to-tail sequences, which gives a high chemical regularity of the polypropylene chain. The occurrence of head-to-head and tail-to-tail sequences induces chemical defects along the PP chain [13].

An important concept in understanding the link between the structure of polypropylene and its properties is tacticity. The relative orientation of each methyl group relate to methyl groups of neighbouring monomers has a strong effect on the finished polymer's ability to form crystals, because each methyl group occupies space and constrains backbone bending [13].

The methyl branching implies an asymmetrical carbon C^* (tertiary carbon) in the propylene group (CH_2-C^*HCH_3). Two stereo-isomeric configurations result from this asymmetrical carbon. For the explanation it is useful to represent the polymer in the zigzag planar conformation to exhibit three typical stereo-configurations: isotactic, syndiotactic and atactic [13].

3.2.1   Isotactic Polypropylene

Isotactic polypropylene (iPP), in which all the methyl groups are positioned on the same side of the zigzag plane, results from polymerization of only one isomeric configuration form of propylene monomer (Figure 3.4) [13].

$$\text{www}-CH_2-CH-CH_2-CH-CH_2-CH-CH_2-CH-CH_2-CH-\text{www}$$
$$\underset{CH_3}{|} \quad \underset{CH_3}{|} \quad \underset{CH_3}{|} \quad \underset{CH_3}{|} \quad \underset{CH_3}{|}$$
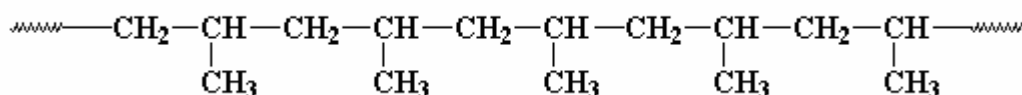
Figure 3.4 Isotactic polypropylene [15]

To select one isomeric configuration during polymerization it is necessary to use catalysts. The most common commercial catalysts used for preparation of iPP are Ziegler-

Natta catalysts. The original Ziegler-Natta catalysts are a complex of transition metal halides, usually titanium trichloride (TiCl3), with an organometallic compound, typically aluminium triethyl or aluminium tributyl as cocatalyst to initiate the polymerization [16]. Zeigler-Natta catalysts are multi-sited catalysts, containing several reactive sites. As a result, the polypropylene produced can include polymer molecules with a broad range of molecular weights which differed extensively in their properties [17].

3.2.2 Syndiotactic Polypropylene

Syndiotactic polypropylene (sPP) is defined by methyl groups arranged alternatively on both side of the zigzag chain, and is obtained by alternative addition of the two stereo-isomeric configuration form of propylene monomer (Figure 3.5) [13].
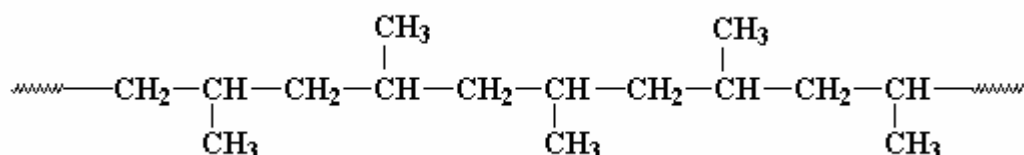
Figure 3.5 Syndiotactic polypropylene [15]

Contrary to isotactic polypropylene, syndiotactic polypropylene is now being produced commercially using metallocenes; commercial production is not possible with Ziegler-Natta catalysts [17]. Metallocenes are organometallic compounds with a sandwich-like spatial arrangement, consisting of a transition metal (iron, titanium, zirconium) situated between two cyclic organic compounds. In contrast to Ziegler-Natta catalysts, metallocene catalysts are single-sited - they have identical active sites and properties such as molecular weight and stereostructure can be tailored to meet the needs of the application [18 - 20].

3.2.3 Atactic Polypropylene

Unlike most other vinyl polymers, useful polypropylene cannot be made by radical polymerization. The material that results from such a process has methyl groups arranged randomly, and so is called atactic. The lack of long-range order prevents any crystallinity in such a material, giving an amorphous material with very little strength and few redeeming qualities (Figure 3.6) [15].
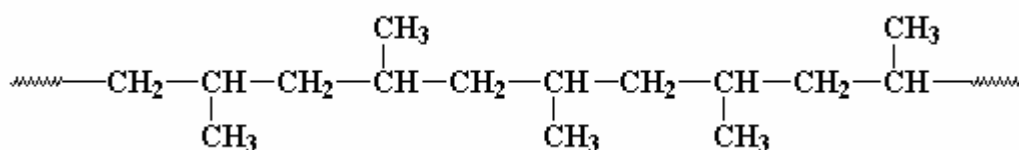

Figure 3.6 Atactic polypropylene [15]

3.2.4   Properties of Polypropylene

Comparison of properties of all polypropylene stereo-isomers is given in Table 3.1 [21].

Table 3.1 Properties of isotactic, syndiotactic and atactic PP [21]

Property	Isotactic PP	Syndiotactic PP	Atactic PP
Density [$kg.m^{-3}$]	920- 940	800 - 910	850 - 900
Melting temperature [ºC]	165	135	-
Solubility in hydrocarbons	no	middle	high
Yield strength	high	middle	very low

3.3   Crystal Structures of Isotactic Polypropylene

The isotactic form is the most regular since the methyl groups are all disposed on one side of the molecule. Such molecules cannot crystallize in a planar zigzag form because of the steric hindrance of the methyl groups. They crystallize in a helix with three molecules being required for one turn of the helix [22]. The helix can be either right- or left-handed, with a periodicity of 0.65 nm. The position of the methyl groups with respect to the chain axis can be either up or down. As a consequence, four possibilities relative to a reference axis (Figure 3.7) can be determined for a three-fold helix of iPP in the crystalline state [23].
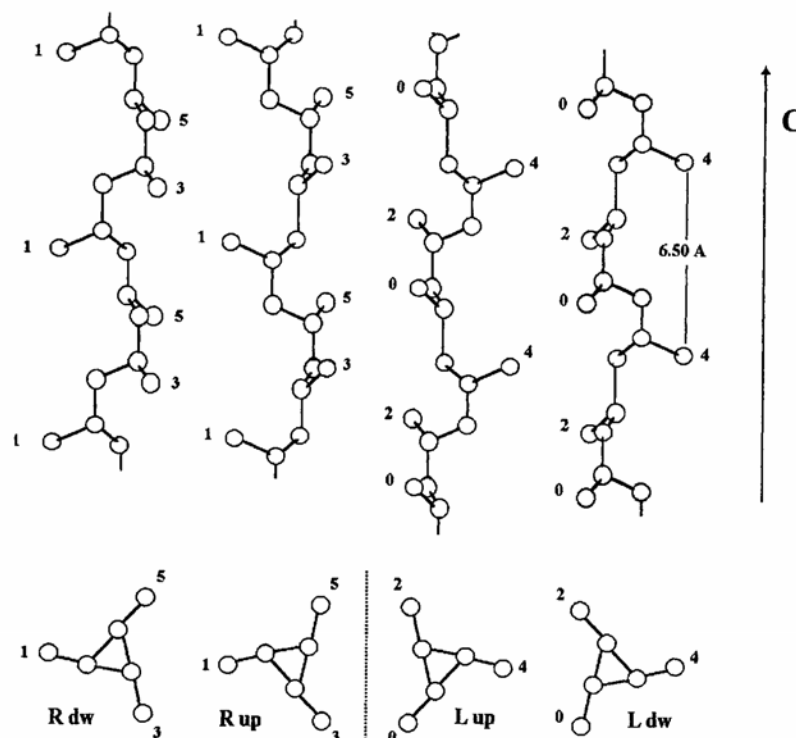
Figure 3.7 Four possible insertions of an iPP chain in the crystal lattice [14]

Chain folding accounts for formation of iPP lamellar structures are displayed in Figure 3.8 [14].
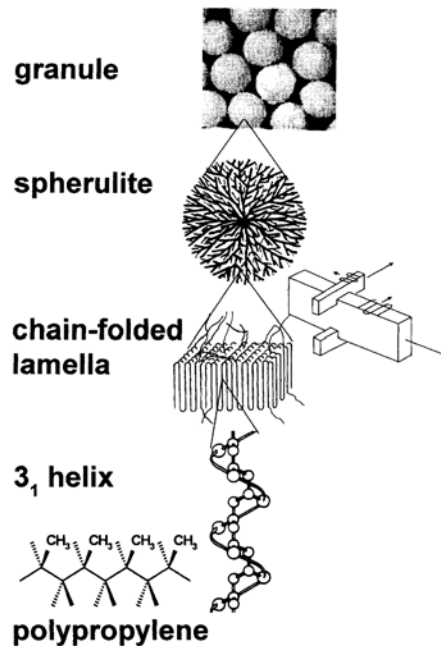
Figure 3.8 Polypropylene molecular and supermolecular architectures [14]

Isotactic polypropylene can exist in different morphological forms, depending on the tacticity and the crystallization conditions, such as pressure, temperature, and cooling rate. Different forms can coexist, and one crystalline form can change into another as conditions change [14].

The monoclinic lattice of the α-form in isotactic polypropylene was identified by Natta and Corradini. Shortly afterwards, a polymorph with a hexagonal lattice was recognized and designated as the β-form. An ever rarer third polymorph was found, based on a triclinic lattice; this was called the γ-form. In addition to these crystal structures, a quenched crystal form, called the smectic form by Natta and Corradini, was also observed in iPP [24].

3.3.1 α-form of Isotactic Polypropylene

The most common crystalline form of iPP is α-form (Figure 3.9). This form is obtained under normal processing conditions. Polymer chains in the α-form of isotactic polypropylene (α-iPP) form a helical structure in a monoclinic unit cell [27, 28], which was reported to be a = 0.666 nm, b = 2.078 nm, c = 0.6495 nm, β = 99.62° and α = γ = 90° [25]. The crystallographic density of α-form was calculated to be 0.936 g/cm^3 [26].
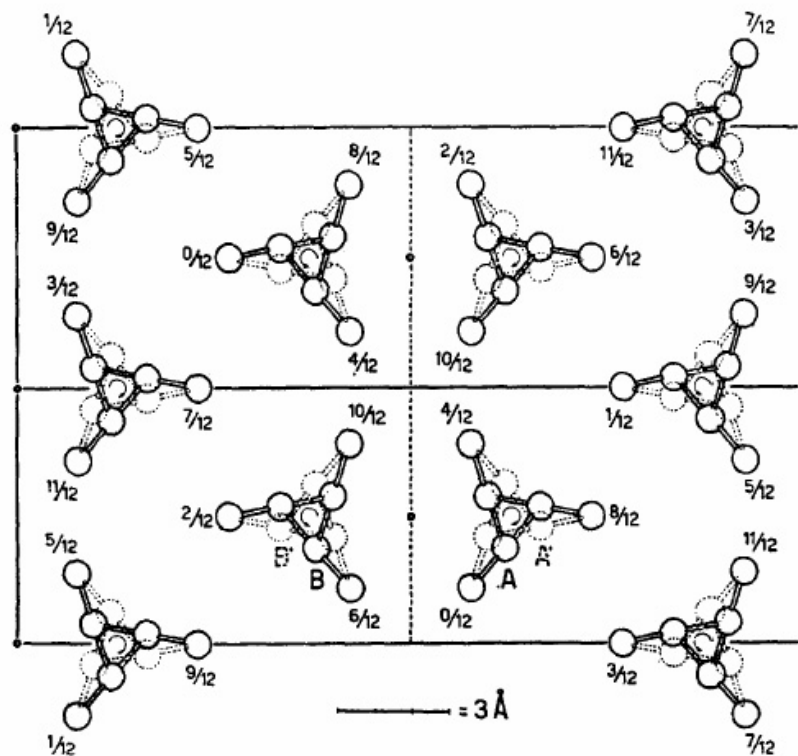
Figure 3.9 Crystal structure of α- iPP [14]

The crystal structure produces positive, negative, and mixed birefringence. Negative birefringence results from spherulites in which radial lamellas are dominant, while positive birefringence is due to spherulites with predominantly tangential lamellas. It has been recognized that this lamellar branching is characterized by a constant angle between tangential and radial lamellas (80° or 100°) [26]. At low temperature, the tangential lamellas develop at almost the same time as the radial leading lamellas. The thicknesses of radial and tangential lamellas are thus similar in the range of 20-25 nm. At high temperature, the cross-hatched lamellas grow after the radial lamellas, and therefore, are thinner. Radial lamellas are 40 nm thick while tangential lamellas only 25-30 nm thick. The thickness of radial and tangential lamellas increases with decreasing isotacticity [14].

Both negatively and positively birefringent spherulites form a Maltese cross pattern under crossed polarizers. In spherulites with mixed birefringence, neither tangential nor radial lamellas are predominant, and a distinct Maltese cross is not formed. The birefringence changes from positive to negative with increasing crystallization temperature, as the tangential lamellas undergo premelting [27, 29].

Owing to the non-equilibrium feature of the polypropylene's crystal structure and under favourable thermal conditions, the α-forms of the samples are susceptible to the recrystallization (α_1 to α_2). Exothermic recrystallization is superimposed on the endothermic melting processes. Recrystallization is a time- and temperature- dependent process, therefore decreasing the heating rate increases the proportion of more perfectly formed structure with a higher melting temperature [30].

The most reliable value of the equilibrium melting point of the α-form is ranging between 185°C and 209°C [26].

3.3.2 β-form of Isotactic Polypropylene

The β-form of isotactic polypropylene is less common and with more disorder than the α-form. β-form was identified in 1959 by Keith and co-workers [14] and for many years has been referred to have a hexagonal crystalline structure. It was suggested that the hexagonal lattice possess a unit cell of a = 1.908 nm, c = 0.649 nm, γ = 120° and α = β = 90° [31]. However, it has been verified by Varga and some other authors that the crystal arrangement of the β-form is trigonal [32]. The trigonal unit cell of β-form contains three isochiral helices with up-down statistics (Figure 3.10) [14]. The crystallographic density of β-form was calculated to be 0.921 g/cm^3 [26].
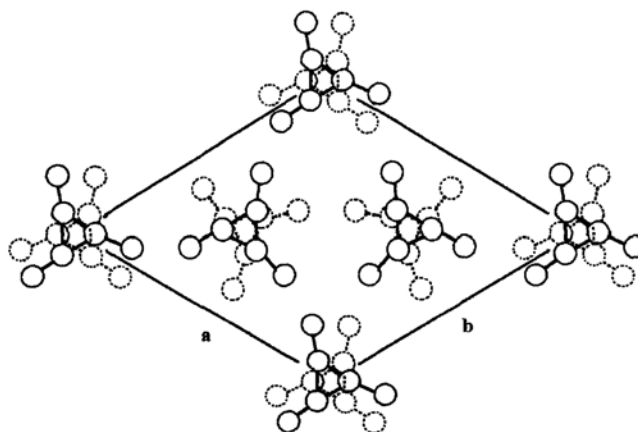
Figure 3.10 The trigonal unit cell of β-iPP [31]

β-form spherulites, characterized by strong negative birefringence, could be sporadically obtained when iPP is crystallized in the 128-132°C temperature range [14].

Almost pure β-form can be obtained with the aid of specific nucleating agents [33]. Crystallization in a temperature gradient is also an efficient way to produce oriented iPP samples with predominant β-form [32]. Studies on β-nucleated iPP (β-iPP) revealed that the formation of pure β-form has an upper (*T(βα)* = 140°C) and a lower (*T(αβ)* = 100-110°C) limit temperature. Between these two temperatures the growth rate of β-spherulites is up to 70 % faster than that of α-spherulites and therefore, formation of β-form is preferred. β-form is metastable relative to α-form (T_m = 155°C versus 180°C), it has lower density and is unstable upon stretching, which produces a transition to α-iPP or to the 'smectic' form depending on whether the sample is processed above or below 60°C [34, 35].

An interesting feature of the β-spherulitic growth is the β to α modification transition (βα-growth transition). This was observed on the growing crystal front under appropriate thermal conditions. Compared with the formation of pure β-polypropylene, the transition has the same upper and lower critical temperatures. The high critical temperature of growth transition, which takes place above 140°C was observed by Varga [36] during the stepwise crystallization of non-nucleated iPP and later during the isothermal crystallization of β-nucleated iPP in the presence of high-selective nucleating agent [32]. Lotz [37, 38] observed that theβα-growth transition occurs if the samples are cooled below the low critical temperature at approximately 100°C during the crystal growth. According

to Varga [32, 18] it can be generally stated that the βα-growth transition always takes place if the growth rate of the α-form is higher than that of β-form, i.e. below 100°C ($T(\alpha\beta)$) and over 140°C ($T(\beta\alpha)$).

The β-form can also recrystallize into α-form during heating. Duswalt and Cox [39, 40] and Fujiwara [26] showed that the melting curves of iPP with mixed polymorphic content have a complicated melting profile because of the melting of the α- and β-form and the βα-recrystallization phenomenon. Varga proved that β-iPP samples are susceptible to βα-recrystallization only if they were cooled below a critical temperature before melting. This critical recooling temperature is $T_R^* \sim$ 100-105°C. On the other hand, β-iPP samples that were not cooled below T_R^* do not recrystallize into α-form when heated; instead they melt separately like the thermodynamically stable phases [32].

The most reliable value of the equilibrium melting point of the β-form is $T_m^0(\beta)$ = 184±4°C, which was obtained with pure β-form when the disturbance of βα-recrystallization was eliminated [34].

3.3.2.1 Specific β-nucleating Agents

Specific β-nucleating agents are added to iPP for preparation of β-form of isotactic polypropylene. The presence of β-form significantly influences important properties of the material, like mechanical and thermal properties, as is undermentioned. Moreover, degradation of β-iPP is slower. Thus, the β-iPP has been rated as an effective alternative to α-iPP for specific applications.

Table 3.2 β-nucleating agents of iPP [14]

β-Nucleating agent	Advantage	Drawback
γ-Quinacridone	High activity (k-value = 0.8-0.9)	Physical or chemical instability, red colour
Calcium-phtalat	High thermal stability	Moderate activity (k = 0.5-0.7)
Two-component nucleator ($CaCO_3$ + organic acids) Ca stearat + pimelic acid	High activity (k-value = 0.8-0.93)	Free stearic acid
N,N´-dicyclohexyl-2,6-naphthalenedicarboxamide	High activity (β ≈ 80 %)	-
δ-Quinacridone	High activity (k-value = 0.8)	Coloured red
Ca salts of suberic or pimelic acid	High activity (β = 90 %)	-
Diamides of adipic or/and suberic acids	High activity (β = 90 %)	-
Quinacridonequinone	High activity	Coloured brown

The known β-nucleating agents are collected in Table 3.2, indicating their advantages and drawbacks. The most widespread high active β-nucleating agent is a γ-quinacridone red pigment. Some two-component compounds obtained by the reactions of certain organic acids with CaCO, also possess a very high β-nucleating activity. Different calcium and zinc salts of aliphatic and aromatic dicarboxylic acids having high thermal stability, belong to the selective β-nucleants, as well [14].

3.3.2.2   Processing of β-nucleated iPP

For the preparation of β-iPP products, some preconditions should be fulfilled in respect to the processing conditions [14]:

- applying of β-nucleating agents with high activity and selectivity and sufficient thermal stability;
- appropriate selection of the processing parameters for the crystallization in temperature range between $T(\alpha\beta)$ and $T(\beta\alpha)$;
- optimization of the flow and relaxation condition of the melt in order to avoid or to minimize the formation of row-nucleated α-form;
- avoidance of use of additives (filler, pigment, stabilizers etc.) with α-nucleating activity in β-nucleated iPP compounds.

3.3.2.3   Properties of β-iPP

Some properties of β-iPP differ significantly from those of α-iPP. In comparison with α-iPP, β-iPP possesses lower crystal density, melting temperature and fusion enthalpy, but a similar glass transition temperature. The chemical resistance of β-iPP seems to be lower than that of α-iPP [41].

β-iPP compared with α-iPP has a lower E-modulus and yield stress, but higher ultimate tensile strength and strain. The improvement in the latter might be related to the βα-transition occurring during the necking [34] which leads to the formation of α-form of enhanced strength (strainhardening). The impact strength and toughness of β-iPP exceed those of α-iPP (Table 3.3) [42].

Table 3.3 Static tensile characteristics of α- and β-iPP [32]

Property	α-iPP	β-iPP
E-modulus [GPa]	2.0	1.8
Yield stress [MPa]	36.5	29.5
Elongation at yield [%]	~ 12	~ 7
Necking stress [MPa]	27.5	28
Elongation at necking [%]	~ 22	-
Tensile strength [MPa]	39.5	44.0
Elongation at break [%]	~ 420	~ 480

3.3.2.4 *Application of β-iPP*

The application of β-iPP is favoured in some fields, based on its high impact resistance and toughness. Other application fields are exploiting the micro-void formation and strain-hardening characteristics as well as the βα-recrystallization tendency during partial melting of β-iPP. The β-form of isotactic polypropylene is used for industrial pipeline construction, dielectric capacitors (with roughened surface), paper like films, biaxially drawn microporous film (gas exchange membranes) and porous fibers with improved moisture adsorption [14].

3.3.3 γ-form of Isotactic Polypropylene

Turner-Jones assigned a triclinic unit cell to the γ-form of isotactic polypropylene [25]. Later studies applying a Rietveld analysis showed that the γ-form of iPP forms an orthorhombic unit cell. Nevertheless, the original triclinic unit cell can be considered as a part of the orthorhombic unit cell. The main difference of the new model is the nonparallel chain packing in the crystal of the γ-form which is unique in the field of synthetic polymers and was introduced by Meille (Figure 3.11) [43].

The orthorhombic unit cell of the γ-form is formed by bilayers composed of two parallel helices. The direction of the chain-axis in adjacent bilayers is tilted with an angle of 80°. This is a unique packing arrangement for polymers but has been known e.g. for fatty acids. The dimensions of the unit cell are a = 0.854 nm, b = 0.993 nm, c = 4.241 nm. Lotz have made a remarkable work to support this nonparallel chain packing model [44]. The crystallographic density of γ-form was calculated to be 0.954 g/cm^3 [26].

The γ-form can be observed in low molecular weight iPP or in iPP crystallized at elevated pressure above 200 MPa [26].

The equilibrium melting temperature of γ-iPP at atmospheric pressure has a value of $T_m^0(\gamma)$ = 187.6°C and the high molecular weight iPP samples crystallized at high pressure melt above 150°C [23].
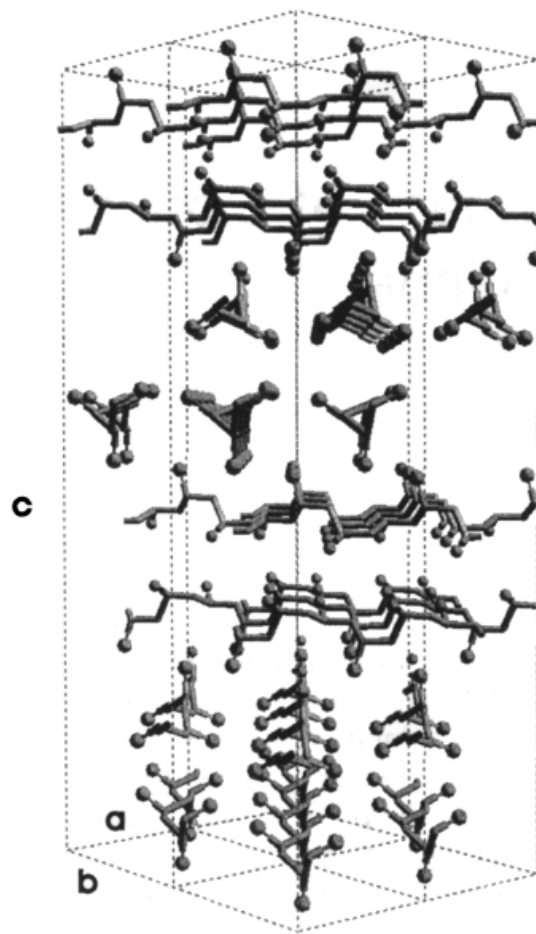
Figure 3.11 Four unit cells of the γ-form of iPP [43]

3.3.4   Smectic Form

The mesomorphic or smectic form of polypropylene is a form intermediates between crystalline and amorphous forms. Early experiments indicated that this form might be a paracrystalline form resulting from deformed or distorted lattice structures. Polymer chains have been shown to form helical structures, but the unit cell and lamellar structures have not been well resolved yet. Experiments indicate a lack of lamellar order in addition to a low density and small size of ordered structures. These characteristics result in high clarity, useful in quenched film applications [27].

4 METHODS OF ANALYSIS

Isotactic polypropylene is a thermoplastic material in which the supermolecular structure fundamentally depends on both presence of specific nucleators and processing conditions. This dependence particularly originates from iPP polymorphism. Consequently, a smart way to adjust final iPP properties can be based on the control of polymorphic composition by the processing set-up and/or the introduction of specific nucleators. Therefore understanding the interrelations between structure, properties and processing of both pure and specifically nucleated PP is a fundamental presumption for their use. The interrelations can be studied on several structure levels using a variety of experimental methods, such as:

- Molecular level - infrared spectroscopy
- Supermolecular level – X-ray scattering, differential scanning calorimetry
- Microscopic level – electron and light microscopy
- Macroscopic level – mechanical testing [45].

4.1 Thermal Analysis of Polymers

The term thermal analysis (TA) is frequently used to describe analytical experimental techniques which investigate the behaviour of a sample as a function of temperature. This definition is too broad to be of practical use [46]. Table 4.1 lists the most common thermal analysis techniques and their practical application to polymers [47].

Table 4.1 Thermal analysis techniques and examples of their practical application [47]

TA method	Abbreviation	Practical application
Differential scanning calorimetry	DSC	melting temperature glass transition temperature T_g
Differential thermal analysis	DTA	degree and rate of crystallization degree of cure heat of fusion
Thermogravimetry	TG	thermal stability volatility of additives filler content moisture content blend composition
Dynamic mechanical thermal analysis	DMTA	creep effects stress relaxation effects damping properties vibration damping molecular transition other than T_g
Thermomechanical analysis	TMA	degree of linear expansion/contraction with temperature delamination temperature degree of polymer hardness with temperature glass transition temperature

Differential Scanning Calorimetry

Thanks to its versatility and explanatory power, DSC is the most-employed thermal analysis method.

A typical differential scanning calorimeter consists of two sealed cells: a sample cell and a reference cell (which is generally an empty sample pan). Cells are heated, or cooled, uniformly while the heat flow difference between the two is monitored. This can be done at a constant temperature (isothermally), but is more commonly done by changing the temperature at a constant rate, a mode of operation that is also called temperature scanning [48]. Experimental arrangement of a DSC instruments is shown in Figure 4.1.
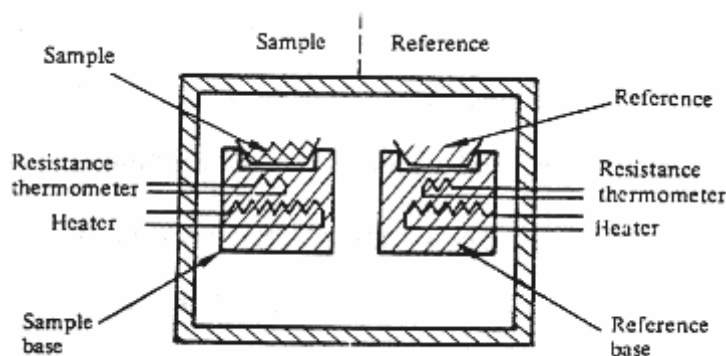
Figure 4.1 Experimental arrangement of a DSC instruments [49]

The sample (in a condensed form such as powder, liquid, or crystal) is generally placed in an aluminum sample pan, which is then placed in the sample cell. The reference consists of a matched empty aluminum sample pan that is placed in the reference cell of the instrument. The sample pans are designed to have a very high thermal conductivity. Sample sizes generally range from 0.1 to 100 mg. The instrument cells are often airtight in order to shield the sample and reference from external thermal perturbations. This also allows experiments to be performed under variable pressures and atmospheres [48].

During the experiment, the instrument detects differences in the heat flow between the sample and reference. This information is sent to an output device (computer), and results in a plot of the differential heat flow between the reference and sample cell as a function of temperature (see Figure 4.2). Generally, the differential heat flow is calculated by subtracting the sample heat flow from the reference heat flow. When following this convention, endothermic processes will show up as positive peaks (above the baseline) while peaks resulting from exothermic processes are negative (below the baseline) [48].
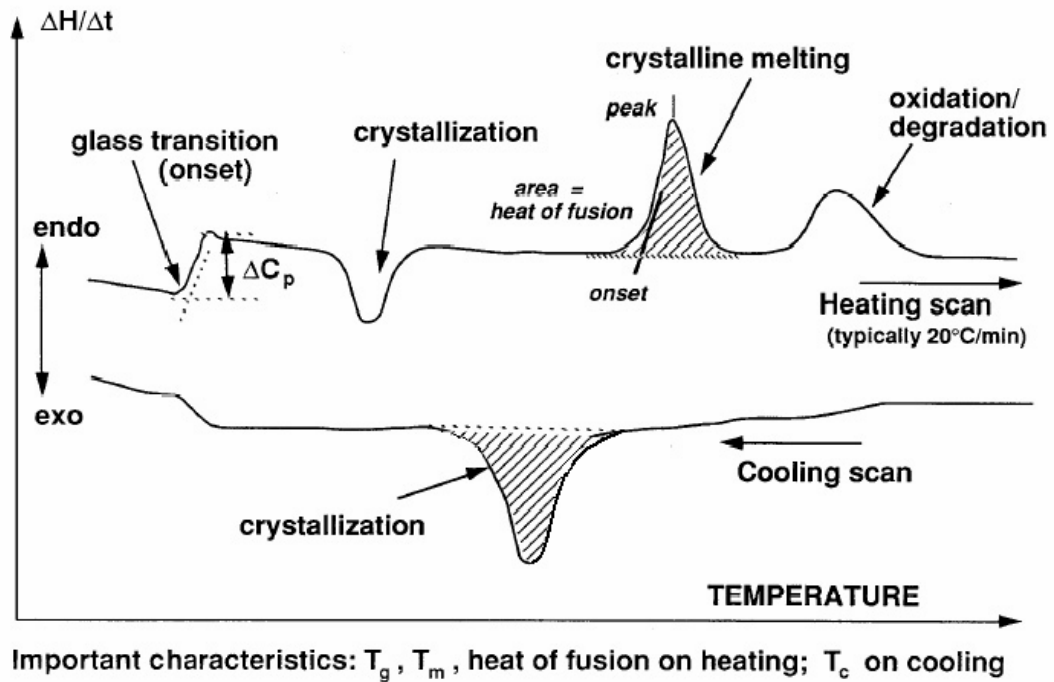
Figure 4.2 Typical polymer DSC thermogram [50]

There are two main types of differential scanning calorimeters - heat flux DSC and power compensation DSC.

In a heat flux calorimeter, heat is transferred to the sample and reference through a disk made of the alloy constantan. The heat transported to the sample and reference is controlled while the instrument monitors the temperature difference between the two. In addition to its function in the heat transfer, this disk serves as part of the temperature-sensing unit. Diagram of a heat flux differential scanning calorimeter is shown in Figure 4.3 [51].
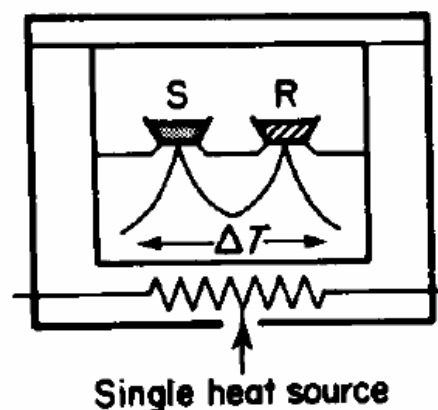
Figure 4.3 Diagram of a heat flux differential scanning calorimeter [51]

In power compensated calorimeters, separate heaters are used for the sample and reference. This is the classic DSC design pioneered by the Perkin-Elmer company. Both the sample and reference are maintained at the same temperature while monitoring the electrical power used by their heaters. The heating elements are kept very small (weighing about 1 gram) in order to ensure that heating, cooling, and thermal equilibration can occur as quickly as possible. Diagram of a power compensated differential scanning calorimeter is shown in Figure 4.4 [51].
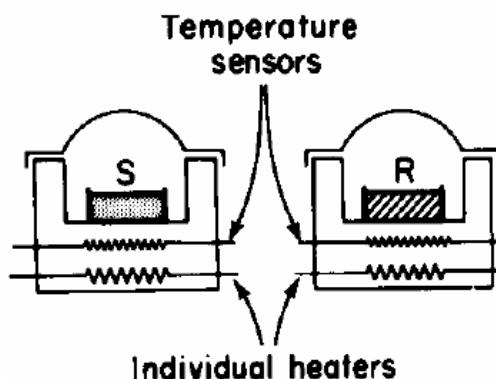
Figure 4.4 Diagram of a power compensated differential scanning calorimeter [51]

4.2 X-ray Scattering

X-ray scattering (diffraction) is the traditional method of crystallographic structure determination, and the standard techniques and analysis procedures can be used in the study of crystalline polymers. The most straightforward application is in the determination of crystal lattice spacing. Other information that can be obtained by X-ray scattering includes crystal size and perfection, the long period in lamellar polymers (lamellar thickness and interlamellar region), the crystallinity (of semi-crystalline polymers), the degree of preferred orientation in polycrystalline samples and, in some recent studies, the conformation of chains in amorphous polymers [52].

X-ray scattering can occur whenever Bragg's law is satisfied. By considering crystals as reflecting gratings for X-rays, Bragg derived equation for the distance d between successive identical planes of atoms in the crystal:

$$d = \frac{n\lambda}{2\sin\theta} \tag{2}$$

where λ is the X-ray wavelength, θ is the angle between the X-ray beam and these atomic planes, and n represents the order of diffraction, a whole number. It turns out that both the X-ray wavelength and the distance between crystals produces a series of spots [47]. See Figure 4. 5.
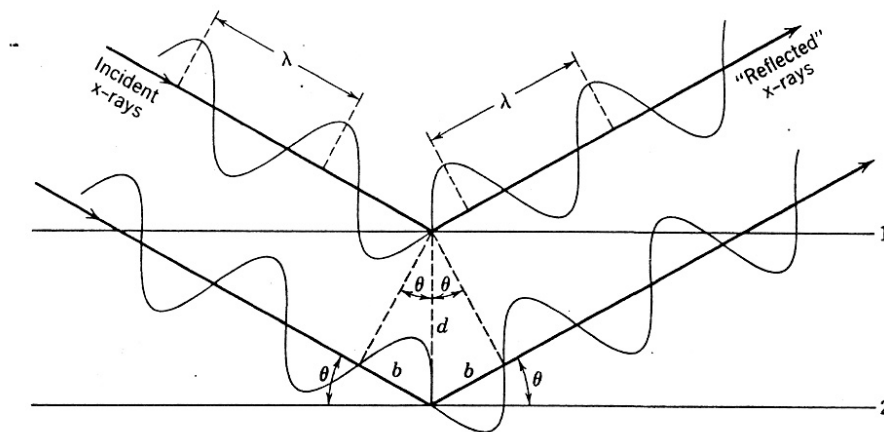
Figure 4.5 Geometry of the Bragg reflection analogy [53]

Only a small range of characteristic X-rays are widely used for diffraction. As an X-ray beam travels through any substance, its intensity decreases with the distance travelled through the substance [54].

With monochromatic radiation, an arbitrary setting of a single crystal in an X-ray beam will not generally produce any diffracted beams. There would therefore be very little information in a single crystal diffraction pattern from using monochromatic radiation. This problem can be overcome by continuously varying λ or θ over a range of values. Practically this is done by:

- using a range of X-ray wavelengths (i.e. white radiation), or
- by rotating the crystal, or using a powder or polycrystalline specimen [54].

Percent Crystallinity in Polymers

Most polymers are semi-crystalline; that is, a certain fraction of the material is amorphous, while the remainder is crystalline. The reason why polymers fail to attain 100 % crystallinity is kinetic, resulting from the inability of the polymer chains to completely disentangle and line up properly in a finite period of cooling or annealing [47].

There are several methods for determining the percent crystallinity in such polymers:

The first method, sometimes called wide-angle X-ray scattering (WAXS), stems from the fact that the intensity of X-ray diffraction depends on the number of electrons involved and is thus proportional to the density. Besides Bragg diffraction lines for the crystalline portion, there is an amorphous halo caused by the amorphous portion of the polymer. This last occurs at a slightly smaller angle than the corresponding crystalline peak, because the atomic spacings are larger. The amorphous halo is broader than the corresponding crystalline peak, because of the molecular disorder [47].

A second method small-angle X-ray scattering (SAXS) involves the determination of the density portion via X-ray analysis of the crystal structure, and determining the theoretical density of a 100 % crystalline material. The density of the amorphous material can be determined from an extrapolation of the density from the melt to the temperature of interest [47].

4.3 Polarized Light Microscopy

The most familiar tool for the study of the material morphology is the light optical microscope. Polarized light microscopy (PLM) is probably the most common method for observing polymer samples. Plane polarized light is used and an analyzer is placed between the sample stage and the eyepiece, and is rotated to the crossed position (zero light transmission) before inserting the sample. The light is transmitted into the image of those parts of the sample that are birefringent (Figure 4.6) [52].

The intensity at any particular position depends on the magnitude of the birefringence, the orientation of the birefringent components with respect to the plane of polarization of the illumination, and the sample thickness, and it follows that the image contrast derives from variation in these from one location to another [52].

This method is especially suitable for studying spherulites because of the difference in birefringence between the crystal lamellas and the non crystalline regions, and because of the different orientations taken by the birefringent lamellas as they radiate out from the centre in all directions: this gives rise to a Maltese cross effect. Birefringence measurements can be made at chosen sites using a compensator inserted into the microscope tube [52].
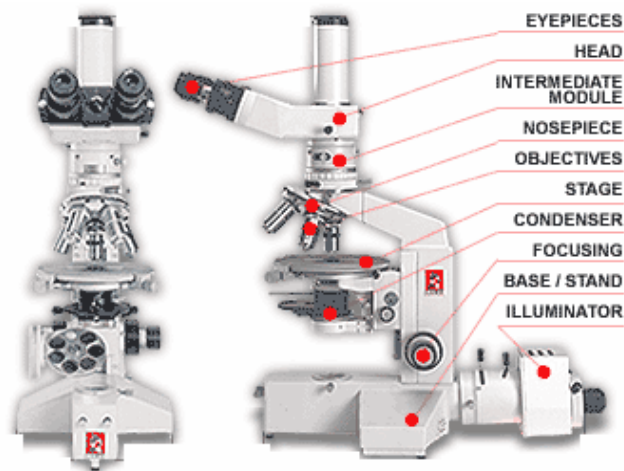
Figure 4.6 Polarized light microscope configuration [55]

The thickness of samples for polarized microscopy is largely depended on the polymer being analyzed. For instance, in case of polypropylene the spherulitic structures are very fine and therefore sections with thickness of several microns are required [47].

II. EXPERIMENTAL

5 MATERIALS

The base material used in this work was iPP Borealis, homopolymer with different melt flow indexes, manufactured by Borealis Group in Copenhagen, Denmark. Some characteristics of these materials, MFI, densities and melting temperatures featured by producer are shown in Appendices A Table 1.

In order to prepare the β-iPP, a specific β-nucleating agent NJ Star NU100 (NU 100), produced by Rika International, Japan, was immixed into PP pellets. The nucleator is based on N,N´-dicyclohexyl-2,6-naphthalenedicarboxamide; its chemical formula and molecular model are shown in Figure 5. 1
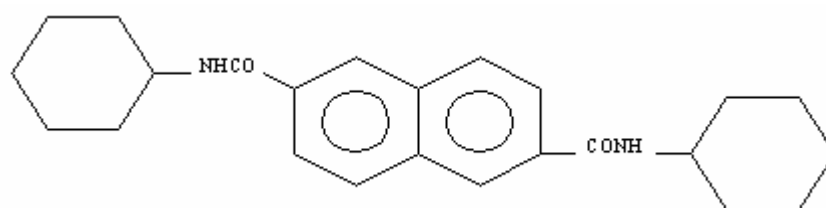
a)
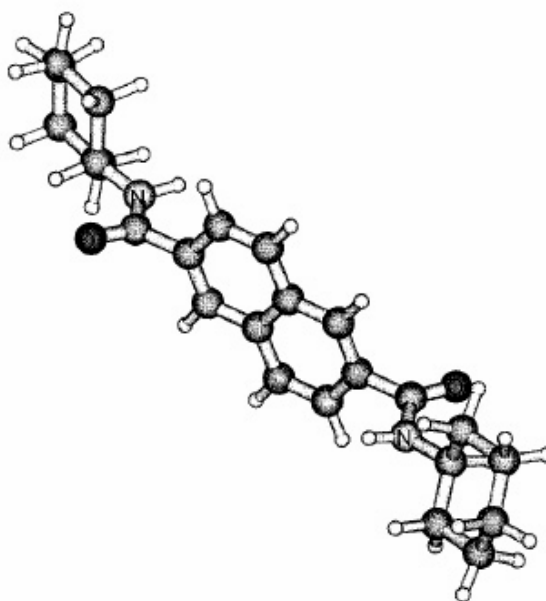
b)

Figure 5.1 Nucleating agent NJ Star NU100: a) chemical formula,
b) molecular model

6 BLENDS PREPARATION

Paraffin oil and subsequently different amount of the nucleating agent NU100 were properly manually immixed into iPP Borealis pellets. Paraffin oil was added for better dispergation of the nucleating agent. Consequently, these blends were premixed in a Brabender twin-screw extruder DSK 42/6D and finally pelletized. The composition of the blends is given in Table 6.1 and processing parameters of extrusion are summarized in Table 6.2. These parameters were put out to provide the best conditions for extrusion of each type of material.

Table 6.1 Composition of blends

Blend no.	wt. % NU100	wt. % PP Borealis	wt. % paraffin oil
1	0.00	100.00	0.00
2	0.01	99.69	0.30
3	0.03	99.67	0.30

Table 6.2 Processing parameters of extrusion

Material	MFI [g/10min]	Temperature of heated zones			Screw speed [min⁻¹]
		T_1 [°C]	T_2 [°C]	T_3 [°C]	
0.01 wt. % NU 100					
BE50	0.3	198	210	220	70
HB205TF	1.0	200	208	215	55
HD601CF	8.0	198	200	210	70
HE125MO	12.0	198	200	210	55
HF136MO	20.0	188	190	195	57
HG455FB	27.0	188	190	195	70
HH450FB	37.0	198	200	210	71
HK060AE	125.0	178	180	190	53
HL504FB	450.0	183	186	190	50
HL508FB	800.0	183	186	190	50
HL612FB	1200.0	187	190	195	55
0.03 wt. % NU 100					
BE50	0.3	205	215	225	70
HB205TF	1.0	200	207	215	50
HD601CF	8.0	200	203	208	65
HE125MO	12.0	195	200	210	55
HF136MO	20.0	182	185	195	57
HG455FB	27.0	178	180	190	70
HH450FB	37.0	173	175	185	71
HK060AE	125.0	187	190	198	53
HL504FB	450.0	181	183	187	47
HL508FB	800.0	181	183	187	50
HL612FB	1200.0	180	182	185	55

7   SAMPLES PREPARATION

Samples for X-ray scattering, DSC and polarized light microscopy were prepared from produced pellets.

7.1   Samples for X-ray Scattering

Samples for X-ray scattering were prepared from the blends plates, which were compression-moulded using a manual press and mould with inside dimensions 125x60x0.5 mm at the following conditions:

- Temperature = 210°C
- Preheating time = 2 min
- Pressing time = 4 min
- Cooling time in a hydraulic press at temperature 60°C = 7 min.

Rectangle samples with dimensions 30x10 mm were cut from the prepared plates.

7.2   Samples for Differential Scanning Calorimetry Analysis

Samples for DSC analysis were prepared from blends plates produced the same way as the samples for X-ray scattering described above with difference in dimensions 125x60x0.2 mm. Thermal conditions were the same.

Cylindrical disks with diameter 4 mm were cut from the prepared plates using a hole-puncher. They were weighed (approximately 5 mg), put into the aluminium pan and covered with the aluminium cover. The pan and the cover were crimped with a special tool supplied by Perkin-Elmer.

7.3   Samples for Polarized Light Microscopy

Samples for polarized light microscopy were prepared the same way as ones for X-ray scattering. Then, they were cut using microtome type FOK GYEM OE-908. The prepared slices of thickness 35 μm were placed on the slide, dropped by paraffin oil and covered by a mount.

8   ANALYSING METHODS AND DEVICES

8.1   Wide Angle X-Ray Scattering

Wide angle X-ray scattering was used in order to investigate relative amount of β-form in the compression-moulded samples. The WAXS patterns were taken with a HZG 3 diffractometer equipped with CuK_α and Bragg-Brentano geometry. Radial scans of intensity vs. diffraction angle *2θ* were recorded in the range from 10° to 30° by steps of 0.05° and length of step scan 5s.

8.2   Differential Scanning Calorimetry Analysis

For the purpose of the crystallization studies, a power-compensated differential scanning calorimeter Perkin-Elmer Pyris 1, was employed. Nitrogen as a purge gas was used and constantly passed 20 ml/s through the heat sink and over the cells. The temperature calibration was performed using indium as a standard.

Samples crystallized in hydraulic press and exposed to WAXS were heated from 50°C up to 190°C with heating rate 10°C/min to obtain melting temperatures and enthalpies of heat fusion.

The controlled non-isothermal crystallization was performed in differential scanning calorimeter using following thermal regime: samples were heated from 50°C to 220°C at a heating rate 50°C/min and annealed at this temperature for 5 min in order to eliminate any previous thermal history of the polymer. Consequently, the samples were cooled to 50°C at given rates 10°C/min and 50°C/min. After that the samples were heated to 190°C at rate 10°C/min in order to observe subsequent melting of the non-isothermally crystallized samples.

To obtain measurements for isothermal crystallization, samples were heated from 50°C to 220°C at a heating rate 50°C/min and then melted at 220°C for 5 min. Consequently, they were rapidly cooled at cooling rate 200°C/min to the crystallization temperature (T_c) 130°C and maintained until the crystallization of the polymer was completed. After that the samples were heated to 190°C at rate 10°C/min with a view to observe subsequent melting of the isothermally crystallized samples.

8.3   Polarized Light Microscopy

In order to study morphology of the crystallized samples, a Zeiss NU optical microscope was used. The samples were placed on the microscope stage and observed in the polarized light. Micrographs of the observed structure were taken using a SONY F-717 digital camera. Common graphic software was used for editing of final images.

III.   RESULTS AND DISCUSSION

9 NON-ISOTHERMALLY CRYSTALLIZED SAMPLES

9.1 Samples Crystallized in Hydraulic Press

k- value

k-value (β-form content) was determined to observe nucleation efficiency of the used nucleator in compression-moulded samples. The proportions of the β-form in the samples were calculated from X-ray diffractograms according to Turner-Jones et al. as follows [25]:

$$k - value = \frac{H_\beta}{H_{\alpha 1} + H_{\alpha 2} + H_{\alpha 3} + H_\beta} \tag{3}$$

where $H_{\alpha 1}$, $H_{\alpha 2}$, $H_{\alpha 3}$ are the intensities of α-diffraction peaks corresponding to angles $2\theta = 14.2°$, 17.0° and 18.8°, respectively, and H_β is the intensity of the β peak at $2\theta = 16.2°$. The *k-value* approximately implies the relative content of β-form in the sample. The ratio of the integral intensities diffracted by a crystalline part (I_c) and total integral intensities (I) was used to determine crystallinity, X_c [25]:

$$X_c = \frac{I_c}{I} \cdot 100 \quad (\%) \tag{4}$$

The analyses of pure and nucleated samples crystallized in hydraulic press were carried out by DSC. The relative crystallinity, *k-value*, melting temperature (T_m) and melting heat (ΔH_m) of each sample are summarized in Appendices A Table 2.

In all cases the crystallinity of the samples is nearly 50 %. In case of the samples without NU 100, the highest crystallinity (53 %) shows material HL508FB with MFI 800.0 g/10 min. On the other hand, the lowest crystallinity (43 %) exhibits material HH450FB with MFI 37.0 g/10 min. In case of the samples with 0.01 wt. % NU 100, the highest crystallinity (47 %) show materials HB205TF with MFI 1.0 g/10 min and HK060AE with MFI 125.0 g/10 min. On the other hand, the lowest crystallinity (41 %) exhibit materials HD601CF with MFI 8.0 g/10 min and HH450FB with MFI 37.0 g/10 min. β-form content of these low-nucleated samples strongly depends on MFI. In case of the samples with 0.03 wt. % NU 100 the highest crystallinity (48 %) shows material HL504FB with MFI 450.0 g/10 min. The lowest crystallinity (41 %) exhibit the same materials as in previous case (HD601CF, HH450FB).

Melting temperature was considered as maximum of endothermic melting peak. As can be seen in the A Table 2, no significant trend between MFI and melting temperature or melting heat can be recognized. As for most of samples containing 0.01 wt. % NU 100 and all samples containing 0.03 wt. % NU 100, the undershoot of DSC baseline during heating caused by recrystallization of α-form into β-form was detected. Therefore, the melting heat could not be calculated. The thermograms are described thereinafter.

9.1.1   PP without NU 100

The dependence of crystallinity and *k-value* on MFI of the samples without NU 100 is shown in Figure 9.1 and described hereinbefore. β-form content of pure samples is neglectable or in the most cases zero.
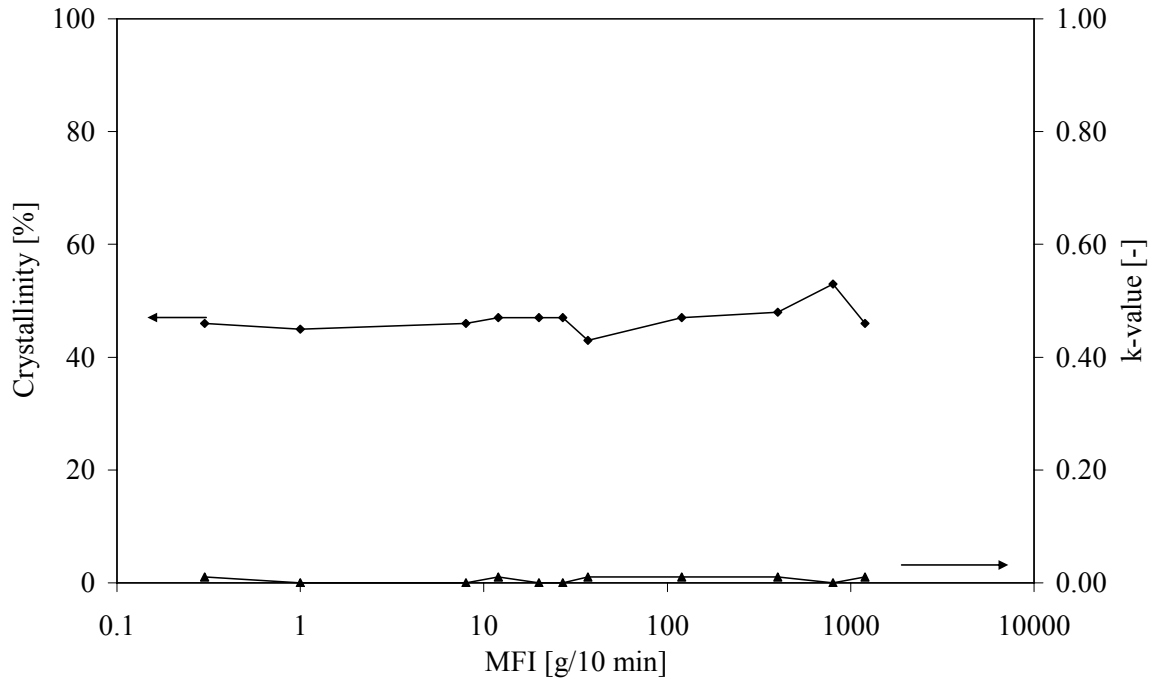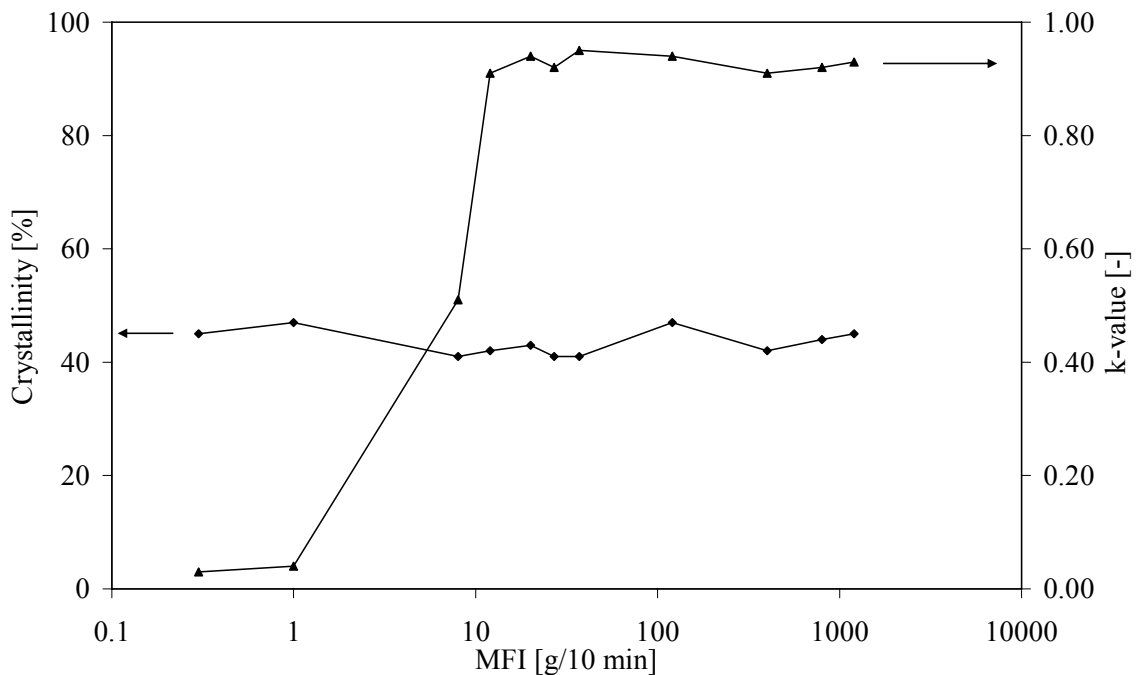

Figure 9.1 Dependence of crystallinity and *k-value* on MFI of the samples without NU 100

Figure 9.2 presents melting thermograms of samples with different MFI without NU 100 crystallized in hydraulic press. The melting peaks of α-form are very well seen, however, no β-form melting endotherm is observed. Moreover, an interesting feature is the doubling of α-form melting peaks. The doubling is particularly significant in the case of samples with high MFI. This doubling can be explained by α_1 to α_2 recrystallization during heating. Application of the fast crystallization conditions leads to the creation of less regular and less stable structure. Subsequent slow heating can then cause the perfection of such structure.
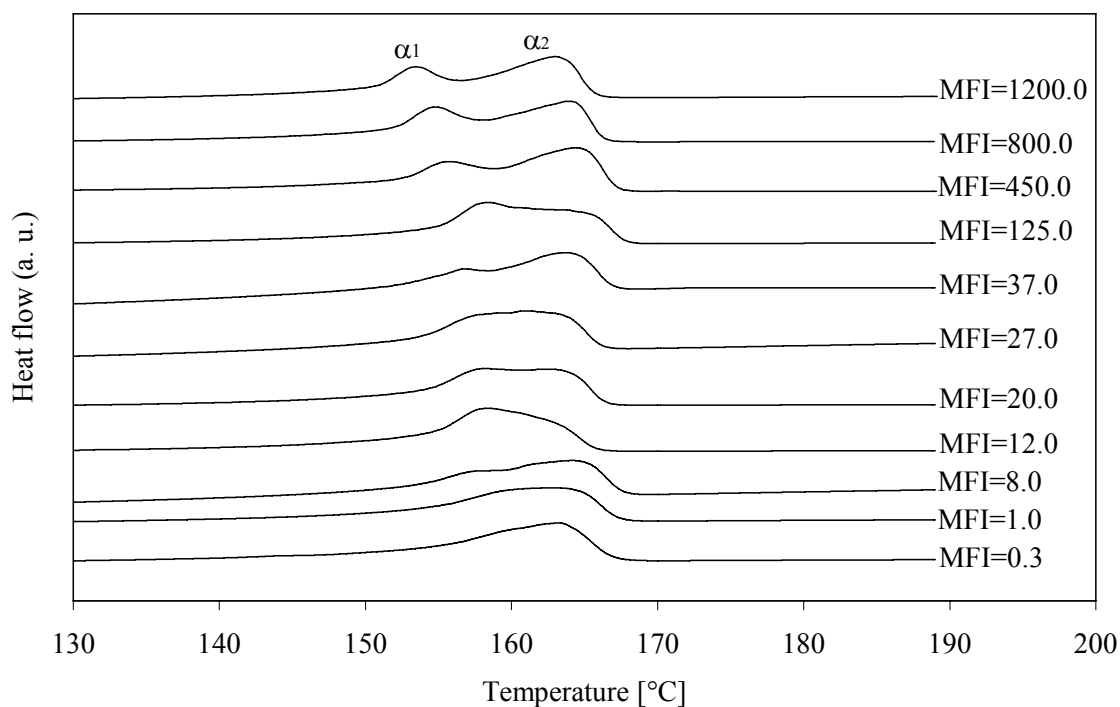
Figure 9.2 Melting thermograms of samples without NU 100 crystallized in hydraulic press

In detail, the morphology of the pure iPP samples with different MFI was studied by means of polarized microscopy. The micrographs in two different scales are shown in Figure 9.3. The spherulites with distinct Maltese-crosses can be observed. The biggest α-spherulites are seen in materials with MFI 1.0, 27.0, 37.0 and 1200.0 g/10 min. No β-spherulites can be recognized.
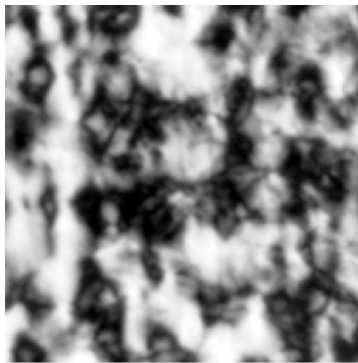
MFI=0.3   MFI=1.0   MFI=8.0
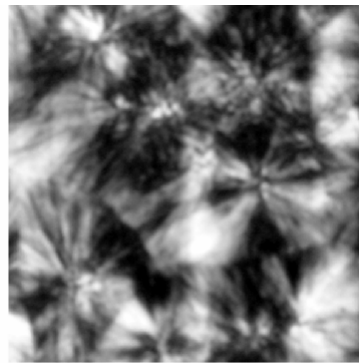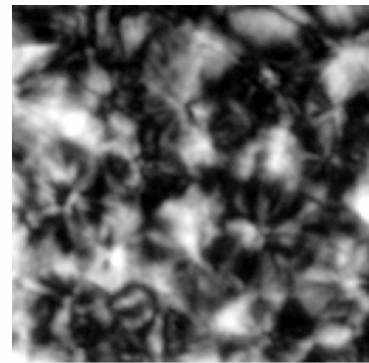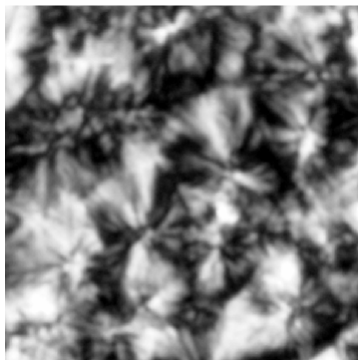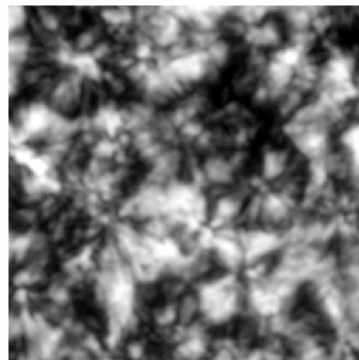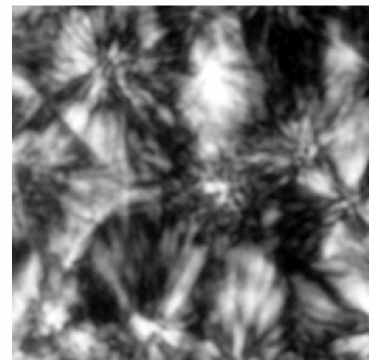
MFI=12.0   MFI=20.0   MFI=27.0
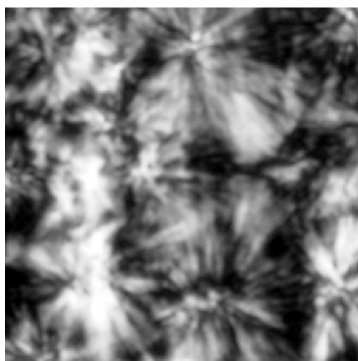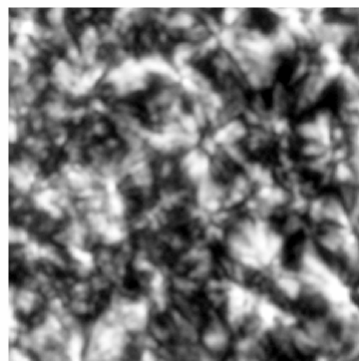
MFI=37.0   MFI=125.0   MFI=450.0
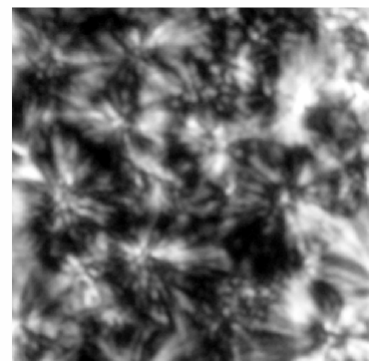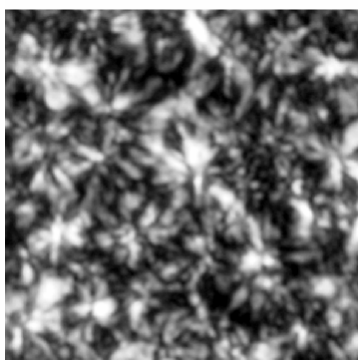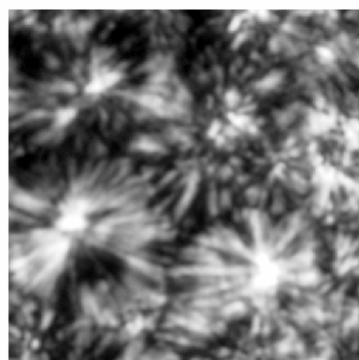
MFI=800.0   MFI=1200.0
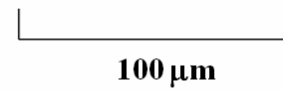
100 μm
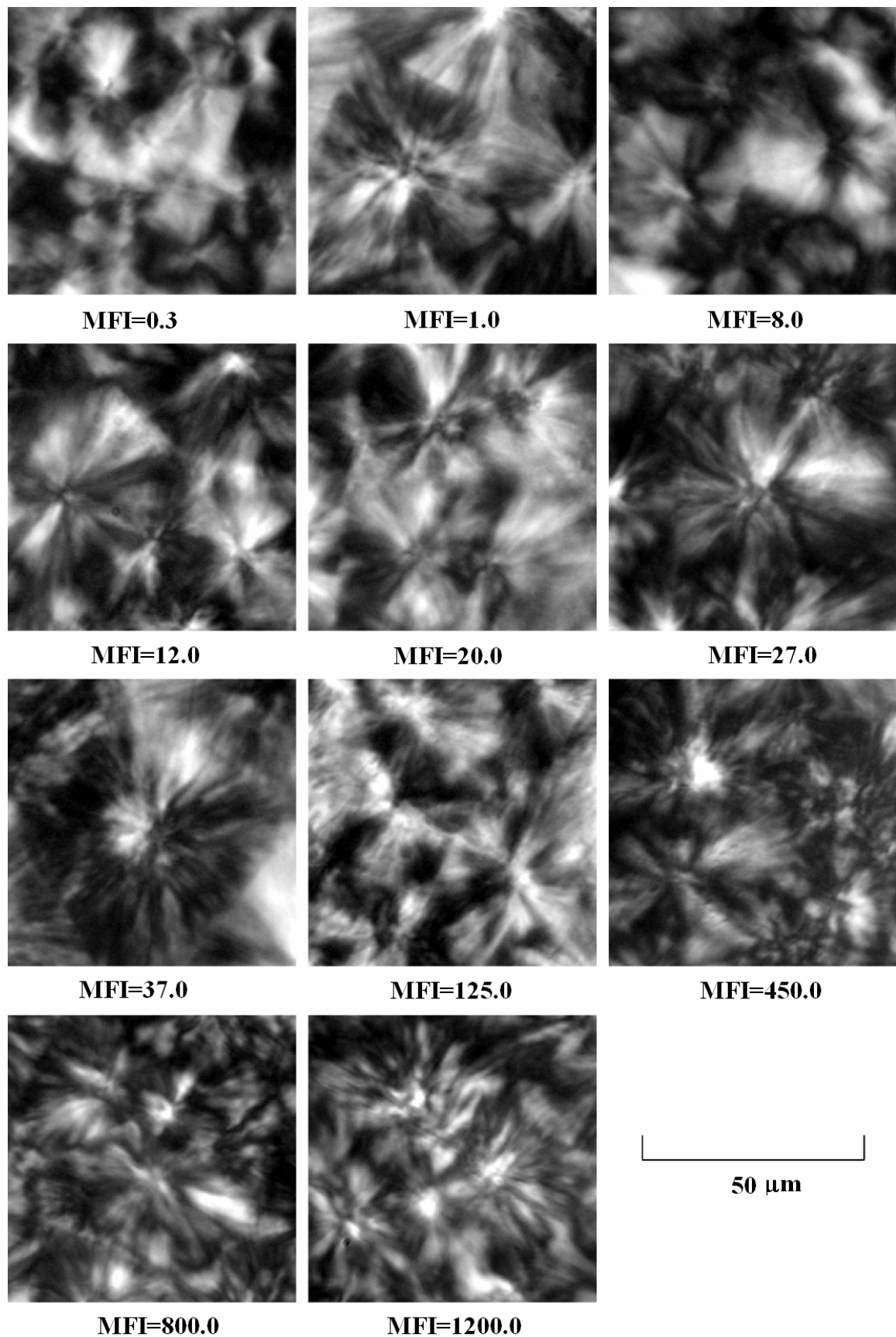
Figure 9.3 Morphology of the pure iPP samples with different MFI in two different scales

9.1.2 PP with 0.01 wt. % NU 100

The dependence of crystallinity and *k-value* on MFI of the samples with 0.01 wt. % NU 100 are shown in Figure 9.4 and described hereinbefore. The crystallinity of all samples is quite stable. The step change of β-form content between materials with MFI 1.0 g/10 min and 12.0 g/10 min (from *k-value* 0.04 to 0.91) can be clearly seen in figure. Based upon this observation, the molecular structure (MFI) seems to influence the efficiency of the NU 100 nucleator. The low MFI decreases the NU 100 efficiency.

Figure 9.4 Dependence of crystallinity and *k-value* on MFI of the samples with 0.01 wt. % NU 100

Figure 9.5 presents melting thermograms of samples with different MFI containing 0.01 wt. % NU 100 crystallized in hydraulic press. In all samples, expect of samples with MFI 0.3 and 1.0 g/10min, α-peaks and also β-peaks can be observed. In the case of samples with very low MFI (i.e. 0.3 and 1.0 g/10 min) only the α-form endotherm can be seen. The sample of MFI 8.0 g/10 min shows next to α-form melting peak also very small β-form melting peak. The melting curves of samples with higher MFI have a complicated profile with doubled β-form endotherm, consequent undershoot of baseline caused by β- to α-form recrystallization process and final melting peak (sometimes doubled) of α-form. The doubled melting peak of α-form or β-form is caused by the perfection of the structure within the same crystal form. However, the exothermic undershoot of baseline is caused by crystallization of melted β-form into α-form. The DSC data are in good agreement with WAXS measurements (see A Table 2).
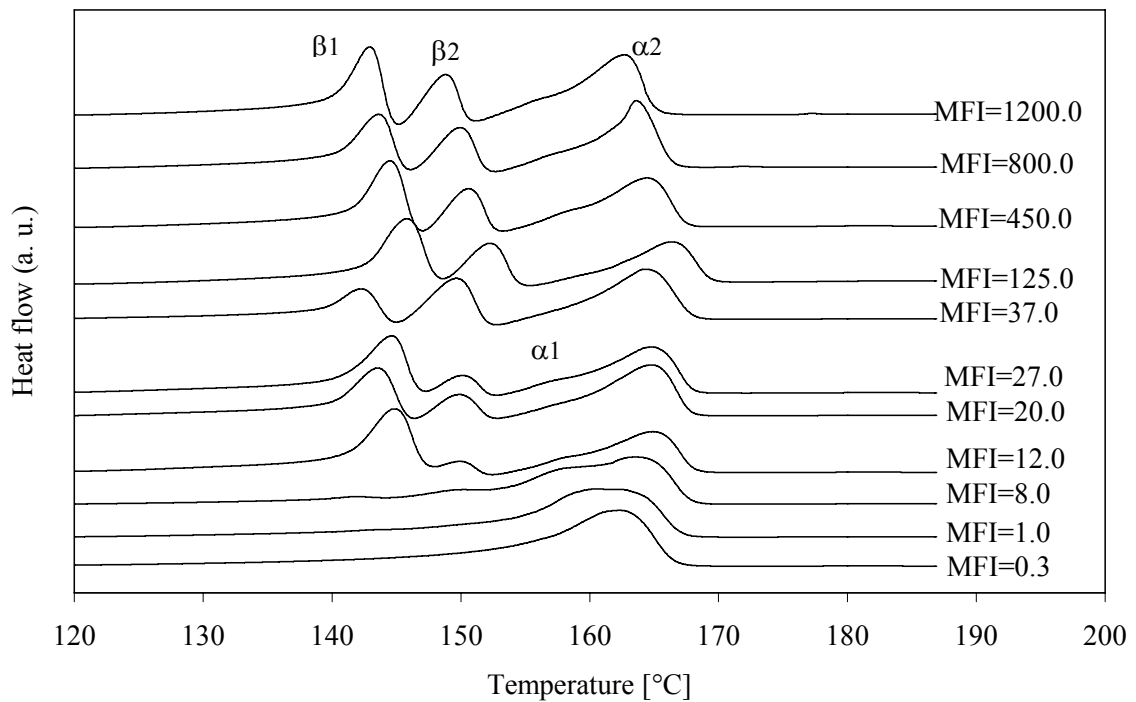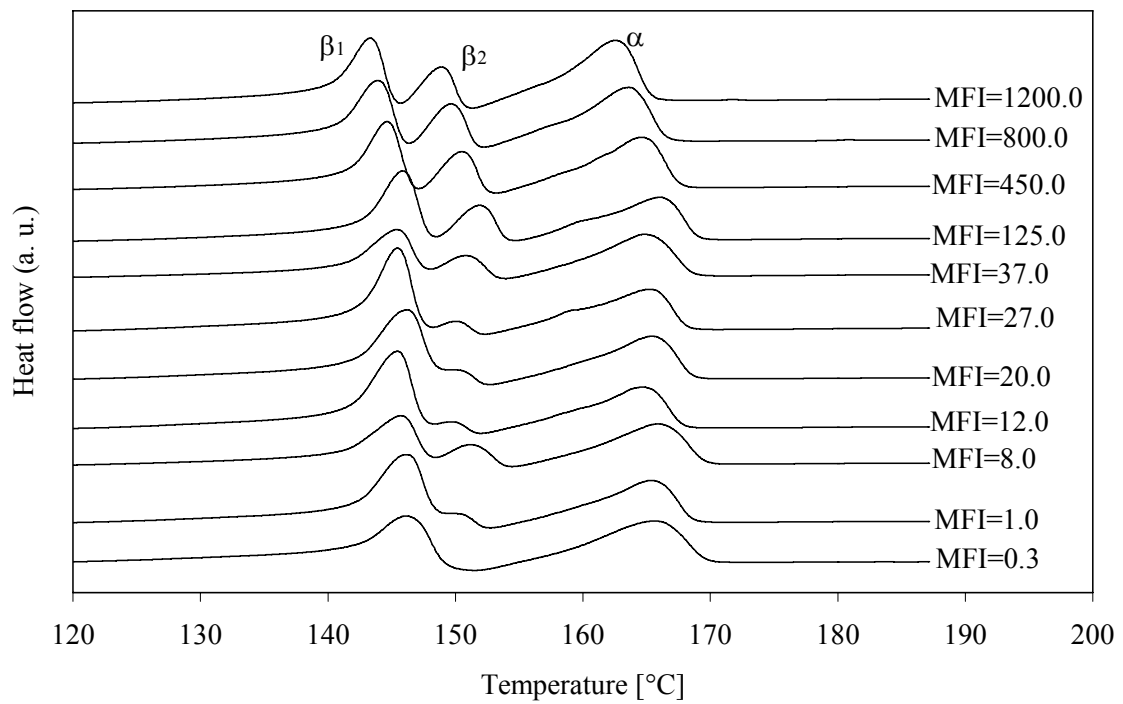
Figure 9.5 Melting thermograms of samples with 0.01 wt. % NU 100 crystallized in hydraulic press

In detail, the morphology of the iPP samples with 0.01 wt. % NU 100 and with different MFI is shown in Figure 9.6 in two different scales. Besides α-spherulites the β-spherulites can be recognized in some cases. The structure of sample with MFI 0.3 g/10 min consists of fine α-spherulites. However, the samples with MFI 1.0 and 8.0 g/10 min show larger α- and β-pherulites. The later mentioned are more frequent in the sample with MFI 8.0 g/10 min. In samples with higher MFI the fine-grained structure containing predominantly β-spherulites originated.
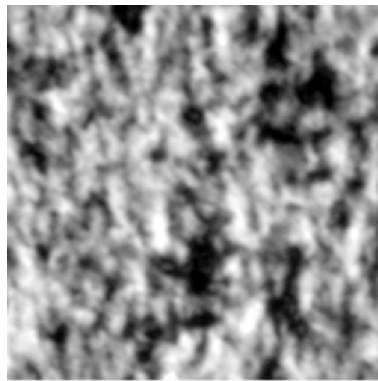
MFI=0.3   MFI=1.0   MFI=8.0
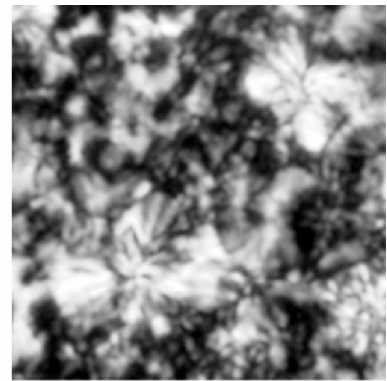
MFI=12.0   MFI=20.0   MFI=27.0

MFI=37.0   MFI=125.0   MFI=450.0

MFI=800.0   MFI=1200.0

100 μm

MFI=0.3   **MFI=1.0**   **MFI=8.0**
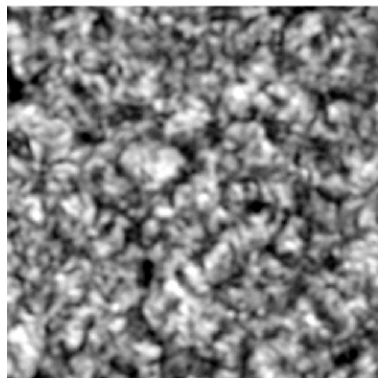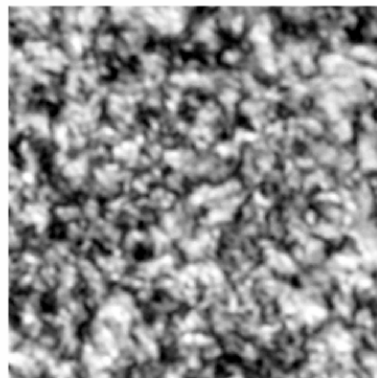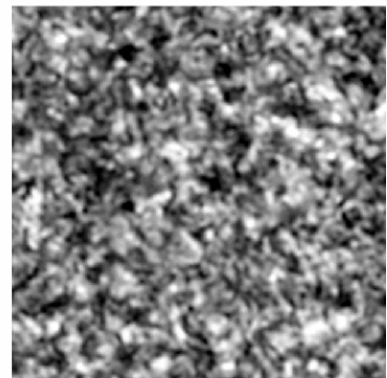
**MFI=12.0**   **MFI=20.0**   **MFI=27.0**
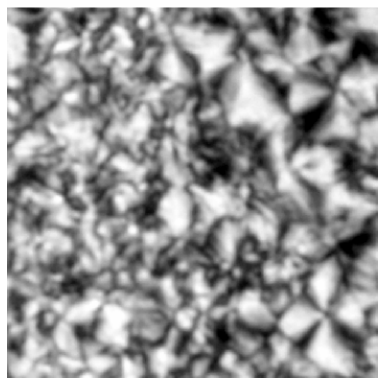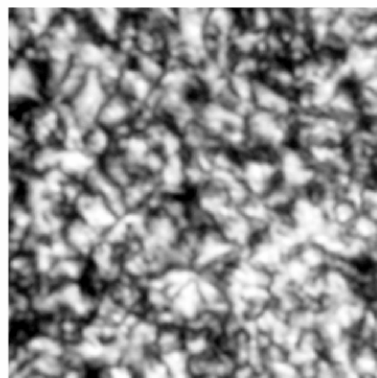
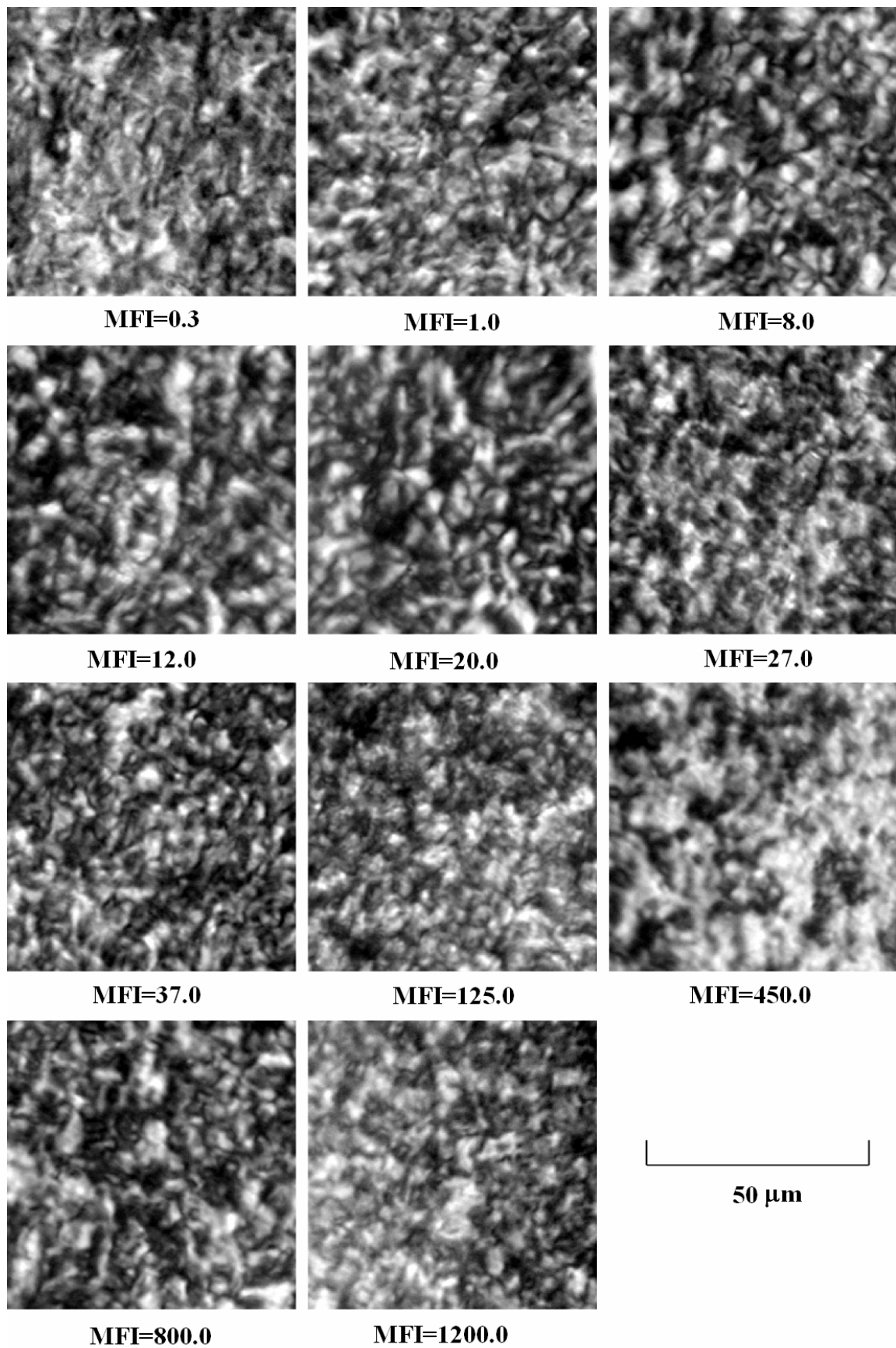**MFI=37.0**   **MFI=125.0**   **MFI=450.0**
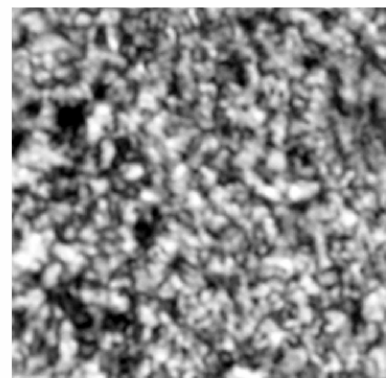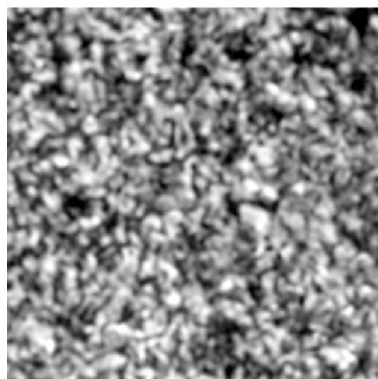
MFI=800.0   **MFI=1200.0**
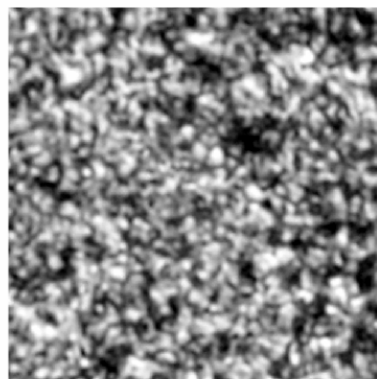
50 μm
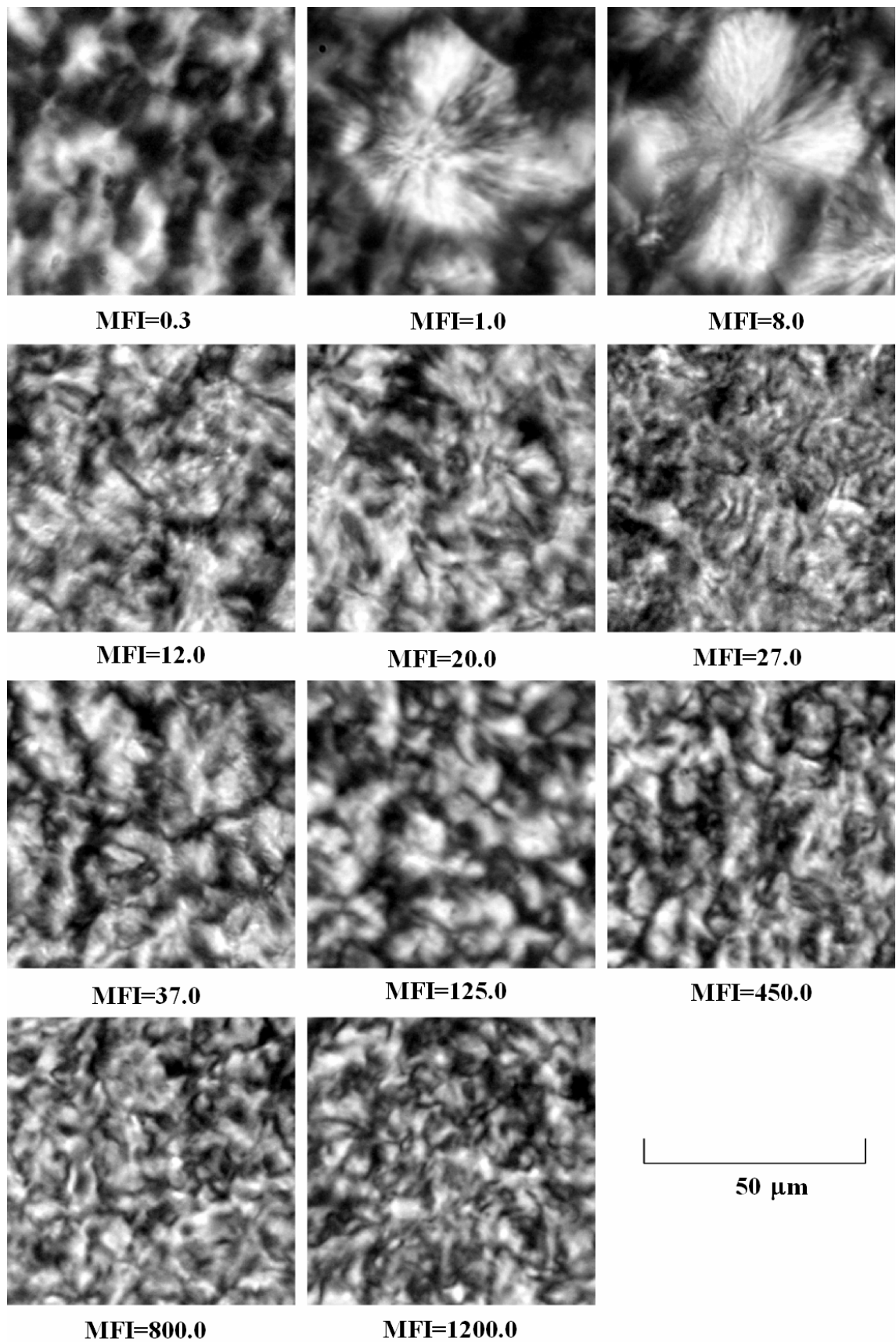
Figure 9.6 Morphology of the iPP samples containing 0.01 wt. % NU 100 with different MFI in two different scales

9.1.3 PP with 0.03 wt. % NU 100

The dependence of crystallinity and *k-value* on MFI of the samples with 0.03 wt. % NU 100 is shown in Figure 9.7. It can be seen that crystallinity of all samples is quite stable (at interval 40 to 50 %). *k-value* of these high-nucleated samples ranges around 0.9.
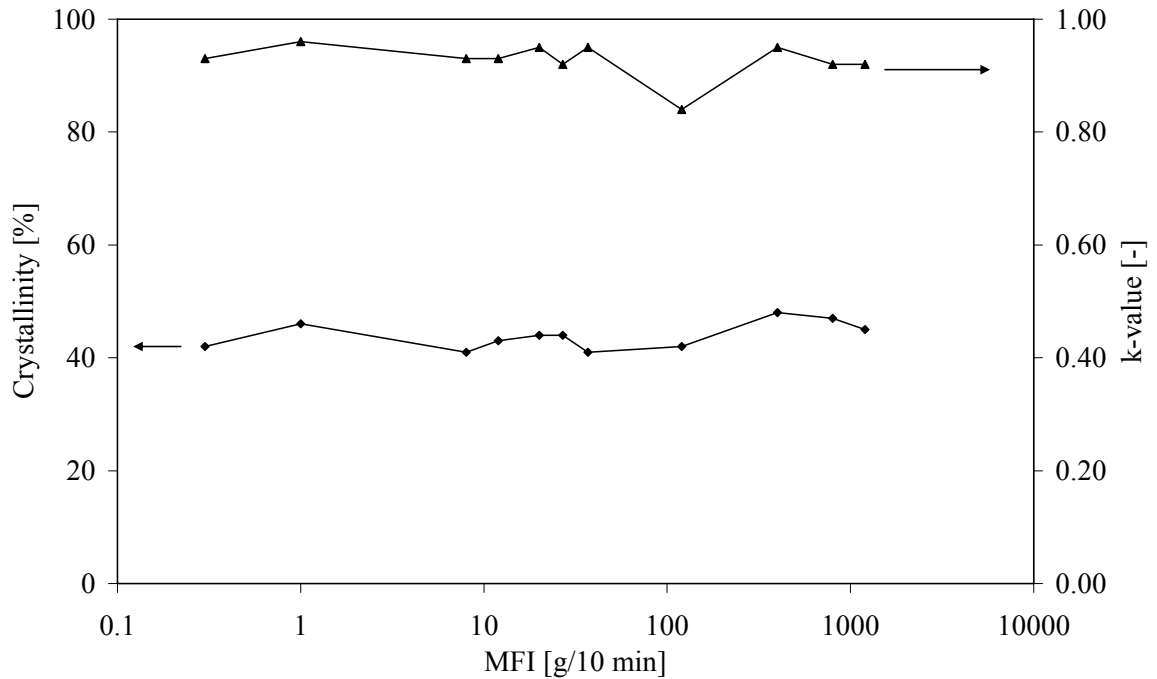
Figure 9.7 Dependence of crystallinity and *k-value* on MFI of the samples with 0.03 wt. % NU 100

Figure 9.8 presents melting thermograms of these high-nucleated samples crystallized in hydraulic press. Beside α-peaks also β-peaks and in most cases double melting β-peaks can be observed. It is again connected with perfection of the structure (ββ-recrystallization) during heating. It should be also noted, that the samples with high MFI are more sensitive to ββ-recrystallization. The significant undershoot of the DSC baseline was recorded, as well as in the case of low-nucleated samples. It implies significant βα-recrystallization process.

Figure 9.8 Melting thermograms of samples with 0.03 wt. % NU 100 crystallized in hydraulic press

In detail, the morphology of the iPP samples with 0.03 wt. % NU 100 and with different MFI are studied and shown in Figure 9.9 in two different scales. The fine-grained structure originated in all cases of MFI and spherulites are not easy recognizable.
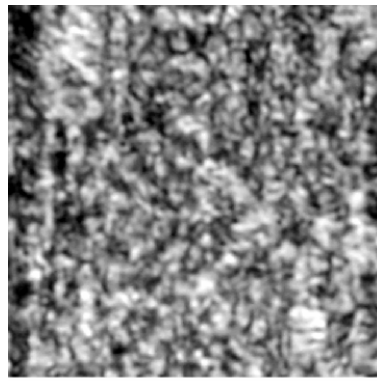
MFI=0.3 MFI=1.0 MFI=8.0
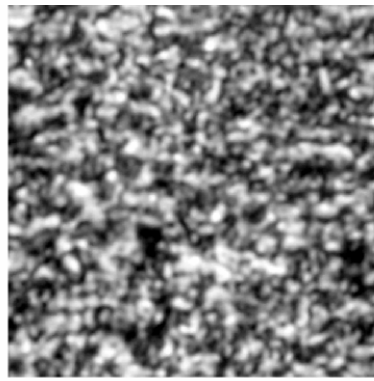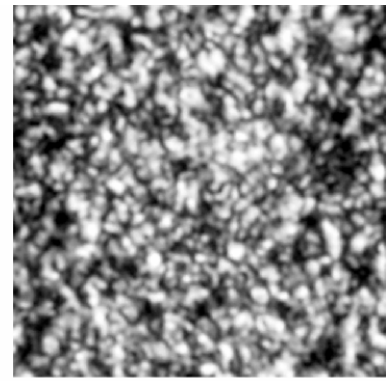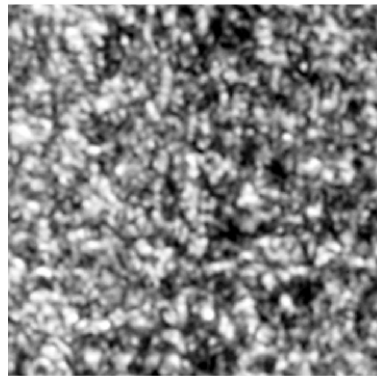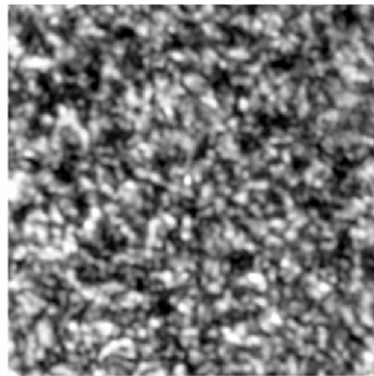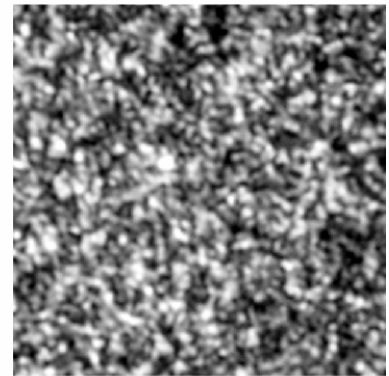
MFI=12.0 MFI=20.0 MFI=27.0
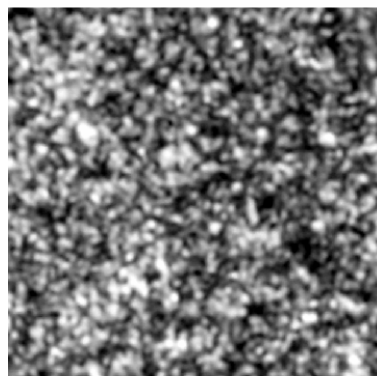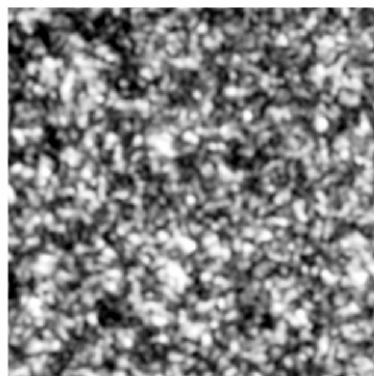
MFI=37.0 MFI=125.0 MFI=450.0
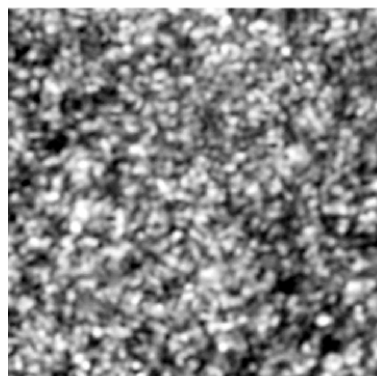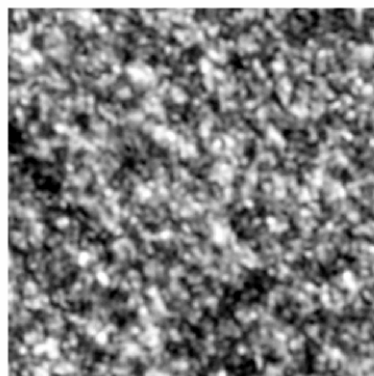
MFI=800.0 MFI=1200.0
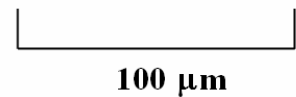
100 μm

Figure 9.9 Morphology of the iPP samples containing 0.03 wt. % NU 100 with different MFI in two different scales

9.2 Samples Crystallized in DSC under Controlled Conditions

To observe the effect of non-isothermal crystallization conditions on the efficiency of β-nucleating agent the samples were cooled at two different cooling rates (10°C/min and 50°C/min). The analysis of pure and nucleated samples crystallized under controlled conditions was carried out by DSC. The measured values such as crystallization temperature, crystallization heat (ΔH_c), crystallization halftime ($t_{1/2}$), melting temperature and melting heat are summarized in Appendices A Table 3.

As is seen in the table, the range of T_c of samples cooled at rate 50°C/min is significantly lower than that of samples cooled at 10°C/min. It is generally known, the temperature range of crystallization is affected by the cooling rate. The higher the cooling rate the lower the temperature range at which the crystallization proceeds. It is apparent that slower cooling rate enables creation of more perfect structure, which gives higher value of the crystallization heat. Gradual crystallization of the melt begins during cooling when potential nucleating barriers are overcome. Thus it is obvious that higher cooling rate allows for higher undercooling of melt and initiation of crystallization at lower temperature [30, 32].

The influence of NU 100 content in the material on the T_c range can be also observed in A Table 3. The crystallization temperature range of the samples with 0.01 wt. % NU 100 is slightly higher than that of neat samples. However, the significant increase of T_c range of high-nucleated samples is observed. This corresponds with known fact that heterogeneous nuclei in the melt accelerate the crystallization [4, 5].

The dependence of crystallization temperature on MFI of the samples containing 0, 0.01 and 0.03 wt. % NU 100 with different cooling rate (10°C/min and 50°C/min) is shown in Figure 9.10 and Figure 9.11. The complex dependence in the case of neat polypropylene crystallized at both cooling rates can be observed. The T_c is probably influenced by the molecular structure (i.e. MFI) of the material. Nevertheless, the dispersion of the T_c values is slighter for the samples containing nucleating agent, especially for the high-nucleated samples. Moreover, in the case of these high-nucleated samples, it can be said that with increasing MFI the T_c rises.
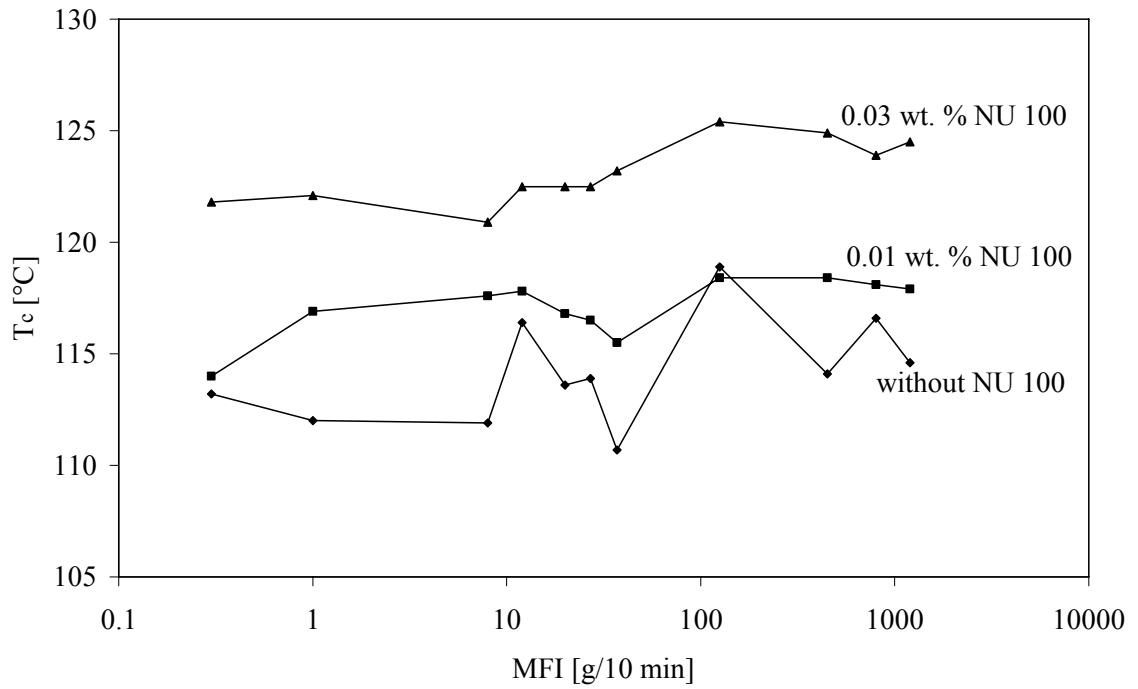
Figure 9.10 Dependence of crystallization temperature on MFI of the samples containing 0, 0.01 and 0.03 wt. % NU 100; crystallization at cooling rate 10°C/min
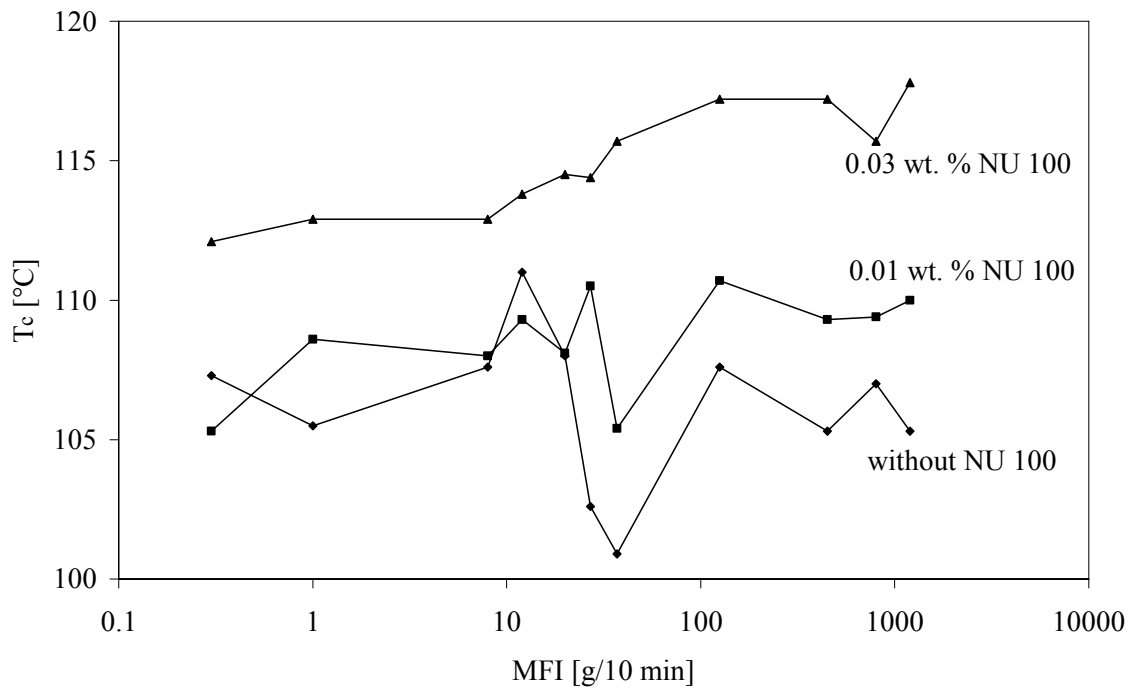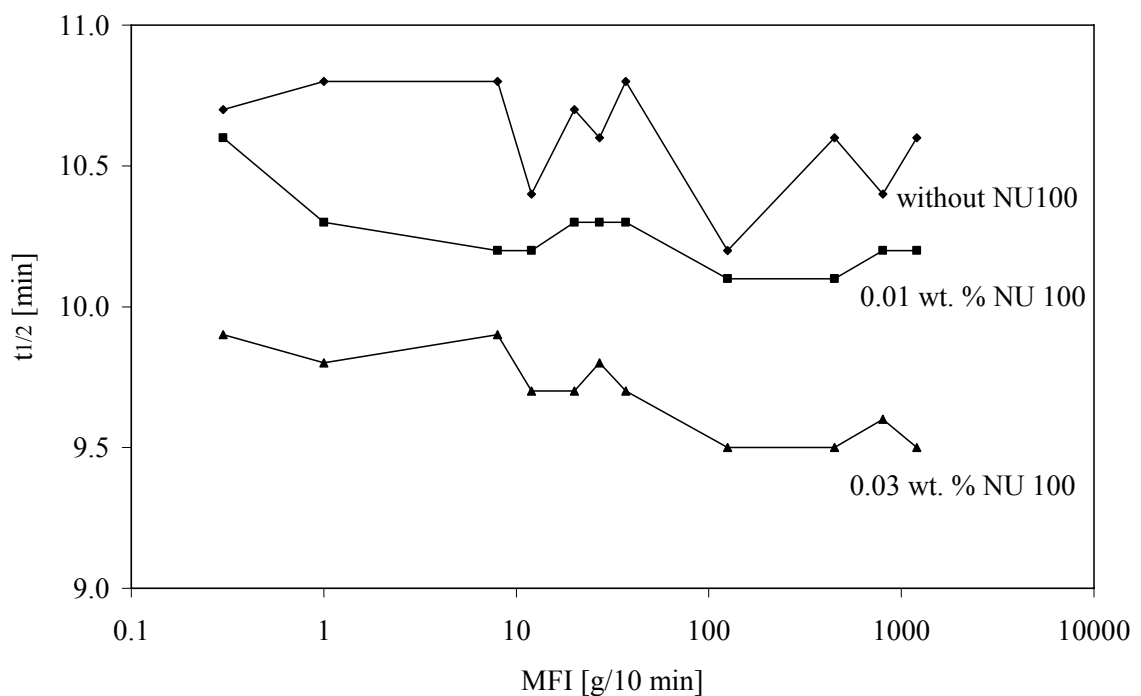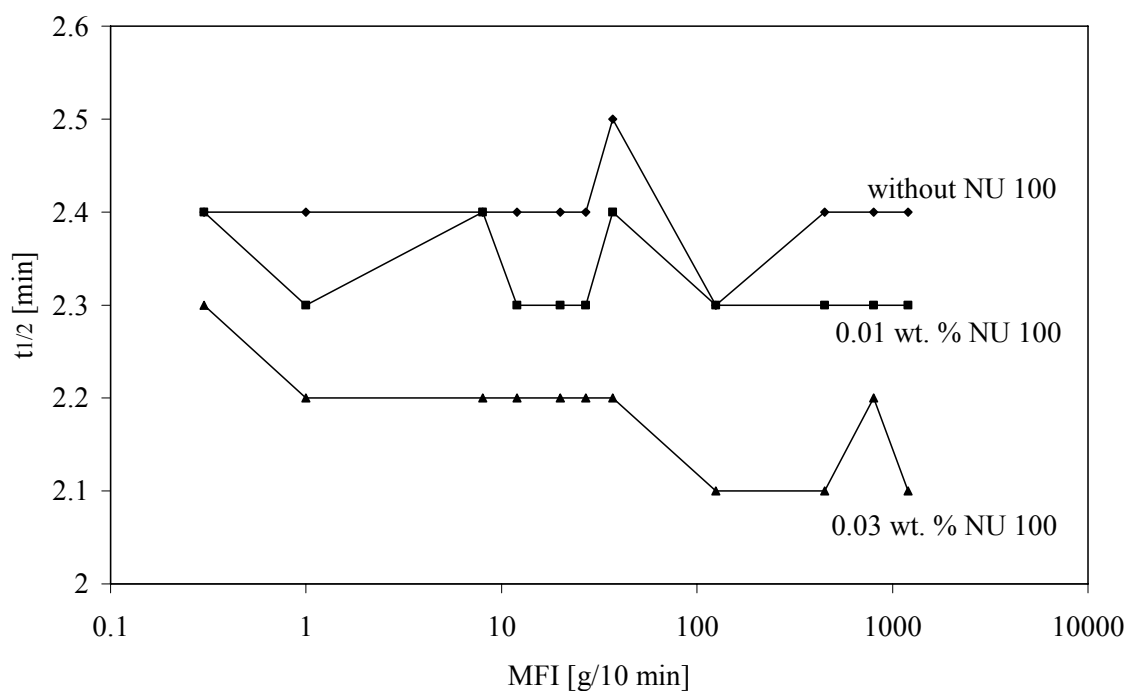

Figure 9.11 Dependence of crystallization temperature on MFI of the samples containing 0, 0.01, 0.03 wt. % NU 100; crystallization at cooling rate 50°C/min

Figure 9.12 and Figure 9.13 show dependence of crystallization halftime on MFI of the samples containing 0, 0.01 and 0.03 wt. % NU 100 crystallized at 10°C/min or 50°C/min. It can be seen, that crystallization halftime decreases with rising amount of the nucleating agent in both cases. The crystallization is time demanding process consisting of two steps: nucleation and growth (see chapters 1.1 and 1.2). In the first step, nucleation, the nuclei are formed which requires the time. In the next step, the crystals grow and again it needs a time. Since in the material with NU 100 the heterogeneous nuclei are present in the melt the time required for crystallization decreases. Regarding the shape of the $t_{1/2}$ dependences on material MFI, it has quite complicated profile, especially in the case of cooling rate 50°C/min. However, as for the cooling rate 10°C/min, the present of nucleator in the material causes compose of the shape and slight decrease of the $t_{1/2}$ with MFI can be recognized (see A Table 3).

As can be seen in A Table 3, no significant trend between MFI and melting temperature or melting heat is evident. As for most of samples containing 0.03 wt. % NU 100 and sample with MFI 1200.0 g/10 min containing 0.01 wt. % NU 100 with cooling rate 50°C/min, the undershoot of DSC curve was detected. Therefore, the melting heat could not be calculated. Thermograms are described thereinafter.

Figure 9.12 Dependence of crystallization halftime on MFI of the samples containing 0, 0.01, 0.03 wt. % NU 100; crystallization at cooling rate 10°C/min

Figure 9.13 Dependence of crystallization halftime on MFI of the samples containing 0, 0.01, 0.03 wt. % NU 100; crystallization at cooling rate 50°C/min

9.2.1 Samples with Different MFI

In order to study the effect of molecular structure on melting behaviour of non-isothermally crystallized neat and nucleated samples the DSC scans are compared in Figures 9.14 – 9.19.

9.2.1.1 PP without NU 100

Figure 9.14 and Figure 9.15 show thermograms of the samples with different MFI without NU 100 non-isothermally crystallized at the cooling rate 10 or 50°C/min. In both cases only α-form melting peaks are observed. Thermograms of the samples with MFI 8.0, 37.0, 450.0, 800.0 and 1200.0 g/10 min crystallized at the cooling rate 10°C/min show double melting peaks indicating the perfection of the structure within the same crystal form ($\alpha\alpha$-recrystallization). In case of the samples crystallized at the cooling rate 50°C/min, all samples expect samples with MFI 0.3 and 1.0 g/10 min, exhibit double melting peaks (see A Table 3). Thus, this effect is particularly more pronounced for samples crystallized at higher cooling rates when less ordered structure originates. It can be also observed, that the high MFI (i.e. 450.0, 800.0 and 1200.0 g/10 min) facilitates the recrystallization process; the doubling of melting endotherm is the most significant. It is caused by the high number of the molecule ends which represent defects in the chains leading to the formation of imperfect crystals with low T_m. Then, during the heating the molecules are released from these imperfect crystals and subsequently arranged into more perfect crystals with high T_m.
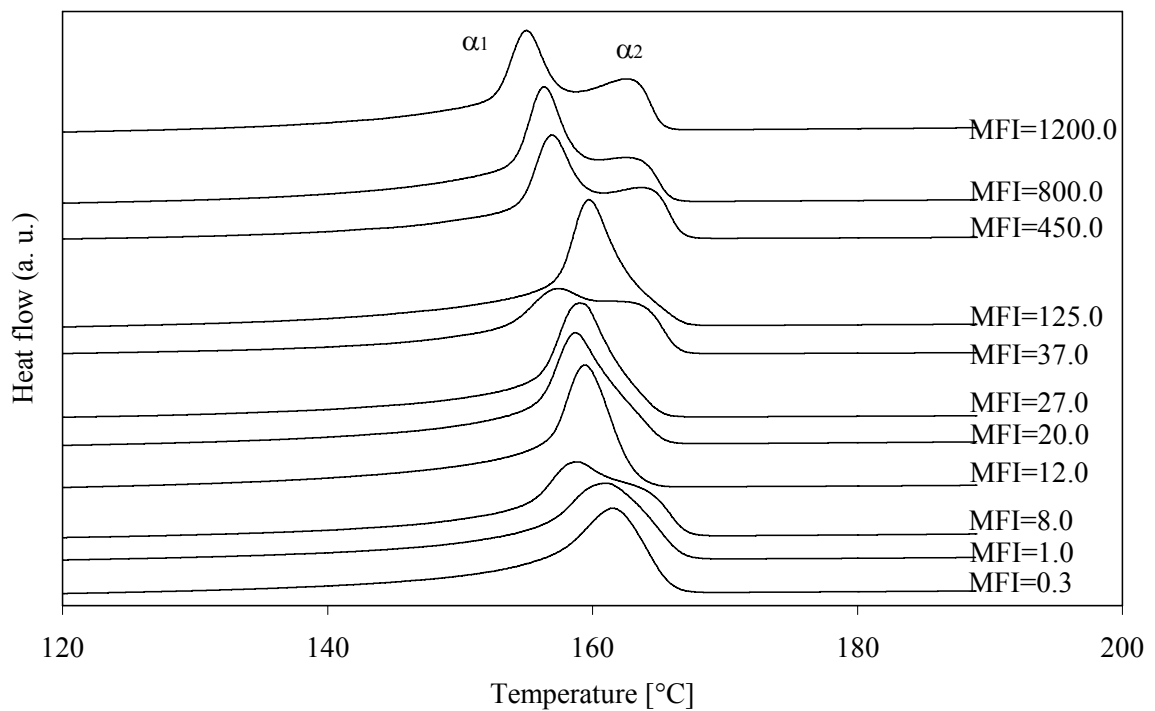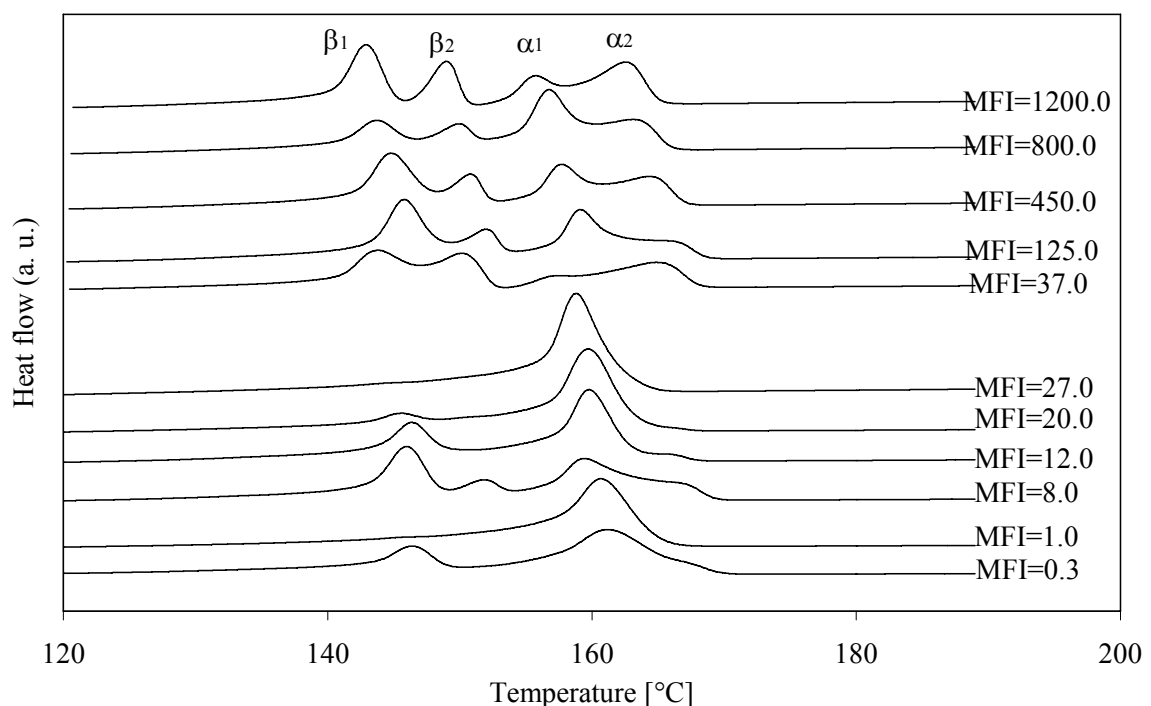
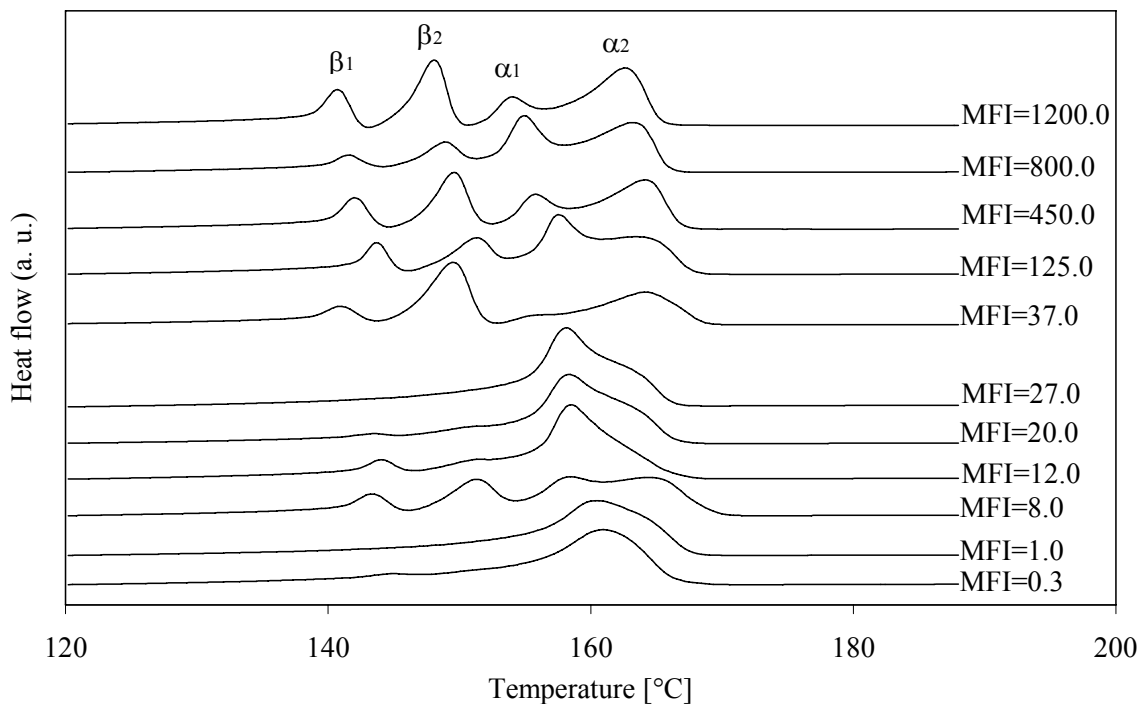Figure 9.14 Melting thermograms of the samples without NU 100 with different MFI crystallized at cooling rate 10°C/min
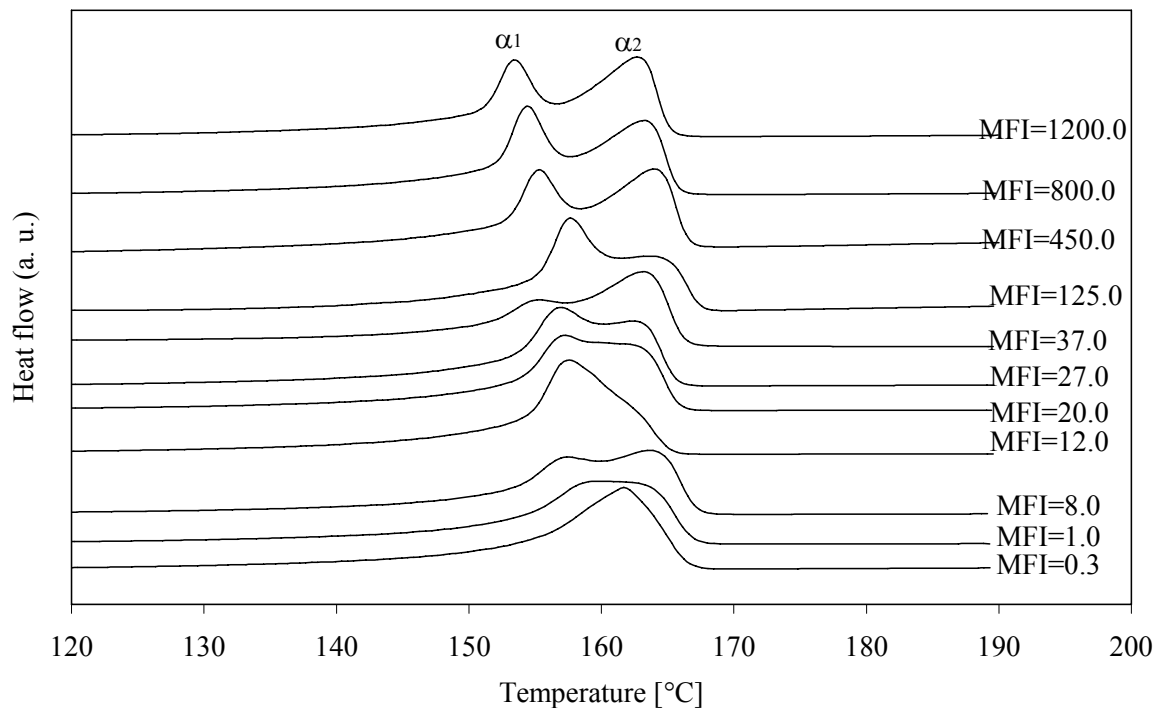
Figure 9.15 Melting thermograms of the samples without NU 100 with different MFI crystallized at cooling rate 50°C/min

9.2.1.2   PP with 0.01 wt. % NU 100

As can be seen from Figure 9.16 and Figure 9.17, the thermograms of the samples containing 0.01 wt. % NU 100 embody beside a melting peak of the α-form, also a melting

peak of β-form. The shape of the melting curves strongly depends on the MFI. The higher is the MFI the more complicated is the melting profile. From the MFI 37.0 and more, even four melting peaks are observed. The first two peaks (T_m = 140 ~ 152°C) are assigned to the β-form melting and the next two peaks (T_m = 156 ~ 168°C) represent the melting of α-form. The doubling of these melting peaks is again ascribed to the perfection of the structure within the same crystal form during heating (αα-recrystallization and ββ-recrystallization). The doubling of the α-melting peak can be also supported by βα-recrystallization which can proceed as well. Very interesting is the fact that some materials crystallizes only into α-form although they are β-nucleated. This is the case of materials with MFI 1.0 and 27.0 g/10 min crystallized at 10°C/min and materials with MFI 0.3, 1.0 and 27.0 g/10 min crystallized at 50°C/min. The material with MFI 20.0 g/10 min shows only very small β-form melting peak for both cases of cooling rates. It is interesting to compare these results with the melting scans of samples crystallized in the hydraulic press (compare Figures 9.16 and 9.5). The scans of samples with MFI 0.3 and 1.0 g/10 min crystallized at hydraulic press possess no β-melting peak as well as the samples crystallized in DSC at 50°C/min. However, sample with MFI 8.0 g/10 min crystallized in press shows only very small β-melting endotherm while in the case of that one crystallized in DSC at 50°C/min the peak is nearly dominant. The scans of materials with higher MFI crystallized in the press show significant β-melting peaks. On the other hand, in the scans of samples with MFI 12.0, 20.0 and 27.0 g/10 min crystallized in DSC at 50°C/min no or very small β-peak can be observed. Therefore, it can be stated, that the crystallization into β-form is influenced by both the crystallization conditions and the molecular structure.
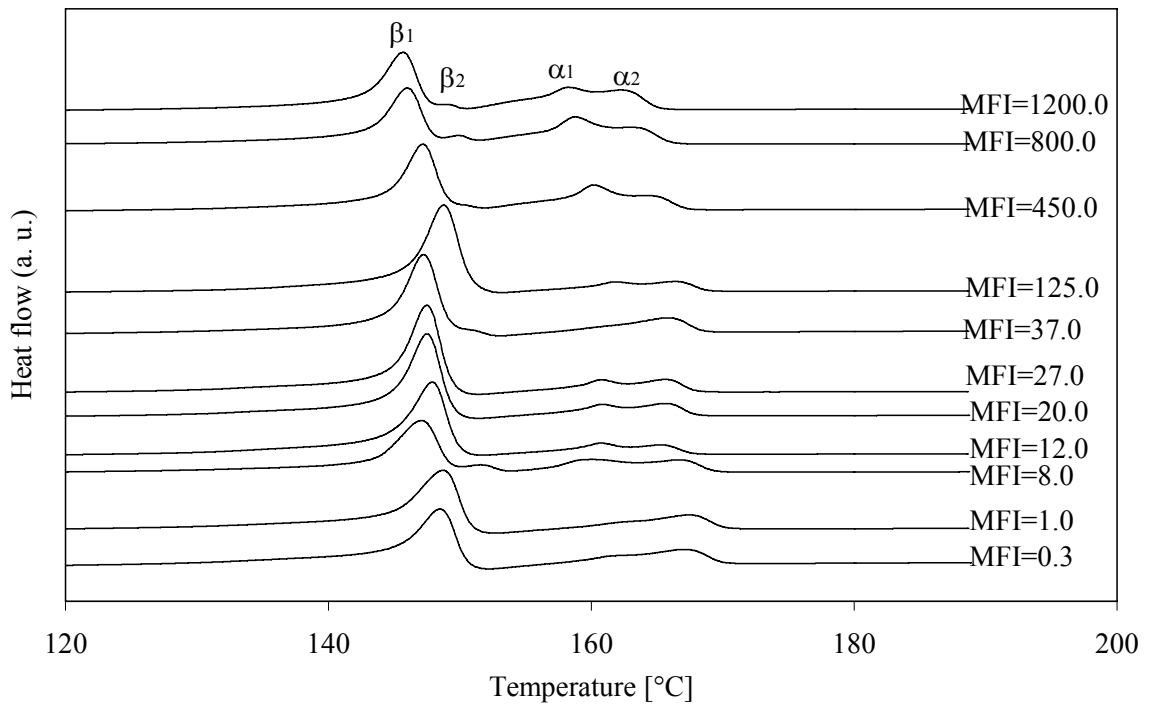

Figure 9.16 Melting thermograms of the samples with 0.01 wt. % NU 100 with different MFI crystallized at cooling rate 10°C/min
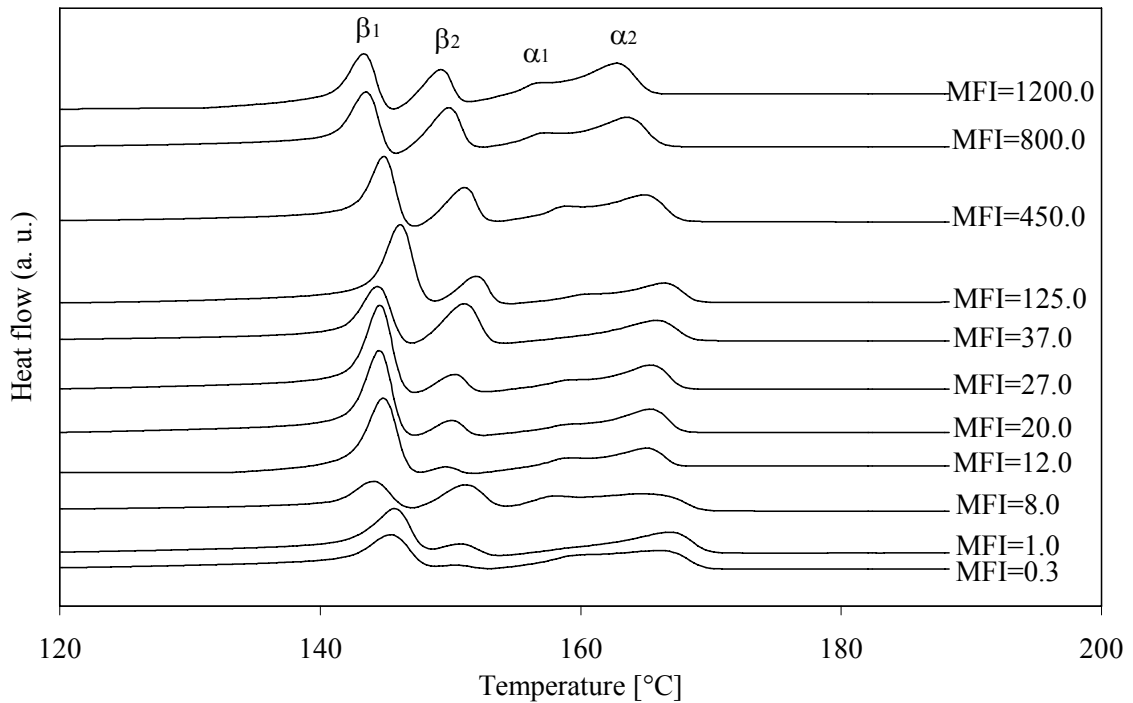
Figure 9.17 Melting thermograms of the samples with 0.01 wt. % NU 100 with different MFI crystallized at cooling rate 50°C/min

9.2.1.3 PP with 0.03 wt. % NU 100

Thermograms of the samples containing 0.03 wt. % NU 100 are displayed in Figures 9.18 and 9.19. It is obvious that the melting endotherms of β-form are predominant. As can be seen in the figures, the shape of the melting curves depends on the MFI. In most cases of the samples non-isothermally crystallized at the cooling rate 50°C/min and some samples crystallized at the cooling rate 10°C/min an undershoot of baseline was detected what implies the β- to α-form recrystallization. The melted β-form can additionally crystallize into α-form with higher T_m (α_2-peak in the figures). In most of samples containing 0.03 wt. % NU 100 a double melting peaks of α-form caused by mentioned βα-recrystallization was also observed (see A Table 3). However, αα-recrystallization could not be excluded. The ββ-recrystallization proceeds mainly in the samples crystallized at 50°C/min when less ordered structure originates.

Figure 9.18 Melting thermograms of the samples with 0.03 wt. % NU 100 with different MFI crystallized at cooling rate 10°C/min

Figure 9.19 Melting thermograms of the samples with 0.03 wt. % NU 100 with different MFI crystallized at cooling rate 50°C/min

9.2.2 Samples with Different Content of NU 100

By virtue of nucleator efficiency observation in each non-isothermally crystallized sample the melting thermographs of variously nucleated material with the certain MFI are compared in the same graphs (Figures 9.20 – 9.41).

9.2.2.1 *MFI 0.3 g/10 min*

Melting thermograms of samples with MFI 0.3 g/10 min with 0, 0.01 and 0.03 wt. % NU 100 crystallized at cooling rate 10 or 50°C/min are shown in Figures 9.20 and 9.21. It can be seen that samples without NU 100 embody only a melting peak of the α-form in both cases. Samples containing 0.01 wt. % NU 100 embody beside a melting peak of the α-form also a very small melting peak of the β-form. In the case of samples containing 0.03 wt. % NU 100 the β-form melting peak becomes dominating. In addition, double melting peaks of α-form were observed, and as for the samples crystallized at 50°C/min also double melting endotherm of β-form was detected (see A Table 3). The recrystallization processes causing these doublings are described earlier in the text. It is evident from these figures, that the addition of only 0.01 wt. % NU 100 is not sufficient to obtain predominant β-form in the material. However, the amount of 0.03 wt. % NU 100 seems to be adequate.
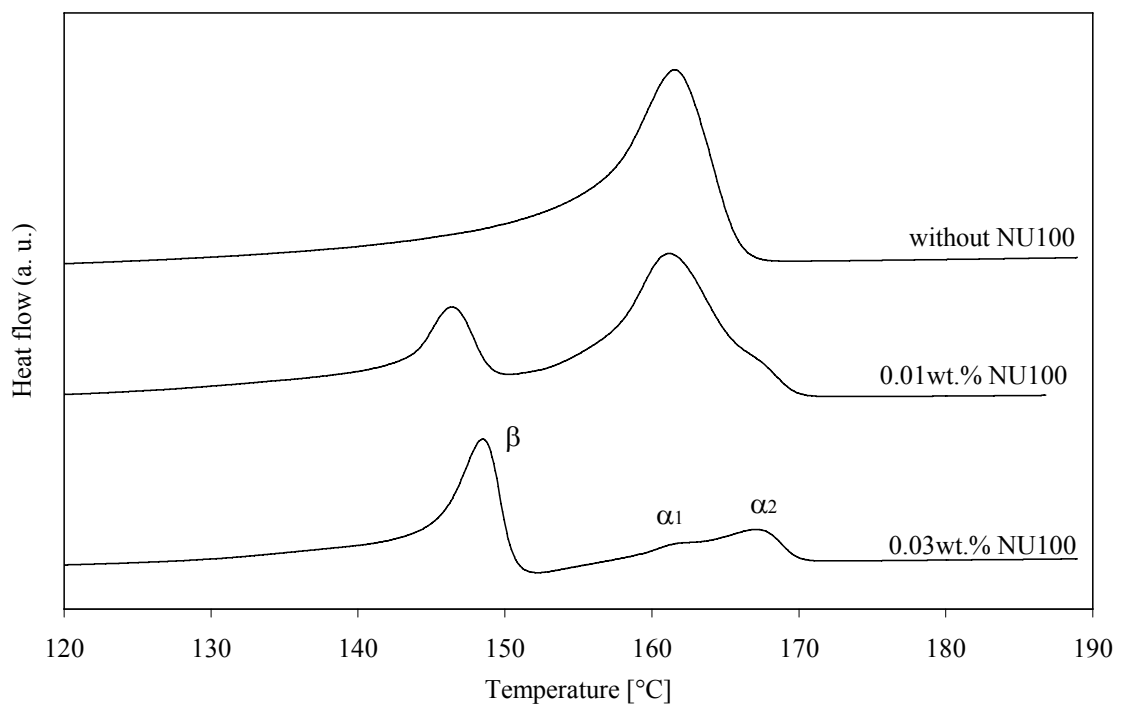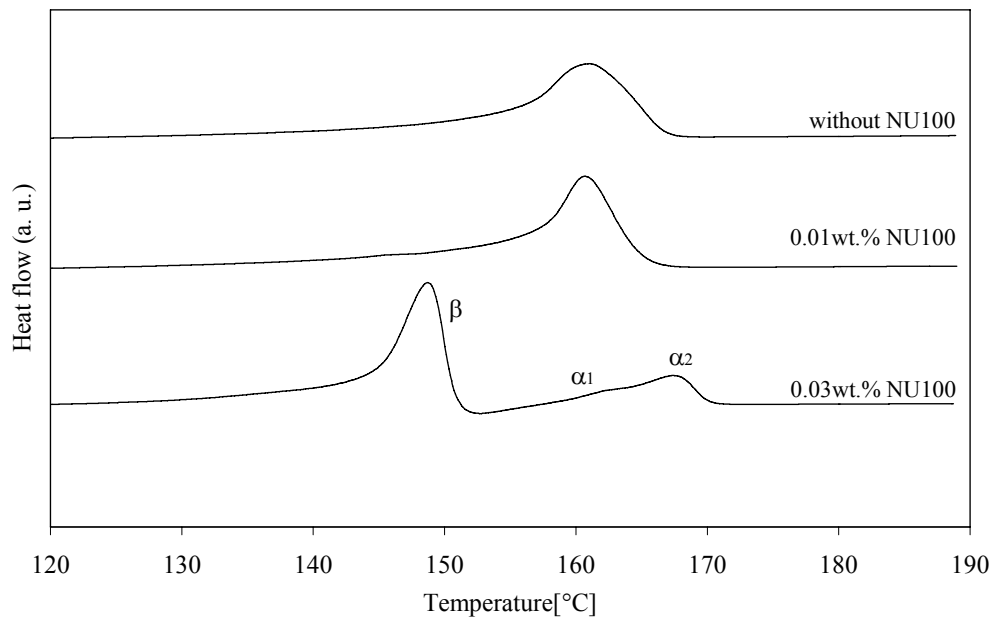

Figure 9.20 Melting thermograms of the samples with MFI 0.3 g/10 min with different content of NU 100 crystallized at cooling rate 10°C/min
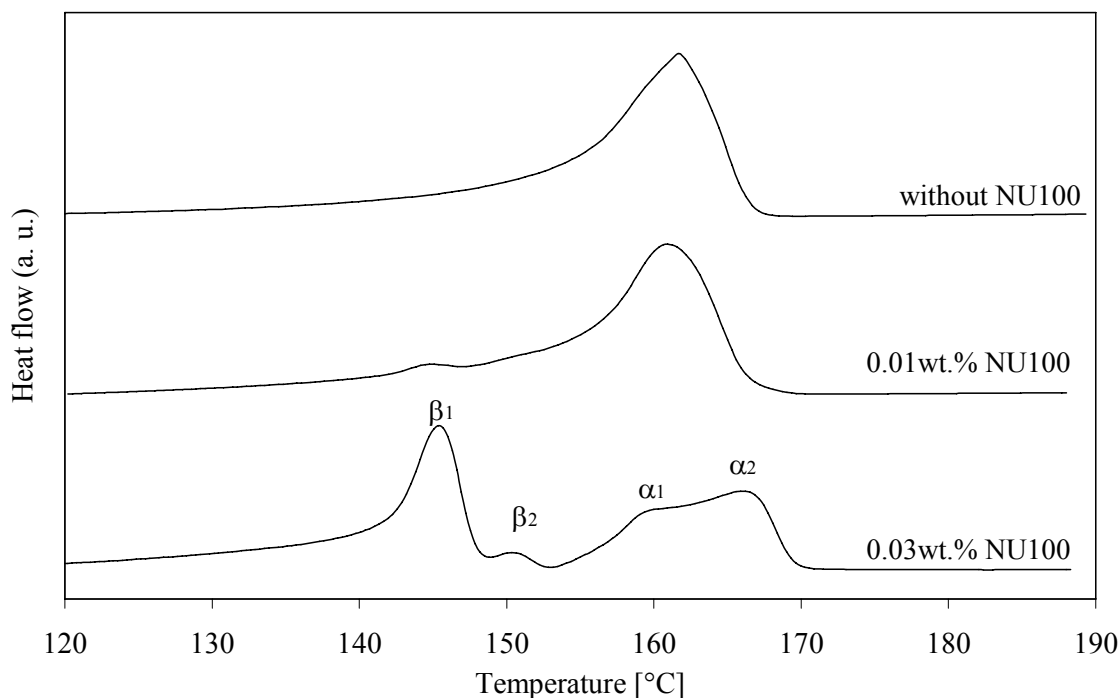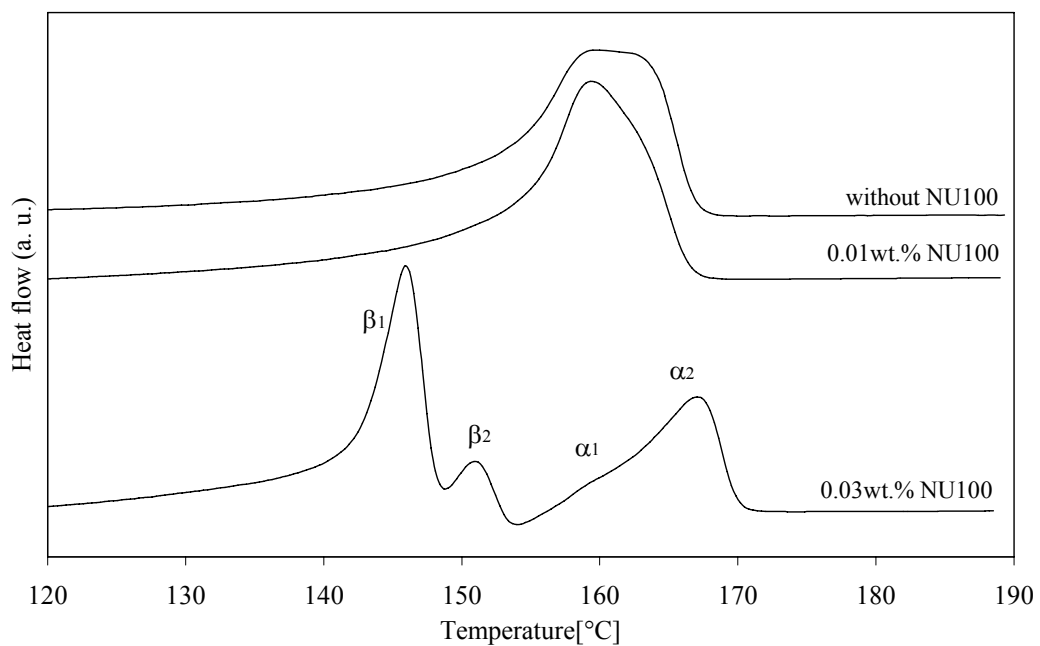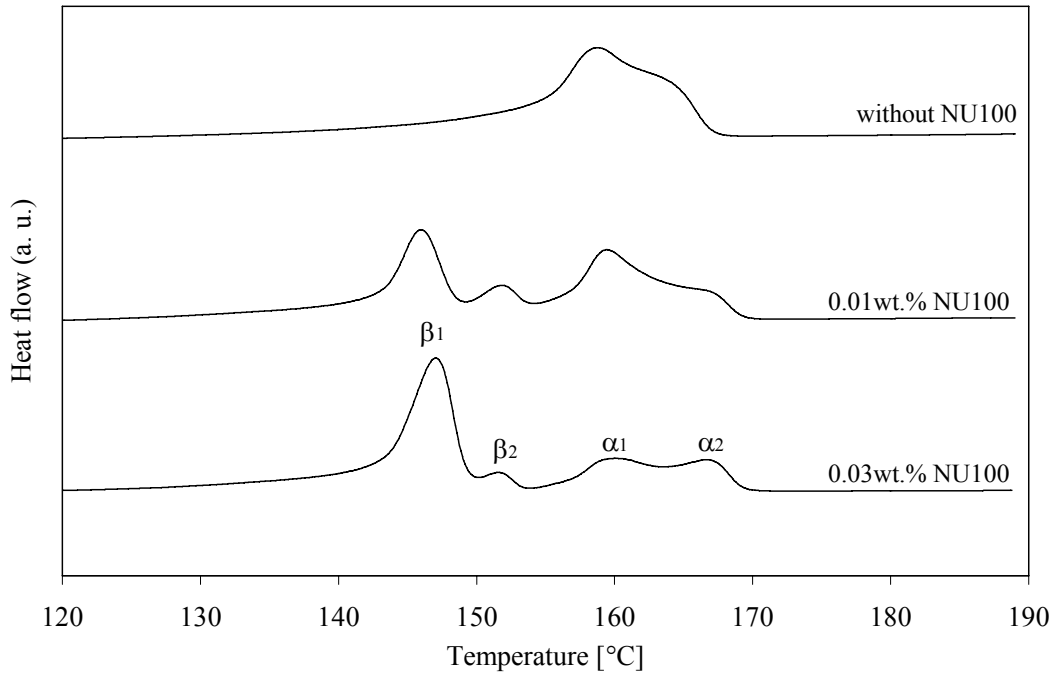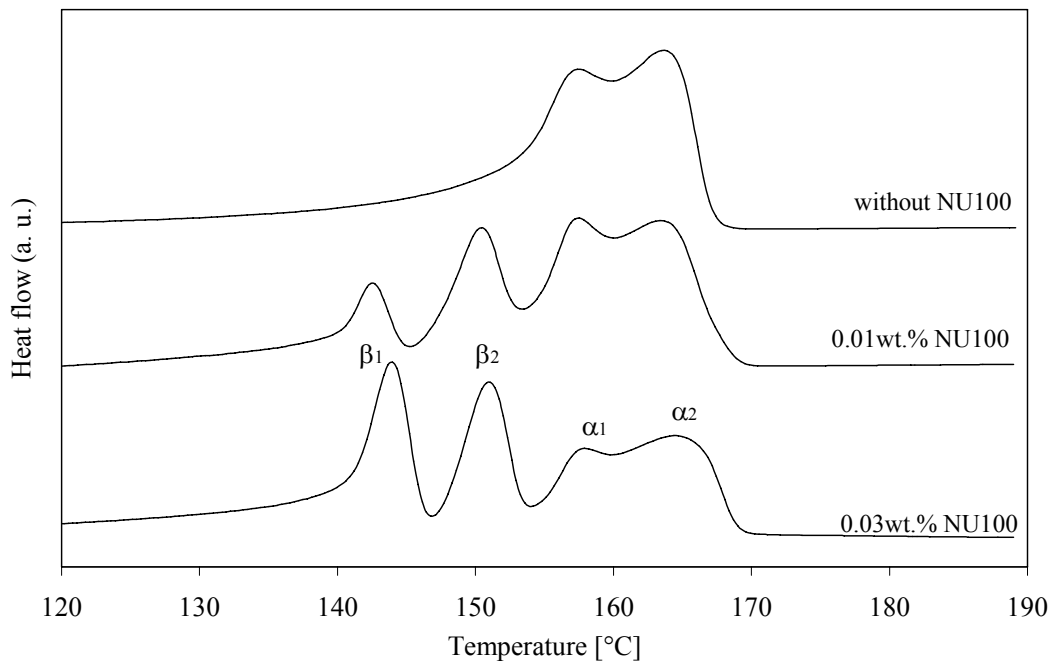
Figure 9.21 Melting thermograms of the samples with MFI 0.3 g/10 min with different content of NU 100 crystallized at cooling rate 50°C/min

9.2.2.2   MFI 1.0 g/10 min

Melting thermograms of the samples with MFI 1.0 g/10 min with 0, 0.01 and 0.03 wt. % NU 100 crystallized at cooling rate 10 or 50°C/min are shown in Figures 9.22 and 9.23. It can be seen that samples without NU 100 embody only a melting peak of the α-form. Moreover, no β-form melting peak can be observed even in the scan of low-nucleated sample. Only the addition of 0.03 wt. % NU 100 leads to the formation of β-form. The dominant β-melting peak is very well seen for both cases of cooling rates. In addition, double melting peaks of α-form were observed and as for the samples crystallized at cooling rate 50°C/min a double melting endotherm of β-form was detected as well as in the case of previous material (i.e. material with MFI 0.3 g/10 min). The recrystallization processes proceed which are indicated by the doubling of melting peaks and also by the significant undershoot of DSC baseline. From these figures it is evident that the addition of low amount of nucleator does not lead to the formation of β-form. Nevertheless, the addition of 0.03 wt. % NU 100 is sufficient.

Figure 9.22 Melting thermograms of the samples with MFI 1.0 g/10 min with different content of NU 100 at cooling rate 10°C/min

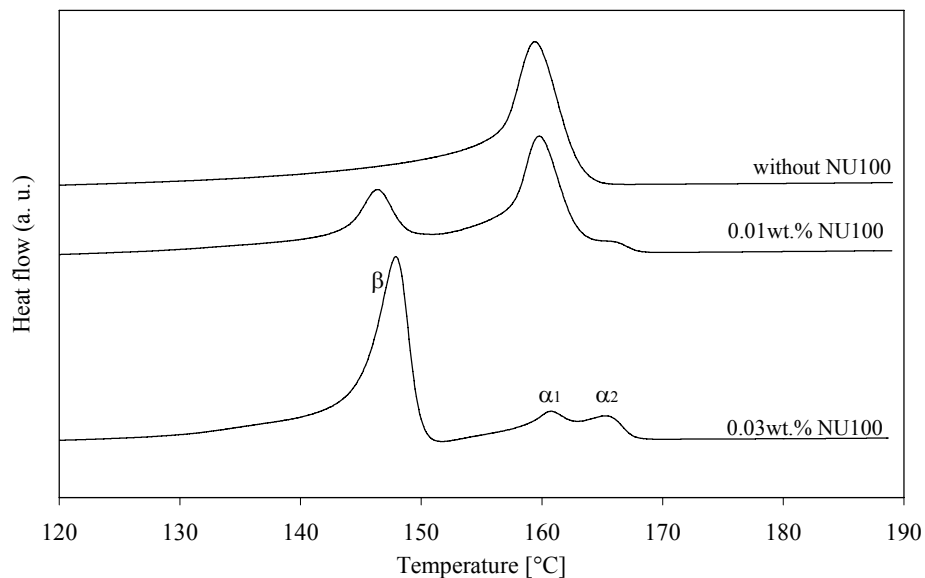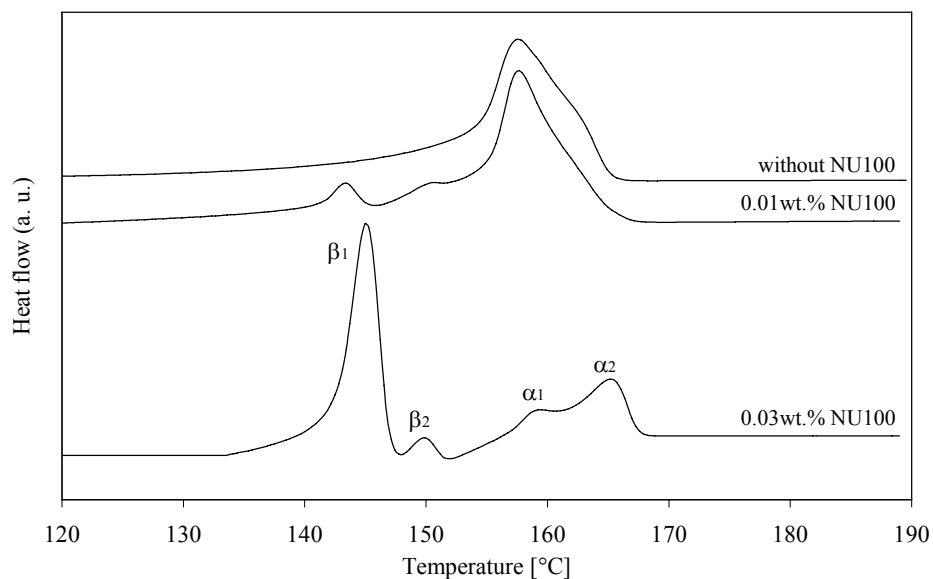
Figure 9.23 Melting thermograms of the samples with MFI 1.0 g/10 min with different content of NU 100 crystallized at cooling rate 50°C/min

9.2.2.3   MFI 8.0 g/10 min

Melting thermograms of the samples with MFI 8.0 g/10 min with 0, 0.01 and 0.03 wt. % NU 100 crystallized at cooling rate 10 or 50°C/min are shown in Figures 9.24 and 9.25. It can be seen that samples without NU 100 embody only a double melting peak of the α-form in both cases. Samples containing 0.01 wt. % NU 100 embody beside a melting peak of the α-form also a double melting peak of the β-form (see A Table 3). The same

situation is in the case of samples containing 0.03 wt. % NU 100. It is clear form the figures that the samples are more sensitive to recrystallization that the samples described before (i.e. samples with MFI 0.3 and 1.0 g/10 min). The doublings of melting peaks proceeds even in the case of neat material. The addition of 0.01 wt. % NU 100 seems to be sufficient to preparation of material with dominant β-form.
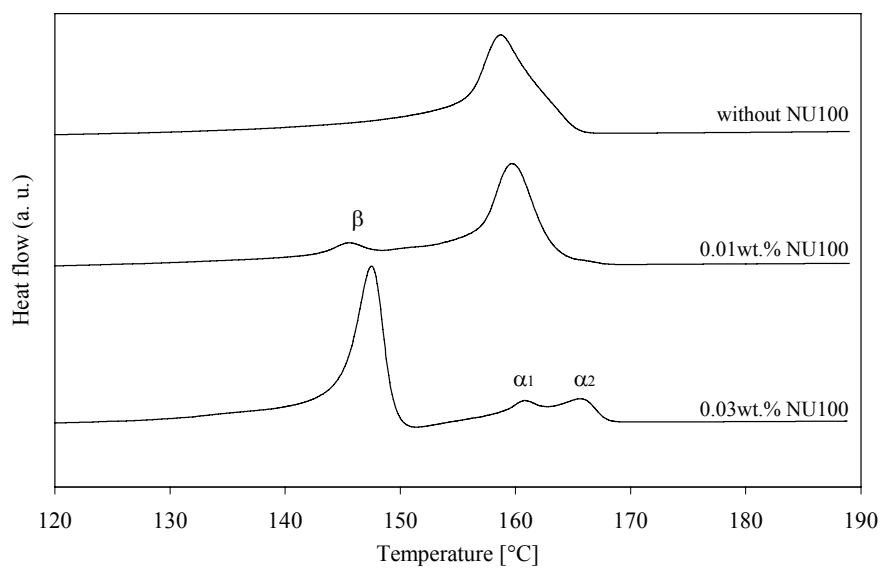

Figure 9.24 Melting thermograms of the samples with MFI 8.0 g/10 min with different content of NU 100 crystallized at cooling rate 10°C/min
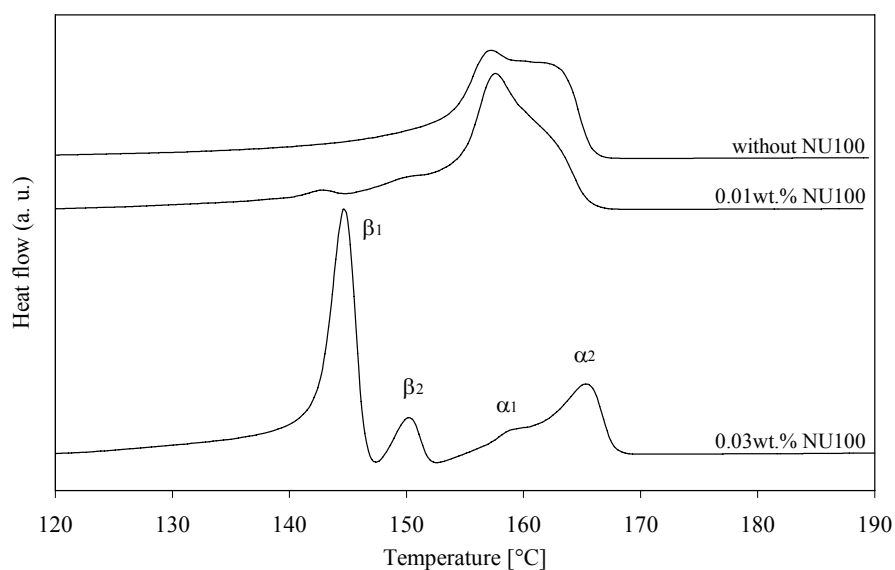

Figure 9.25 Melting thermograms of the samples with MFI 8.0 g/10 min with different content of NU 100 crystallized at cooling rate 50°C/min

9.2.2.4 MFI 12.0 g/10 min

Melting thermograms of the samples with MFI 12.0 g/10 min with 0, 0.01 and 0.03 wt. % NU 100 crystallized at cooling rate 10 or 50°C/min are shown in Figures 9.26 and 9.27. It can be seen that samples without NU 100 embody only a melting peak of the α-form; in case of sample cooled at rate 50°C/min the melting peak is doubled. Samples containing 0.01 wt. % NU 100 contain beside a double melting peak of the α-form also a small melting peak of the β-form. However, the material with 0.03 wt. % NU 100 shows dominant β-melting peak for both cooling rates. The doubled β-peak is observed only in the case of material crystallized at 50°C/min. For preparation of dominant β-form in the material the addition of 0.03 wt. % NU 100 is essential.
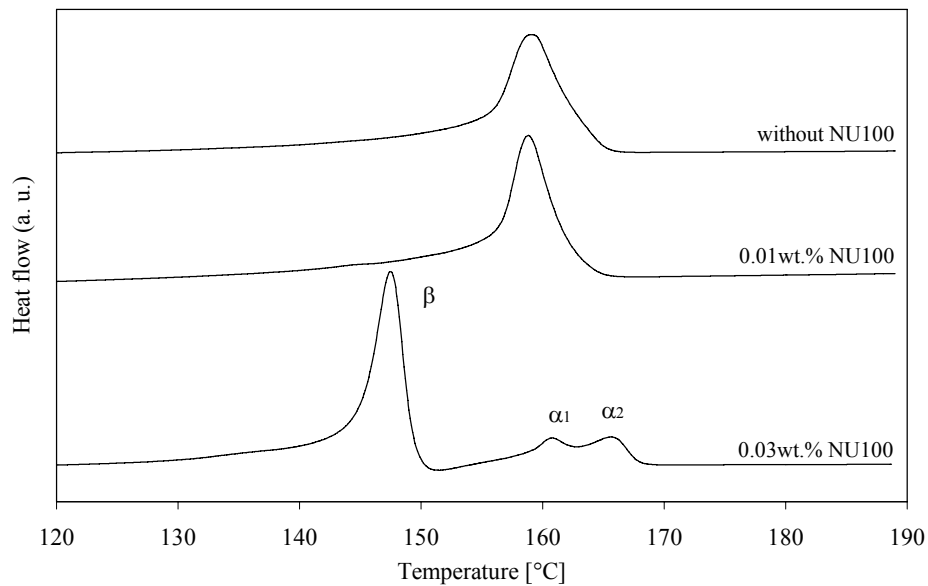

Figure 9.26 Melting thermograms of the samples with MFI 12.0 g/10 min with different content of NU 100 crystallized at cooling rate 10°C/min
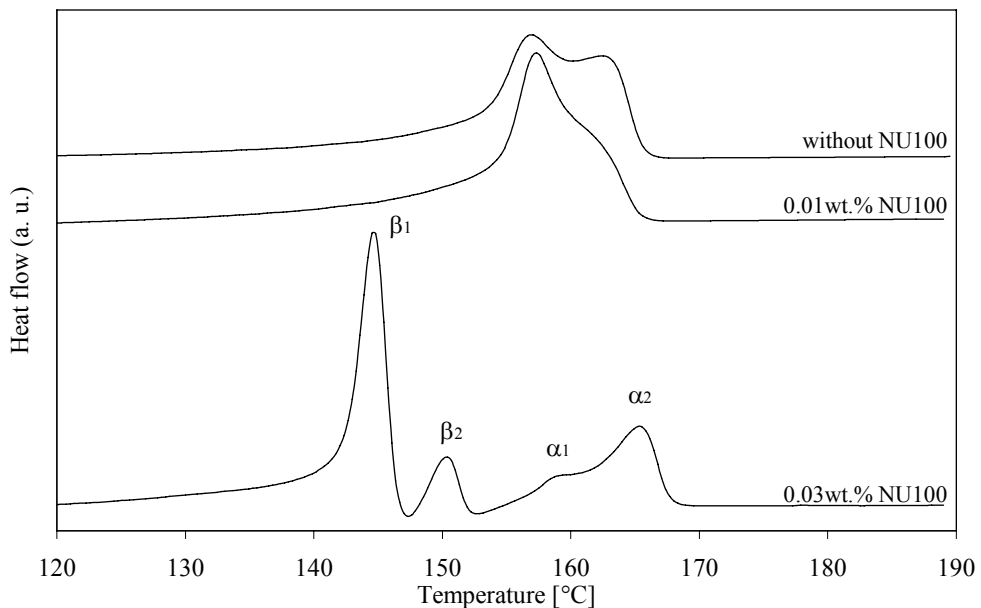

Figure 9.27 Melting thermograms of the samples with MFI 12.0 g/10 min with different content of NU 100 crystallized at cooling rate 50°C/min

9.2.2.5 MFI 20.0 g/10 min

Melting thermograms of the samples with MFI 20.0 g/10 min with 0, 0.01 and 0.03 wt. % NU 100 crystallized at cooling rate 10 or 50°C/min are shown in Figures 9.28 and 9.29. It can be seen that samples without NU 100 embody only a melting peak of the α-form as well as in the case of samples described earlier in the text. Samples containing 0.01 wt. % NU 100 contain beside a melting peak of the α-form also neglectable melting peak of the β-form. The dominant β-melting peak is evident in the scan of high-nucleated sample. Based upon the doubling of melting peaks, it can be said that the samples crystallized at high cooling rate are more sensitive to the recrystallization. As well as for previous discussed material the addition of 0.03 wt. % NU 100 leads to the predominant formation of β-form.
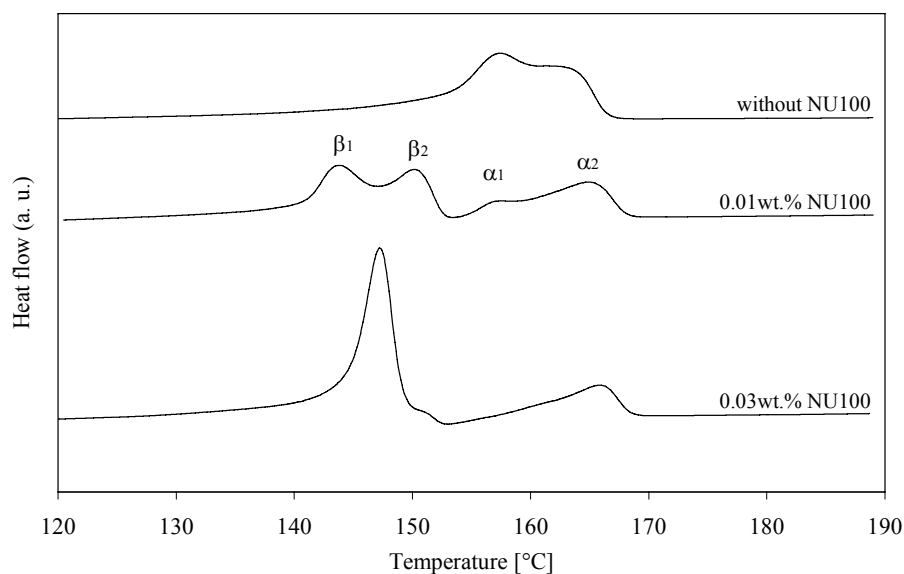
Figure 9.28 Melting thermograms of the samples with MFI 20.0 g/10 min with different content of NU 100 crystallized at cooling rate 10°C/min
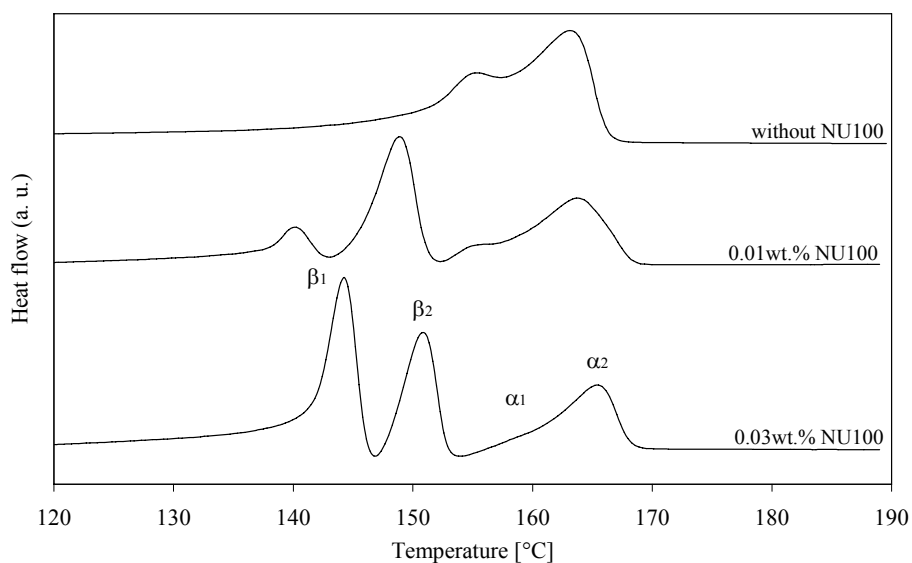
Figure 9.29 Melting thermograms of the samples with MFI 20.0 g/10 min with different content of NU 100 crystallized at cooling rate 50°C/min

9.2.2.6 MFI 27.0 g/10 min

Melting thermograms of the samples with MFI 27.0 g/10 min with 0, 0.01 and 0.03 wt. % NU 100 crystallized at cooling rate 10 or 50°C/min are shown in Figures 9.30 and 9.31. It can be seen that samples without NU 100 embody only a melting peak of the α-form, as well as each discussed material. However, the material with low amount of nucleator also seems to crystallize only into α-form; no β-melting peak is detected. The high-nucleated samples predominantly crystallize into β-form indicating dominant β-melting peak. The recrystallization processes are again more pronounced for samples crystallized at high cooling rate.
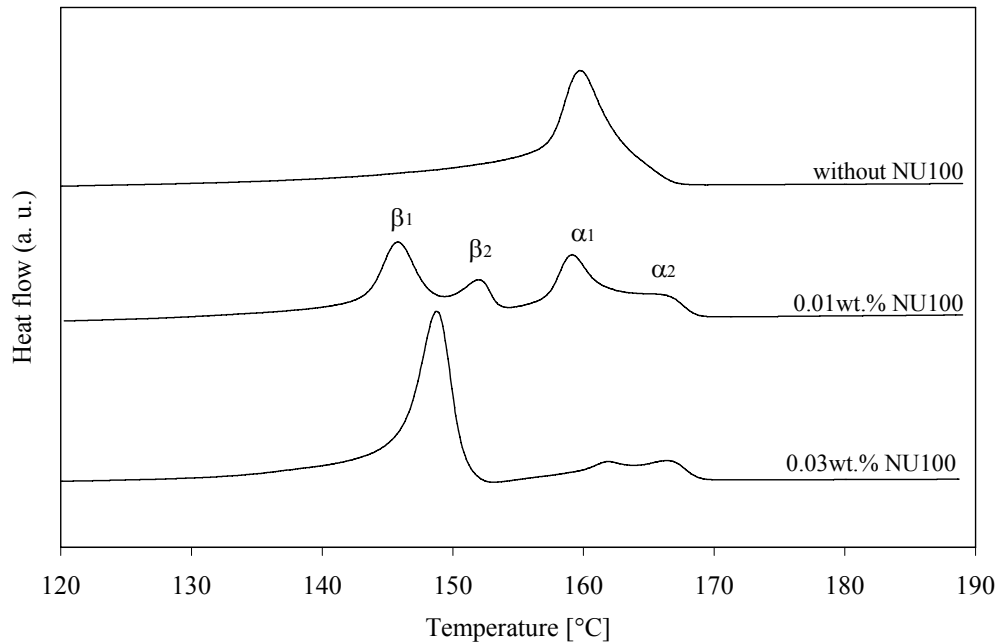

Figure 9.30 Melting thermograms of the samples with MFI 27.0 g/10 min with different content of NU 100 crystallized at cooling rate 10°C/min
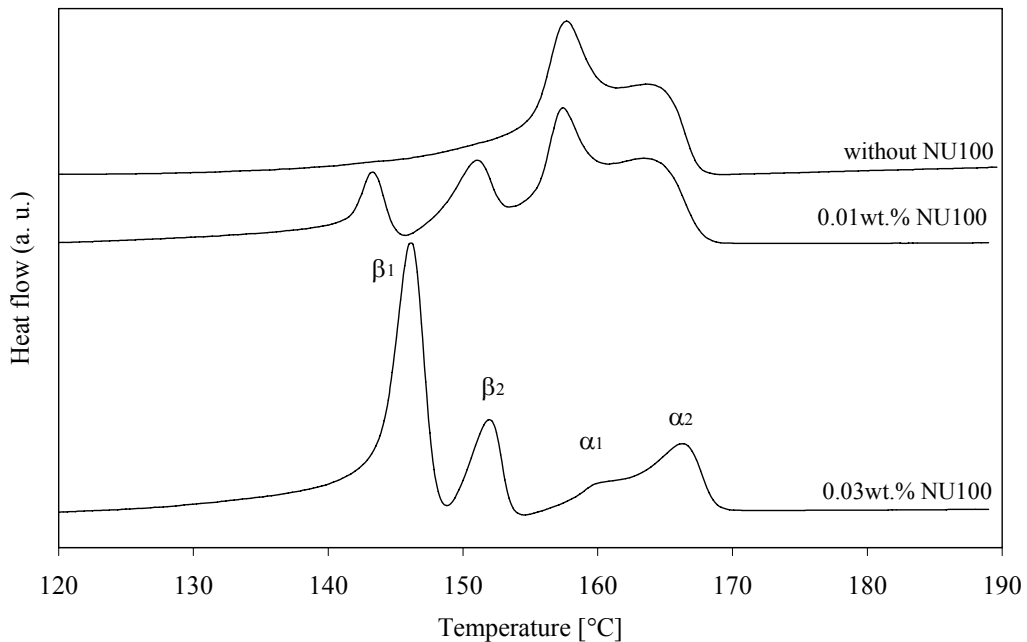

Figure 9.31 Melting thermograms of the samples with MFI 27.0 g/10 min with different content of NU 100 crystallized at cooling rate 50°C/min

9.2.2.7 *MFI 37.0 g/10 min*

Melting thermograms of the samples with MFI 37.0 g/10 min with 0, 0.01 and 0.03 wt. % NU 100 crystallized at cooling rate 10 or 50°C/min are shown in Figures 9.32 and 9.33. The samples without NU 100 embody only a double melting peak of the α-form in both cases. Samples containing 0.01 wt. % NU 100 embody beside a double melting peaks of the α-form also a significant double melting peaks of the β-form (see A Table 3). However, the β-melting peaks are more pronounced for samples containing high amount of nucleator. It should be noted, that the recrystallization processes in this material (i.e. material with MFI 37.0 g/10 min) are more significant, that in the samples with lower MFI. The extent of β-form in the sample with 0.01 wt. % NU 100 seems to be comparable with α-form. The dominant content of β-form is reached by addition of 0.03 wt. % NU 100.
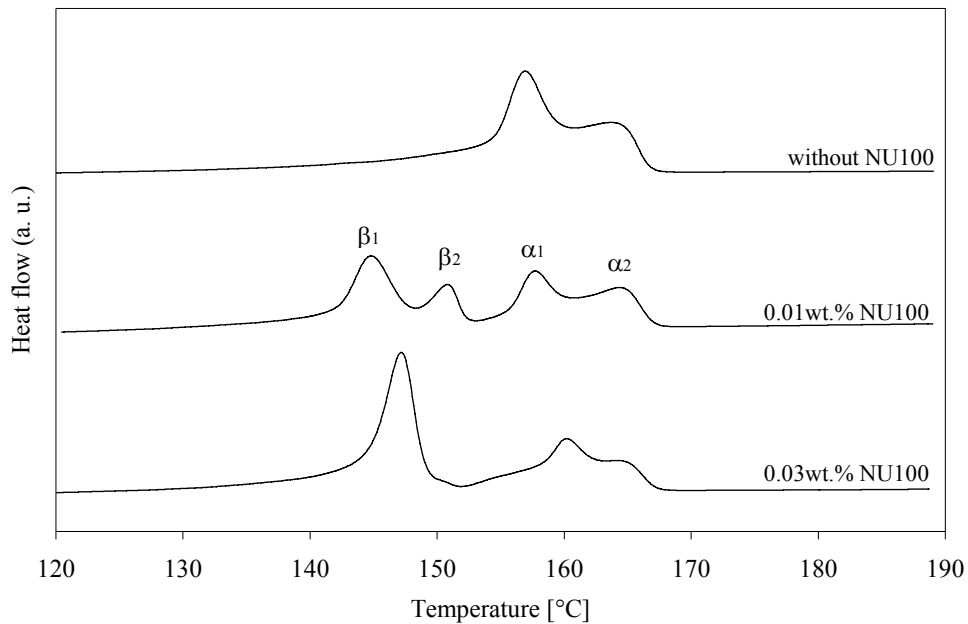

Figure 9.32 Melting thermograms of the samples with MFI 37.0 g/10 min with different content of NU 100 crystallized at cooling rate10°C/min
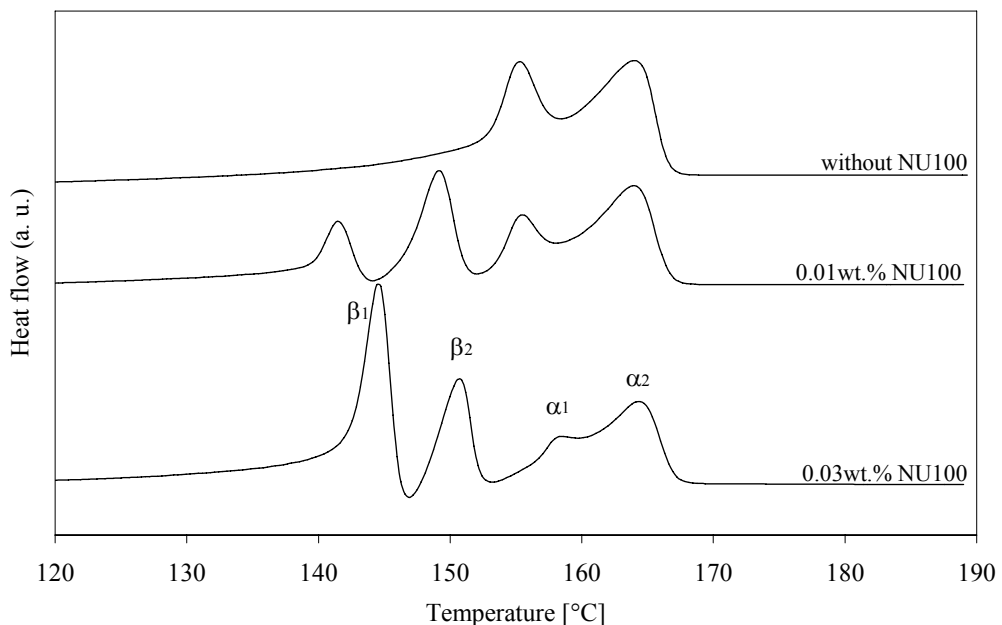

Figure 9.33 Melting thermograms of the samples with MFI 37.0 g/10 min with different content of NU 100 crystallized at cooling rate 50°C/min

9.2.2.8 MFI 125.0 g/10 min

Melting thermograms of the samples with MFI 125.0 g/10min with 0, 0.01 and 0.03 wt. % NU 100 crystallized at cooling rate 10 or 50°C/min are shown in Figures 9.34 and 9.35. As in all cases, samples without NU 100 embody only melting peaks of the α-form. Samples containing 0.01 wt. % NU 100 embody beside a double melting peaks of the α-form also significant double melting peaks of the β-form (see A Table 3). The addition of 0.03 wt. % leads to the dominant formation of β-form.
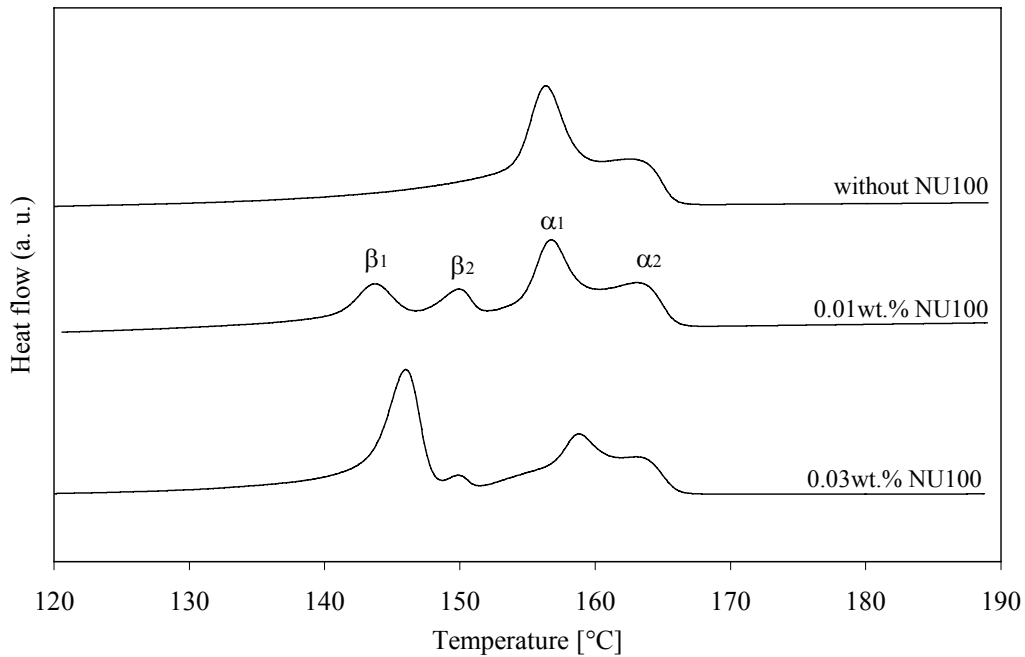

Figure 9.34 Melting thermograms of the samples with MFI 125.0 g/10 min with different content of NU 100 crystallized at cooling rate 10°C/min
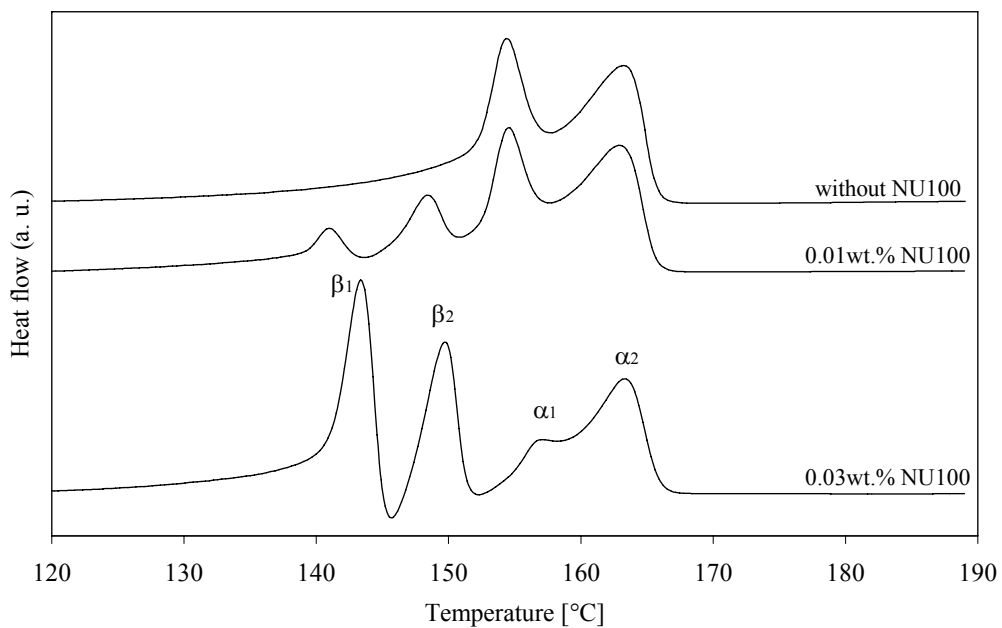

Figure 9.35 Melting thermograms of the samples with MFI 125.0 g/10 min with different content of NU 100 crystallized at cooling rate 50°C/min

9.2.2.9 MFI 450.0 g/10 min

Melting thermograms of the samples with MFI 450.0 g/10min with 0, 0.01 and 0.03 wt. % NU 100 crystallized at cooling rate 10 or 50°C/min are shown in Figures 9.36 and 9.37. The neat samples embody only double melting peaks of the α-form in both cases. Samples containing 0.01 wt. % NU 100 embody beside a double melting peaks of the α-form also significant double melting peaks of the β-form (see A Table 3). However, the dominant β-melting peak is observed in the scan of high-nucleated samples. The recrystallization proceeds in large extent, especially in the case of high cooling rate.
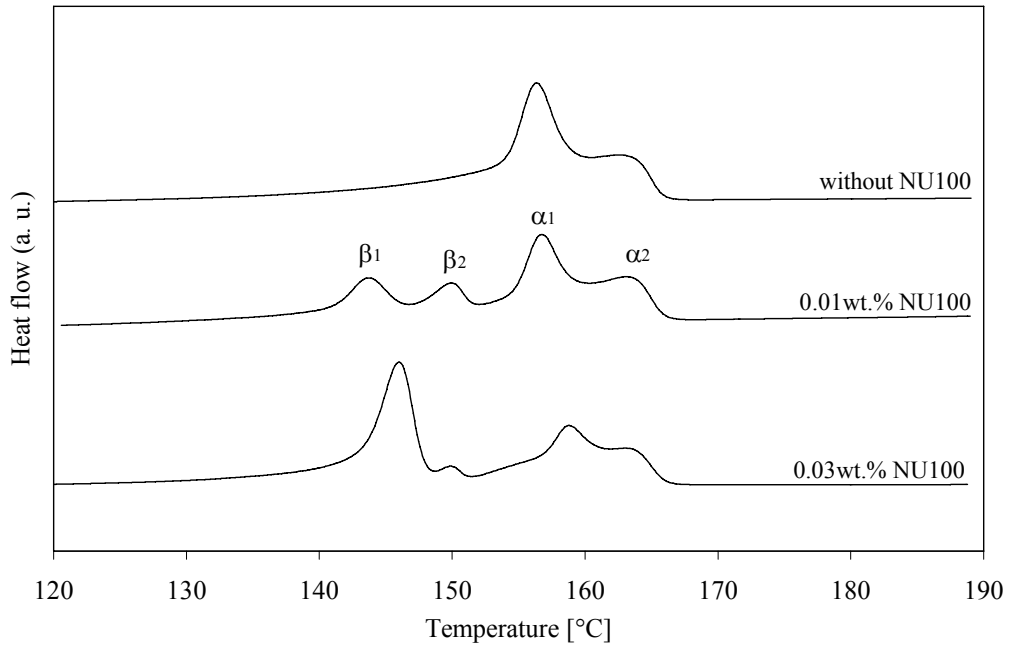

Figure 9.36 Melting thermograms of the samples with MFI 450.0 g/10 min with different content of NU 100 crystallized at cooling rate 10°C/min

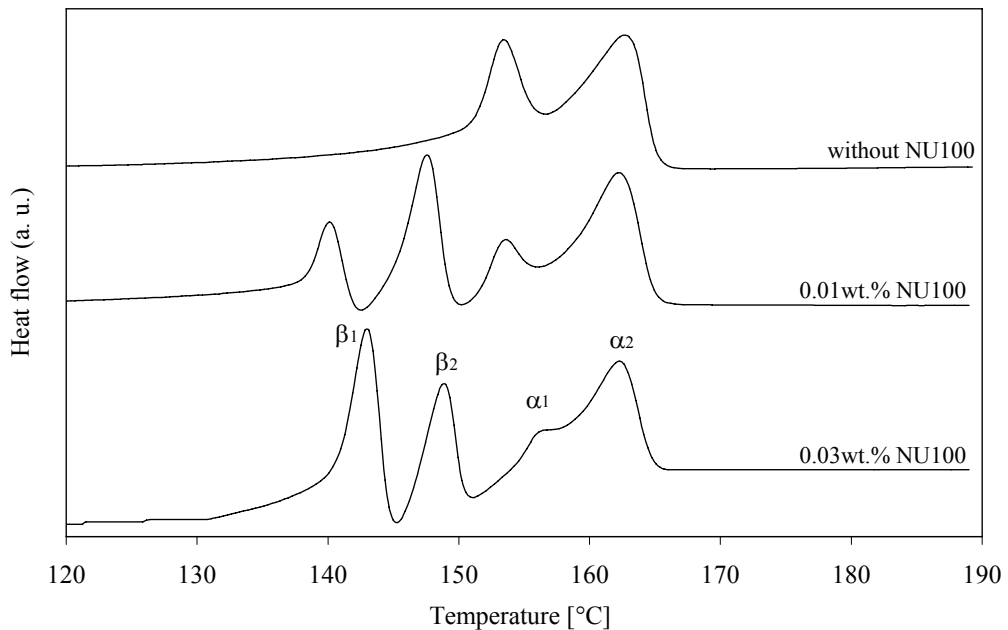Figure 9.37 Melting thermograms of the samples with MFI 450.0 g/10 min with different content of NU 100 crystallized at cooling rate 50°C/min

9.2.2.10 MFI 800.0 g/10 min

Melting thermograms of the samples with MFI 800.0 g/10 min with 0, 0.01 and 0.03 wt. % NU 100 crystallized at cooling rate 10 or 50°C/min are shown in Figures 9.38 and 9.39. The situation is very similar to the samples with MFI 450.0 g/10 min. The addition of 0.3 wt. % NU 100 leads to the dominant content of β-form as well. The recrystallization extent is comparable with that of the previous discussed material (with MFI 450 g/10 min).

Figure 9.38 Melting thermograms of the samples with MFI 800.0 g/10 min with different content of NU 100 crystallized at cooling rate 10°C/min

Figure 9.39 Melting thermograms of the samples with MFI 800.0 g/10 min with different content of NU 100 crystallized at cooling rate 50°C/min

9.2.2.11 MFI 1200.0 g/10 min

Melting thermograms of the samples with MFI 1200.0 g/10min with 0, 0.01 and 0.03 wt. % NU 100 crystallized at cooling rate 10 or 50°C/min are shown in Figures 9.40 and 9.41. The profile of heating scan is again very similar to that of previous discussed materials (i.e. with MFI 450.0 and 800.0 g/10 min).

Figure 9.40 Melting thermograms of the samples with MFI 1200.0 g/10 min with different content of NU 100 crystallized at cooling rate 10°C/min

Figure 9.41 Melting thermograms of the samples with MFI 1200.0 g/10 min with different content of NU 100 crystallized at cooling rate 50°C/min

10 ISOTHERMALLY CRYSTALLIZED SAMPLES

In order to study the effect of isothermal crystallization on efficiency of nucleator the samples were crystallized at 130°C using DSC. The obtained values of crystallization heat, crystallization halftime, melting temperature and melting heat are summarized in Appendices A Table 4.

As can be seen in the table, no significant trend between MFI and melting temperature or melting heat is evident.

Dependence of crystallization heat on MFI of the samples containing 0, 0.01 and 0.03 wt. % NU 100 is shown in Figure 10.1. Crystallization heat decreases with increasing amount of nucleating agent. It can be explained by the fact that the heterogeneous nuclei lead to the formation of high number of small spherulites. Therefore, the extent of amorphous phase between the spherulites increases. Accordingly, the crystallization heat decreases. The shape of the dependence is non-monotonic. Very interesting is the behaviour of the material with MFI 37.0 g/10 min, especially that with 0.01 wt. % NU 100. ΔH_c of all samples slightly increases with rising MFI until the value of MFI 37.0 is reached. Then, the jump decrease in the crystallization heat can be observed. Even in the case of material with 0.01 wt. % NU 100 the jump decrease begins at MFI 27.0 followed by next jump decrease of MFI 37.0. After that, the increase of the ΔH_c occurs. The next evolution of the dependence shape depends on the nucleator content.
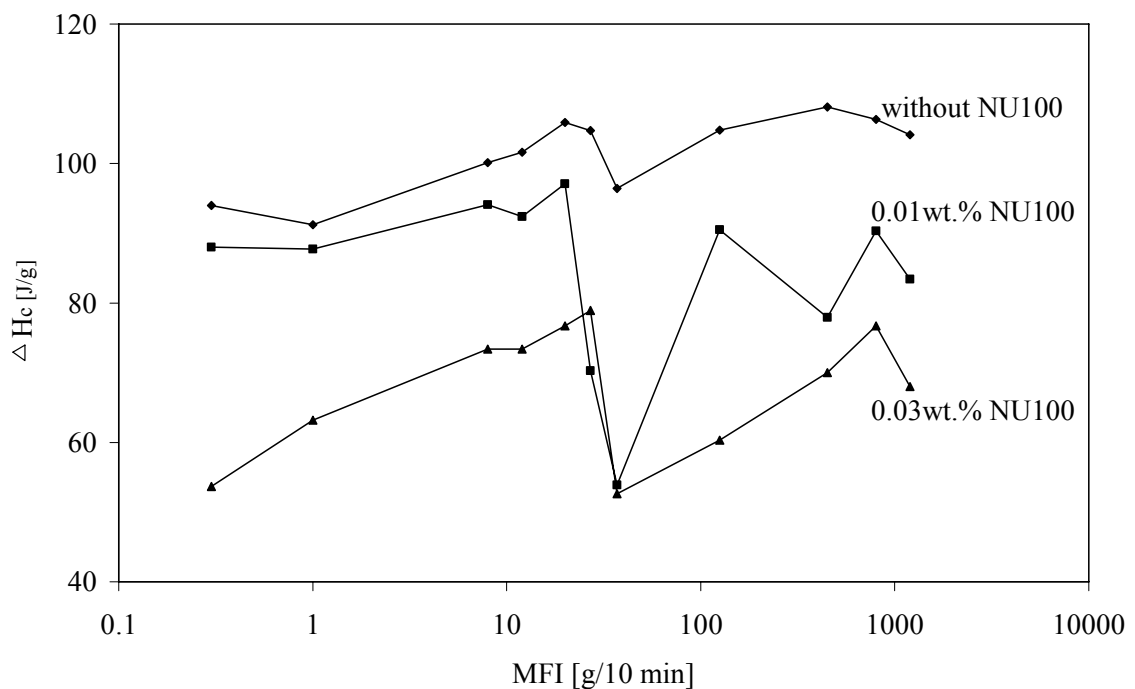
Figure 10.1 Dependence of crystallization heat on MFI of the samples containing 0, 0.01, 0.03 wt. % NU 100

Figure 10.2 shows dependence of crystallization halftime on MFI of the samples containing 0, 0.01 and 0.03 wt. % NU 100. It can be seen, that crystallization halftime is decreasing with rising amounts of the nucleating agent. It corresponds to the well known fact that the present of heterogeneous nuclei in the melt decreases the crystallization time [4, 5]. The shape of the dependence of the neat material is very complex. However, the addition of the nucleator leads to the narrowing of the curve.
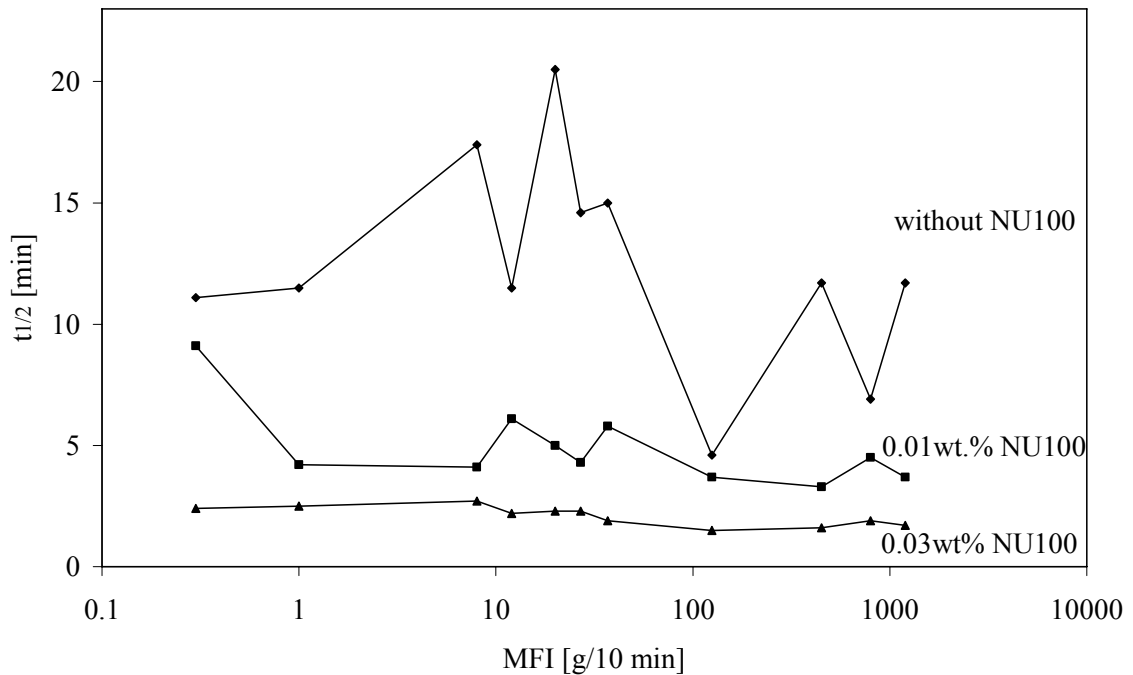

Figure 10.2 Dependence of crystallization halftime on MFI of the samples containing 0, 0.01 and 0.03 wt. % NU 100

10.1 Samples with Different MFI

Crystallization exotherms and melting thermograms of the samples with different MFI and with different amount of NU 100 isothermally crystallized at temperature 130°C are shown in Figures 10.3 - 10.8.

10.1.1 PP without NU 100

Figure 10.3 shows the heat flow evolution during the isothermal crystallization of neat iPP samples. It can be seen that crystallization process strongly depends on MFI. It is evident from the figure that no significant trend between MFI and crystallization time is observed. The shortest crystallization halftime (4.6 min) exhibits material HK060AE with MFI 125.0 g/10 min and the longest crystallization halftime (20.5 min) exhibits material HF136MO with MFI 20.0 g/10 min (see A Table 4). It should be noted, that some materials (materials with MFI 8.0, 12.0, 27.0 and 37.0 g/10 min) show doubled crystallization exotherms. It can be caused by different nucleation mechanism which can be indicated by the presence of the additives in the plastic (these additives are used by producer of the material and the information of them are not available).
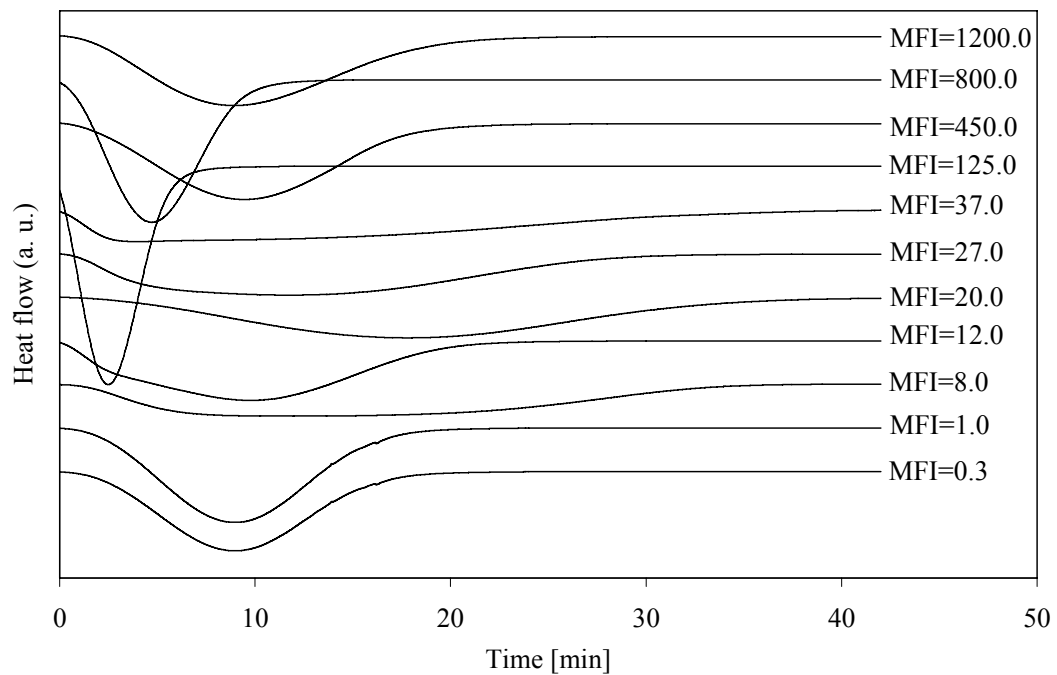
Figure 10.3 Crystallization exotherms of the pure iPP with different MFI

Melting thermograms of the samples with different MFI without NU 100 are shown in Figure 10.4. It is evident that only α-form originates in all cases. The melting temperature shifts to the lower values with increasing MFI. It is caused by formation of crystallites with more imperfections (molecule ends) in the material with high MFI.
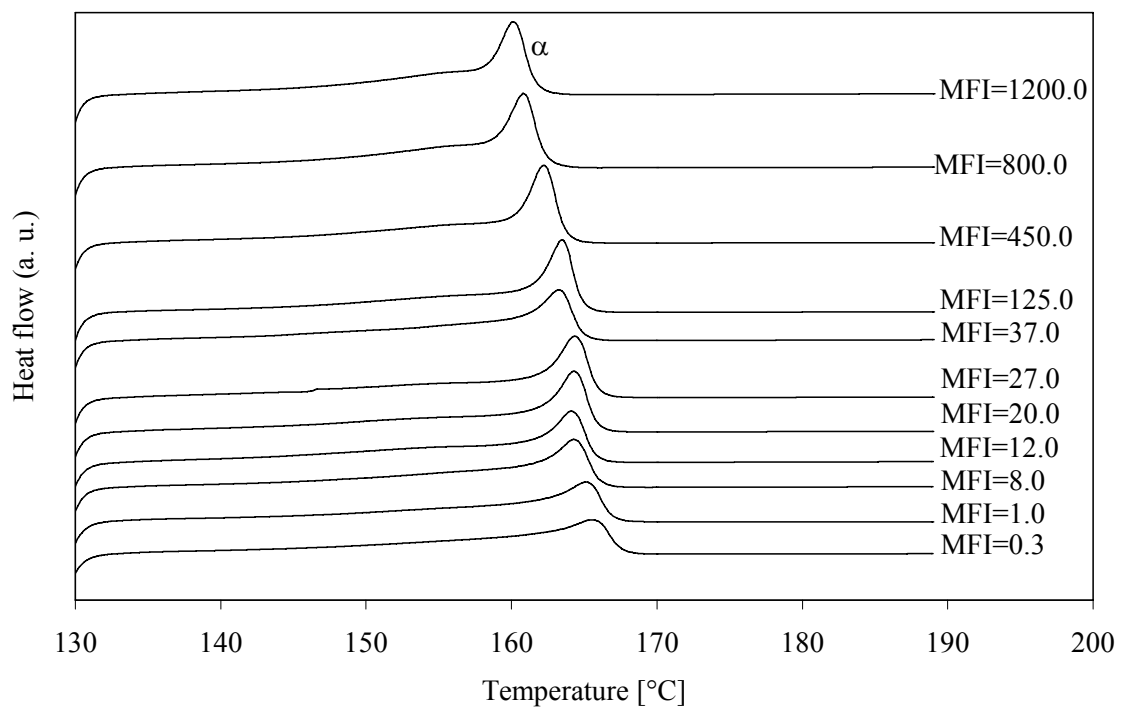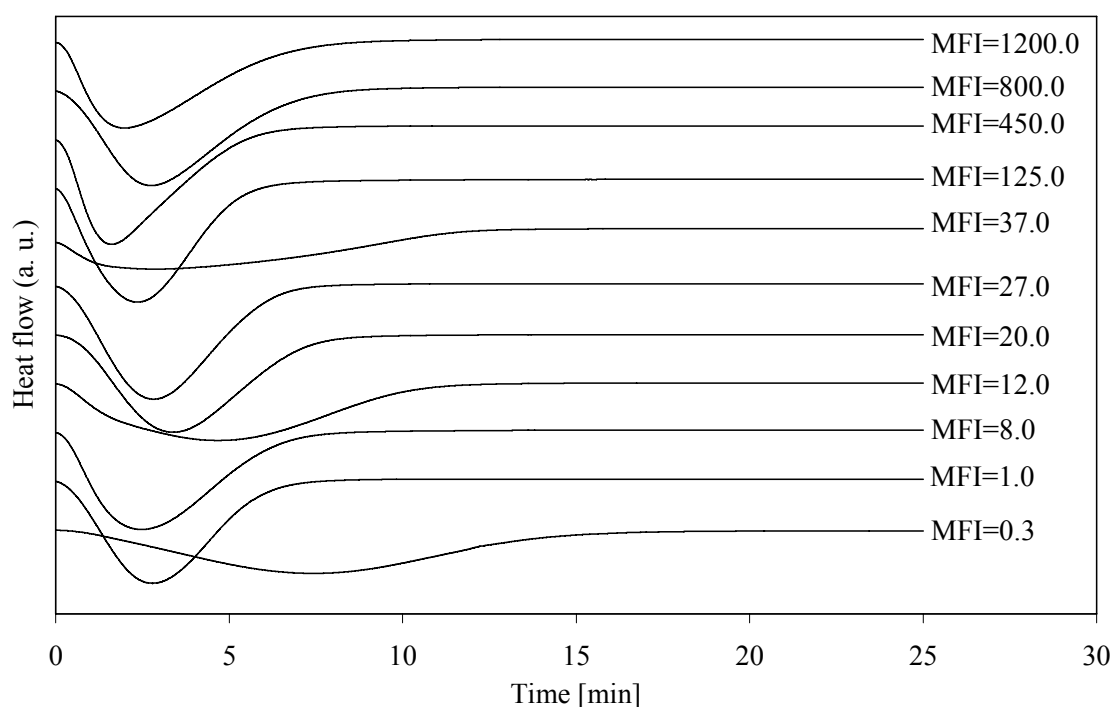
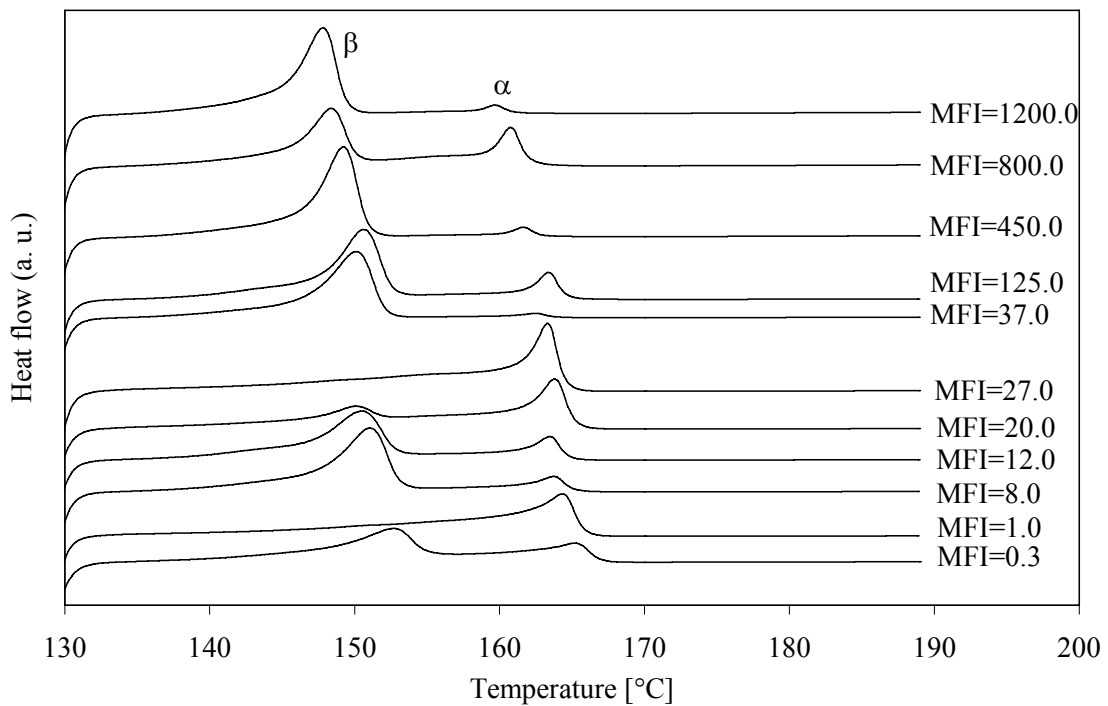

Figure 10.4 Melting thermograms of the samples with different MFI without NU 100

10.1.2 PP with 0.01 wt. % NU 100

Figure 10.5 shows the heat flow evolution during the isothermal crystallization of iPP samples with 0.01 wt. % NU 100. It can be seen that crystallization strongly depends on MFI. It is also evident that no significant trend between MFI and crystallization time is observed. The material HL504FB with MFI 450.0 g/10 min exhibits the shortest crystallization halftime (3.3 min) and material FB50 with MFI 0.3 g/10 min exhibits the longest crystallization halftime (9.1 min). Very interesting is the fact, that some crystallization exotherms (exotherms of materials with MFI 37.0, 450.0 and 1200.0 g/10 min) are asymmetric. Moreover, the material with MFI 12.0 shows doubled crystallization exotherm.

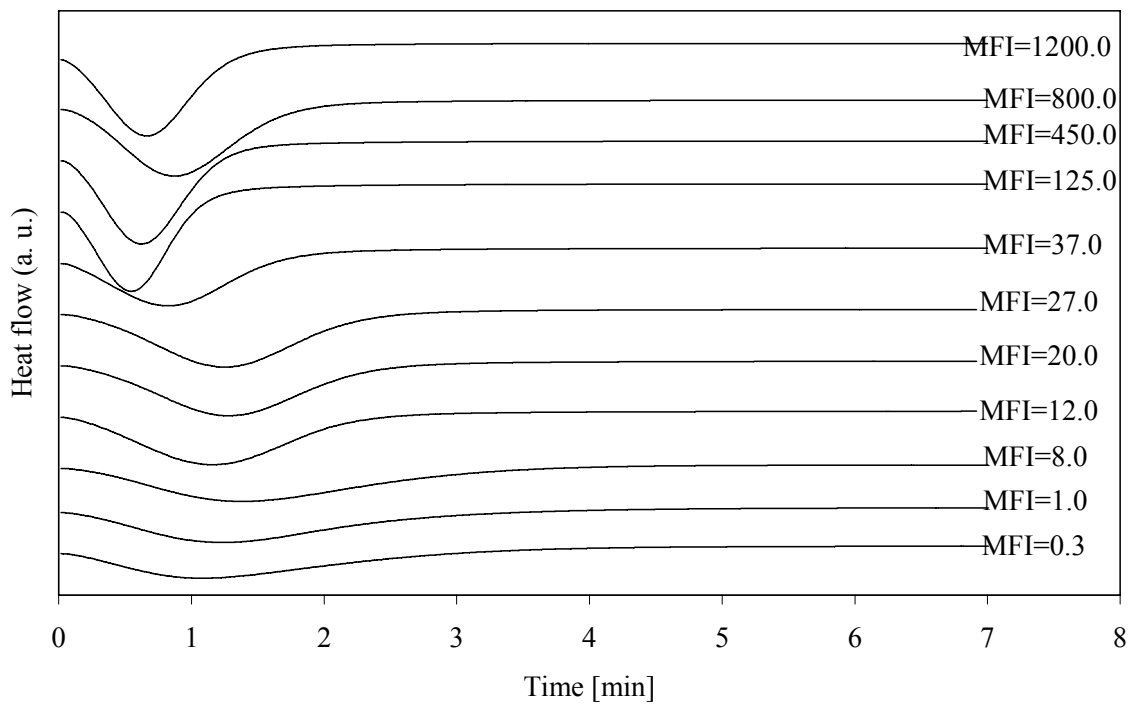Figure 10.5 Crystallization exotherms of the samples with 0.01 wt. % NU 100 with different MFI

Melting thermograms of the samples with different MFI with 0.01 wt. % NU 100 are shown in Figure 10.6. In most cases two endothermic melting peaks can be observed. They are ascribed to the melting of the α-form and β-form. In most cases, the β-peak is dominant indicating the majority content of β-form in the material. However, in the case of materials HB205TF with MFI 1.0 g/10 min, HF136MO with MFI 20.0 g/10 min and HG455FB with MFI 27.0 g/10 min dominating α-form was detected (see A Table 4). As for materials with MFI 1.0 and 27.0 g/10 min even only α-melting peak is observed. The heating scans of these materials are very similar to that of non-isothermally crystallized samples at cooling rate 10°C/min (compare Figures 10.6 and 9.16).

Figure 10.6 Melting thermograms of the samples with different MFI with 0.01 wt. % NU 100

10.1.3 PP with 0.03 wt. % NU100

Figure 10.7 shows the heat flow evolution during the isothermal crystallization of iPP samples with 0.03 wt. % NU 100. Contrary to samples without and with 0.01 wt. % NU 100 the highly-nucleated samples show symmetric single crystallization peaks. Moreover, the crystallization halftime is significantly shorter for the samples with high MFI (from MFI 37.0 g/10 min). The shortest crystallization halftime (1.5 min) exhibits material HK060AE with MFI 125.0 g/10 min and the longest crystallization halftime (2.7 min) exhibits material HD601CF with MFI 8.0 g/10 min.

Melting thermograms of the samples with different MFI with 0.03 wt. % NU 100 are shown in Figure 10.8. In all cases two endothermic peaks ascribed to the melting of α-form and β-form can be observed. The β-melting peak is more significant in all cases indicating the majority content of β-form in the material. It should be also mentioned, that the α-melting peak of materials with high MFI (450.0, 800.0 and 1200.0 g/10 min) is doubled.

Figure 10.7 Crystallization exotherms of the samples with 0.03 wt. % NU 100 with different MFI
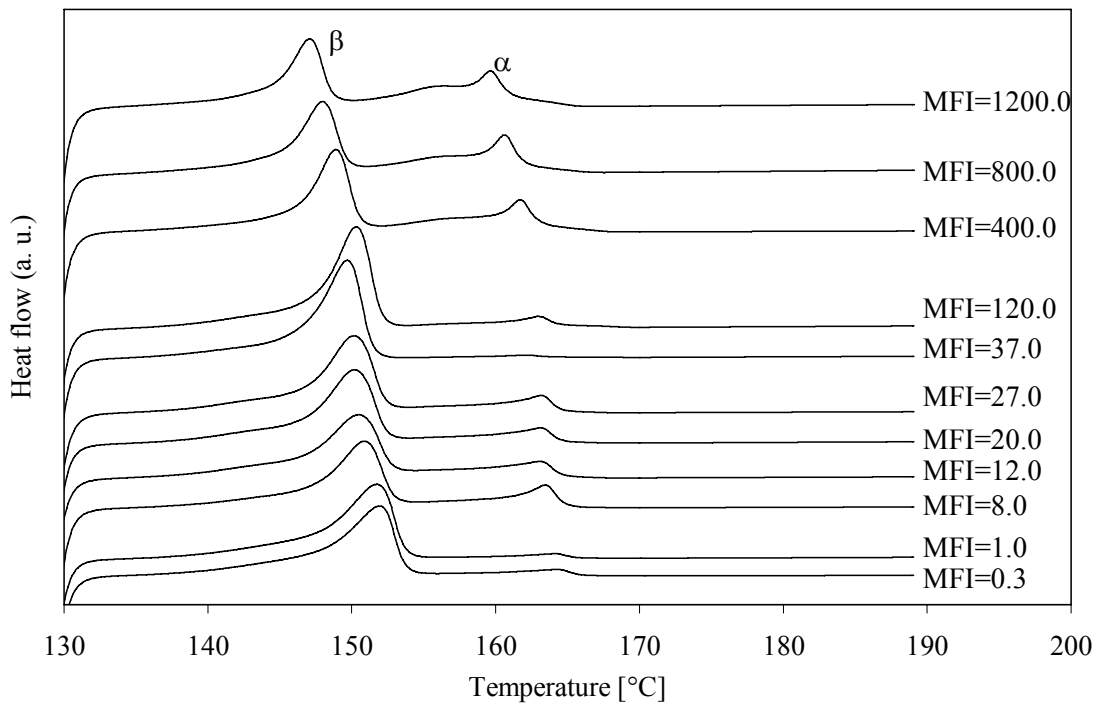
Figure 10.8 Melting thermograms of the samples with different MFI with 0.03 wt. % NU 100

10.2 Samples with Different Content of NU100

In order to compare the crystallization and melting behaviour in dependence of nucleator content in the same material the crystallization exotherms and heating scans of each material are displayed in Figures 10.9 - 10.29. It can be seen that the addition of a nucleating agent causes a sharping and narrowing of the exothermic peak and a shortening of the crystallization time. This fact corresponds with crystallization theory. Generally, it can be seen that samples without NU 100 embody only a melting peak of the α-form. Samples containing 0.01 wt. % NU 100 embody beside a melting peak of the α-form also a melting peak of the β-form. The important founding is that in most cases β-form is predominant, except samples with MFI 1.0, 20.0 and 27.0 g/10 min where mainly α-form is created. The samples containing 0.03 wt. % NU 100 show predominant β-melting peak in all cases of MFI.

10.2.1 MFI 0.3 g/10 min

Figure 10.9 shows crystallization exotherms of the samples with MFI 0.3 g/10 min with different content of NU 100. Only the slight decrease of crystallization time of sample with low amount of nucleator is observed compared to the neat material. However, the high-nucleated material shows very short and narrow endotherm. Melting thermograms of the samples with MFI 0.3 g/10 min with different content of NU 100 are shown in Figure 10.10.
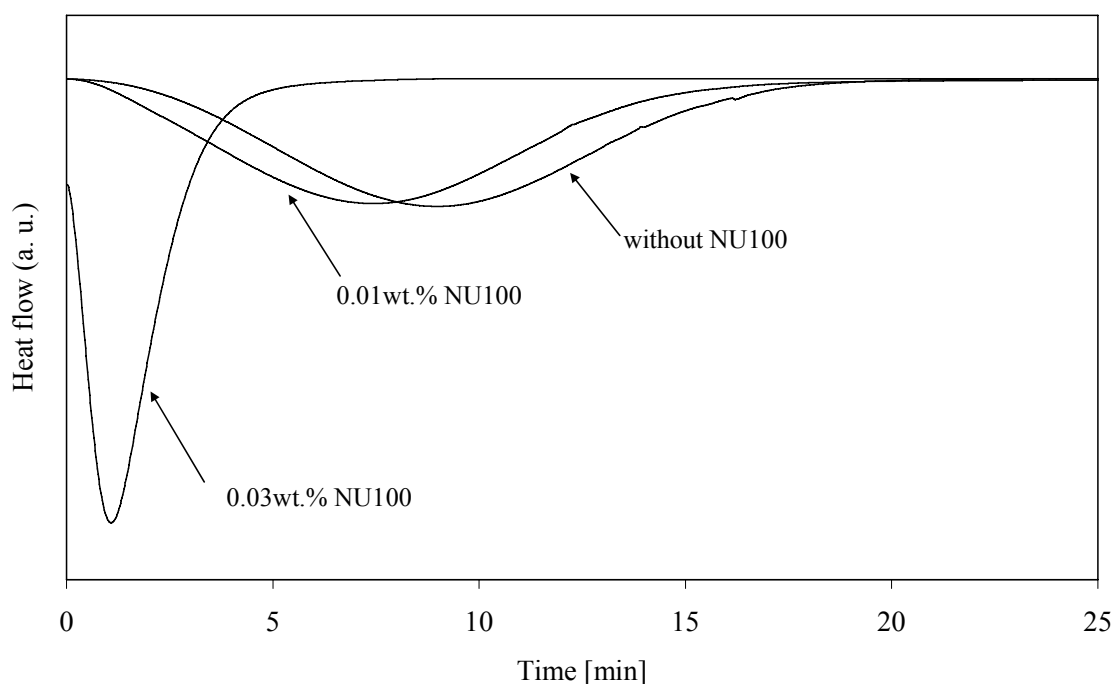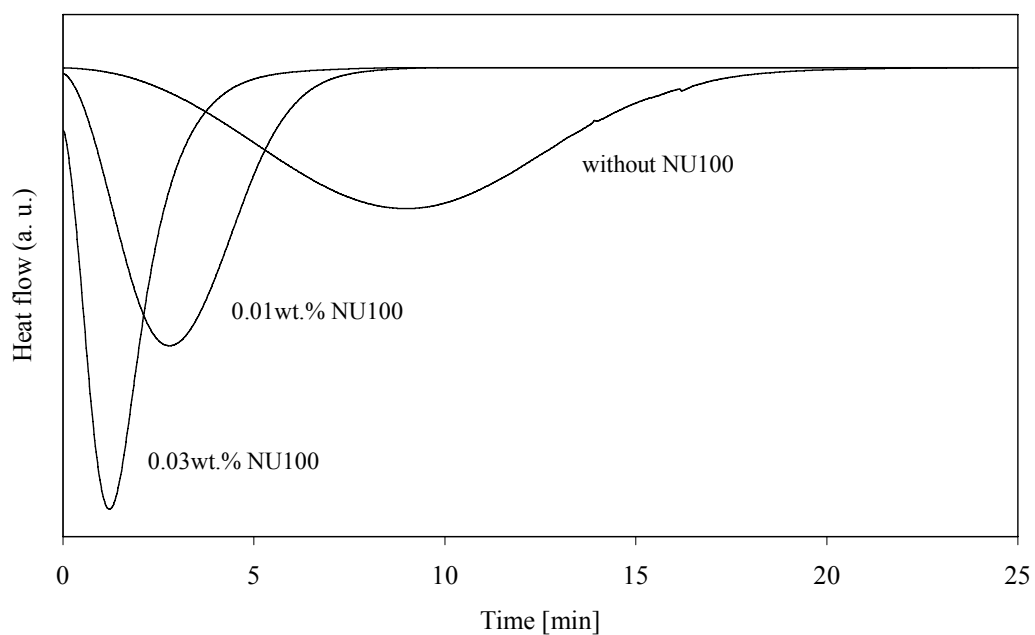

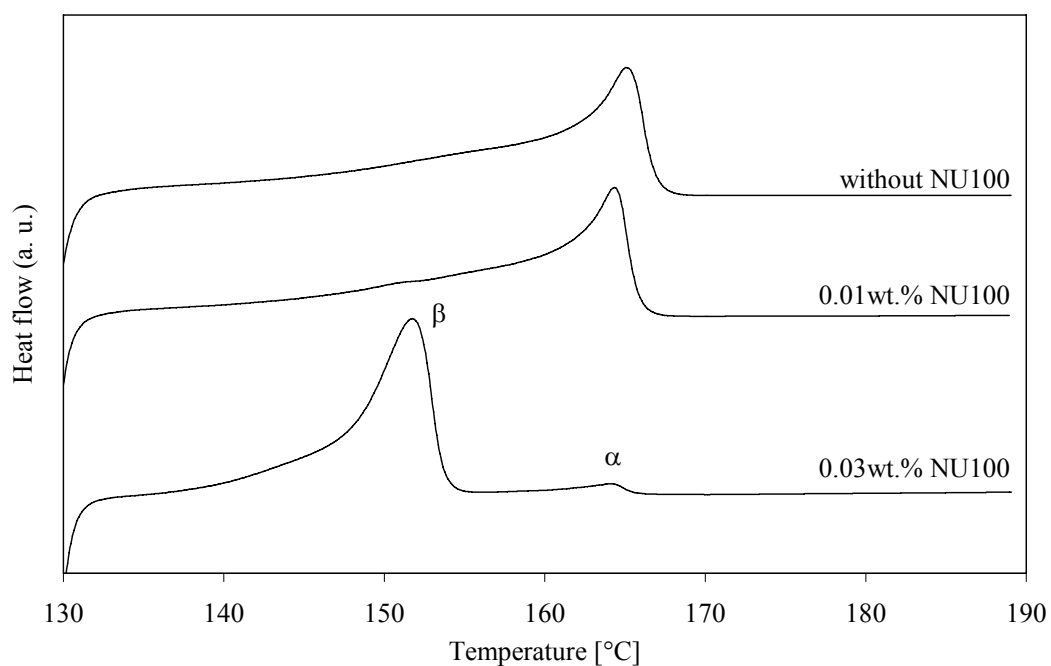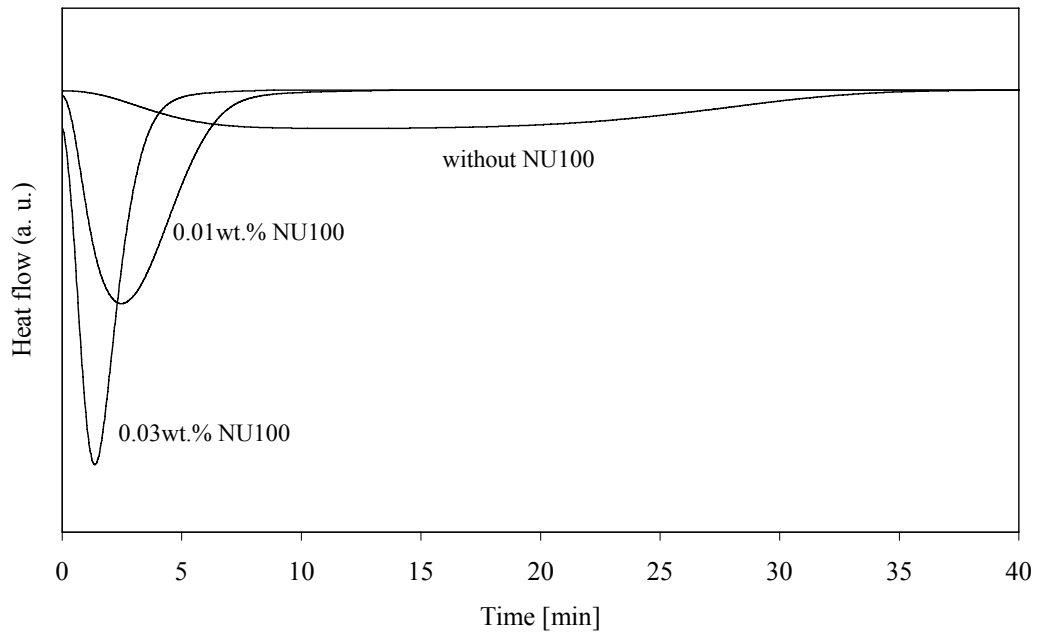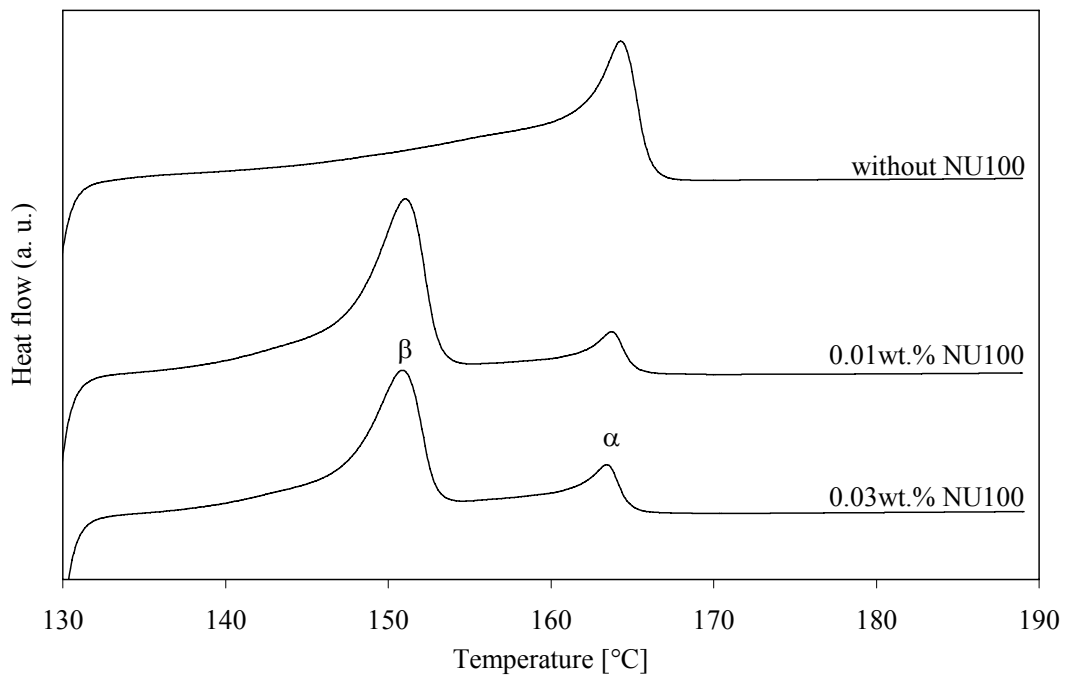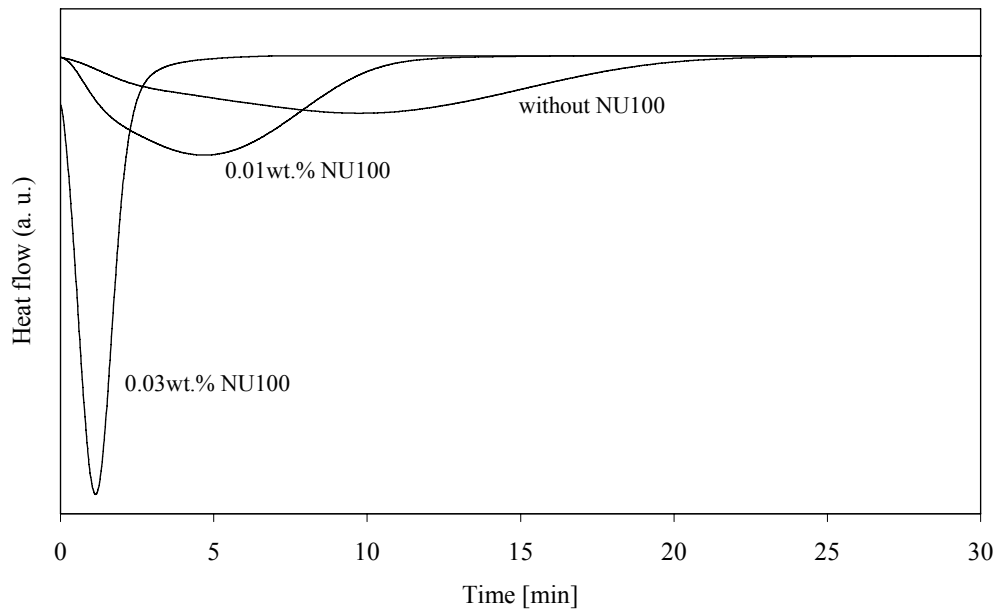Figure 10.9 Crystallization exotherms of the samples with MFI 0.3 g/10 min with different content of NU 100
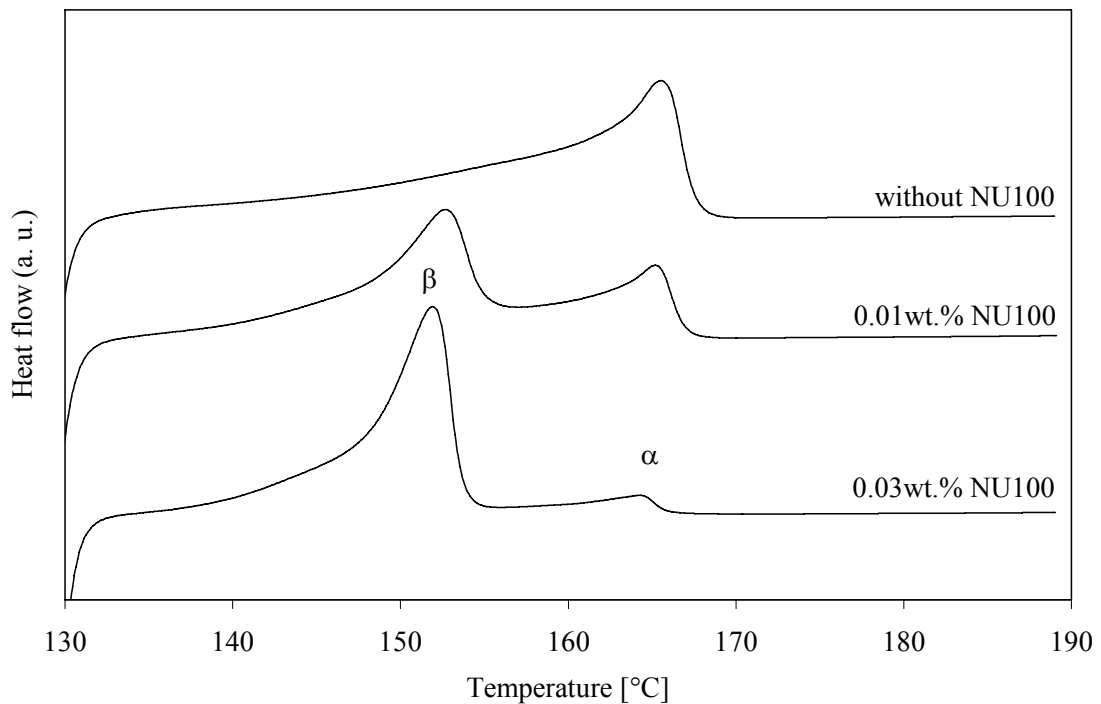
Figure 10.10 Melting thermograms of the samples with MFI 0.3 g/10 min with different content of NU 100

10.2.2 MFI 1.0 g/10 min

Figure 10.11 shows crystallization exotherms of the samples with MFI 1.0 g/10 min with different content of NU 100. Contrary to the previous material (i.e. material with MFI 0.3 g/10 min) the addition of 0.01 wt. % NU 100 causes significant change of crystallization peak; the peak is shorter and narrower. Further addition of nucleator leads to the additional shortening and narrowing of the peak. Melting thermograms of the samples with MFI 1.0 g/10 min with different content of NU 100 are shown in Figure 10.12.

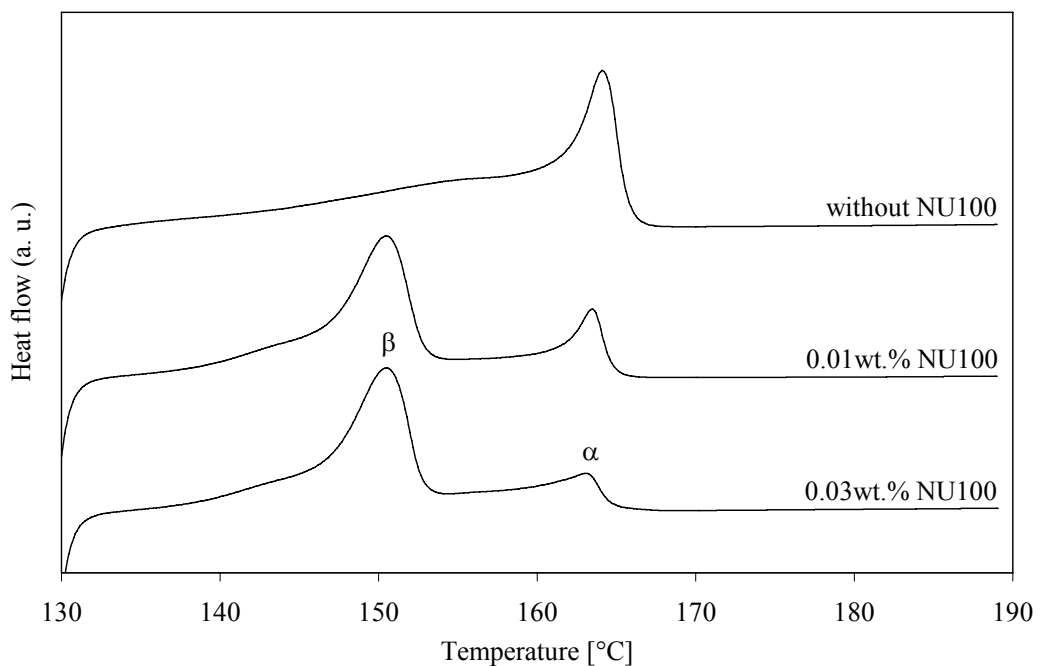Figure 10.11 Crystallization exotherms of the samples with MFI 1.0 g/10 min with different content of NU 100

Figure 10.12 Melting thermograms of the samples with MFI 1.0 g/10 min with different content of NU 100

10.2.3 MFI 8.0 g/10 min

Figure 10.13 shows crystallization exotherms of the samples with MFI 8.0 g/10 min with different content of NU 100. The exotherms of neat and low-nucleated samples are asymmetric while the exotherm of high-nucleated sample is symmetric. The difference in shape of each peak is very significant. Melting thermograms of the samples with MFI 8.0 g/10 min with different content of NU 100 are shown in Figure 10.14.
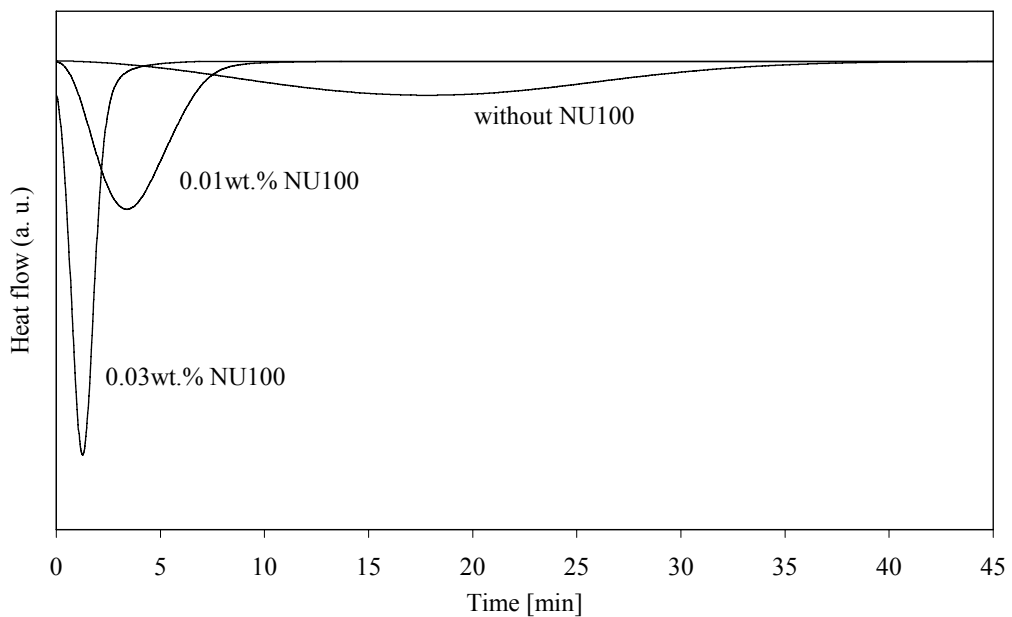

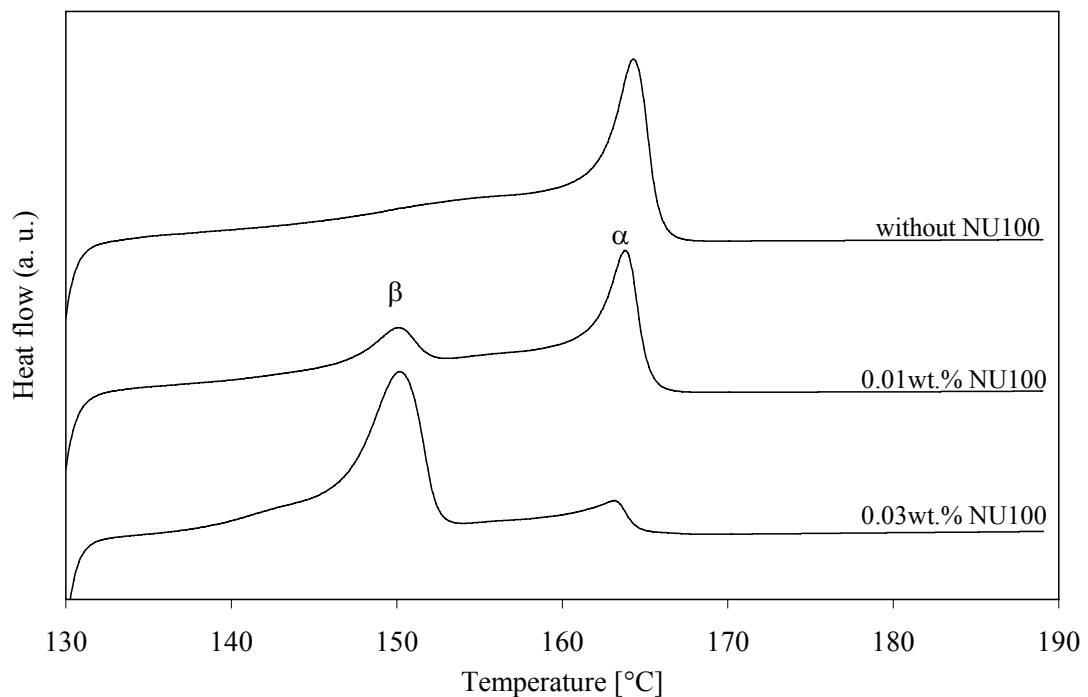Figure 10.13 Crystallization exotherms of the samples with MFI 8.0 g/10 min with different content of NU 100

Figure 10.14 Melting thermograms of the samples with MFI 8.0 g/10 min with different content of NU 100

10.2.4 MFI 12.0 g/10 min

Figure 10.15 shows crystallization exotherms of the samples with MFI 12.0 g/10 min with different content of NU 100. As well as for the previous discussed material (i.e. material with MFI 8.0 g/10 min) the crystallization peaks of neat and low-nucleated samples are asymmetric. Moreover, they are doubled. The high-nucleated sample shows symmetric exotherm. Melting thermograms of the samples with MFI 12.0 g/10 min with different content of NU 100 are shown in Figure 10.16.
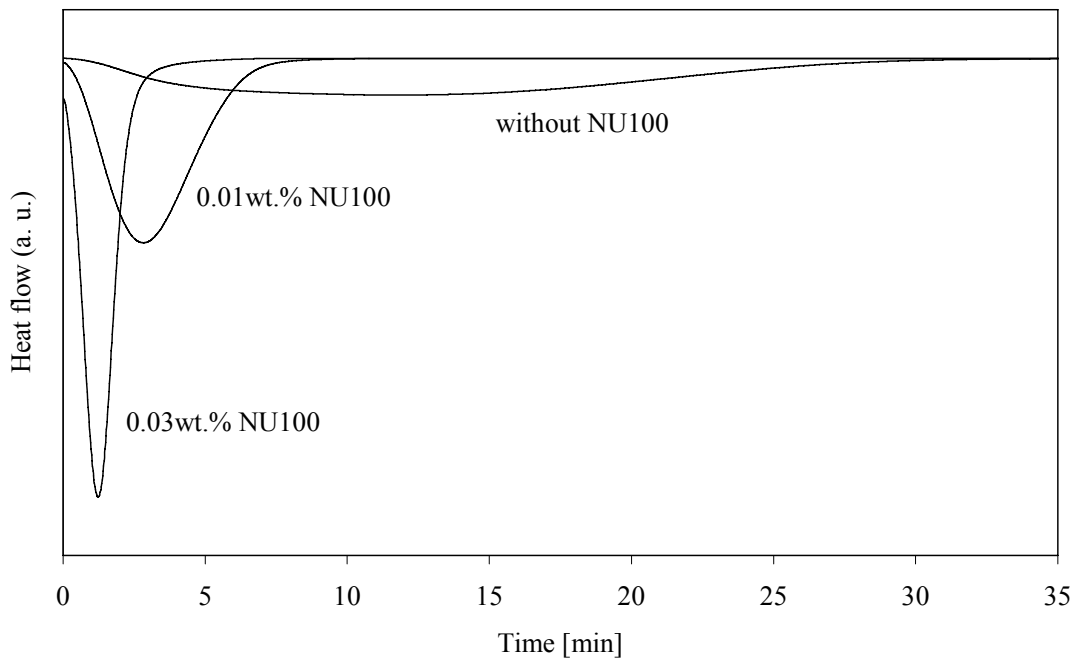

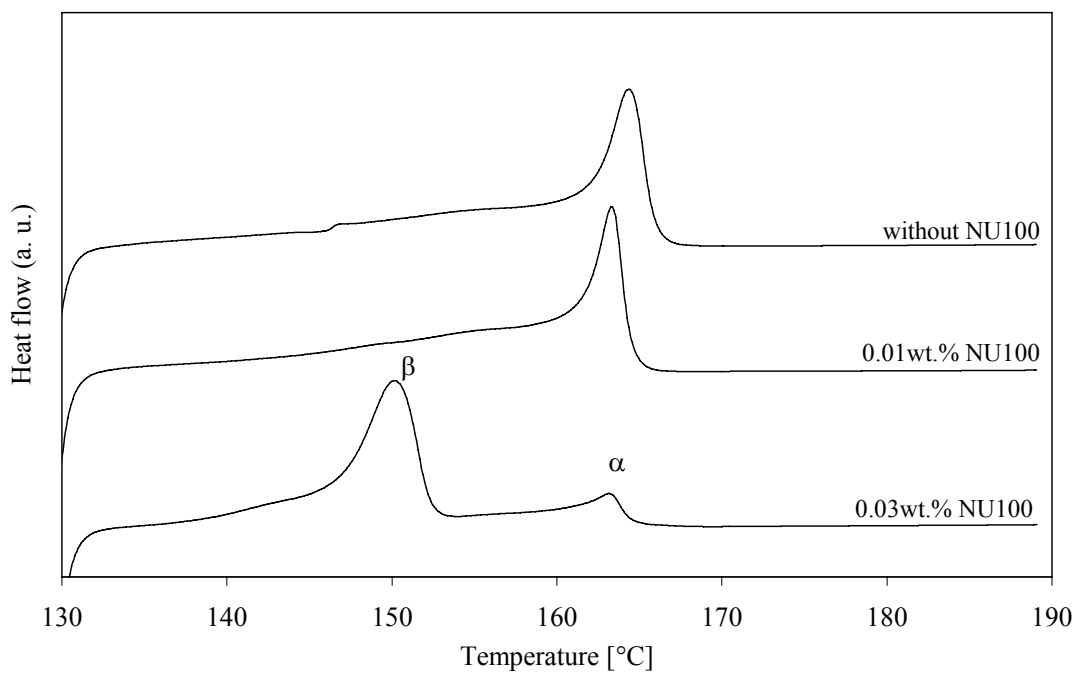Figure 10.15 Crystallization exotherms of the samples with MFI 12.0 g/10 min with different content of NU 100

Figure 10.16 Melting thermograms of the samples with MFI 12.0 g/10 min with different content of NU 100

10.2.5 MFI 20.0 g/10 min

Figure 10.17 shows crystallization exotherms of the samples with MFI 20.0 g/10 min with different content of NU 100. All exotherms show symmetric shape. With increasing content of NU 100 the significant narrowing and shortening of the peak proceed. Melting thermograms of the samples with MFI 20.0 g/10 min with different content of NU 100 are shown in Figure 10.18.
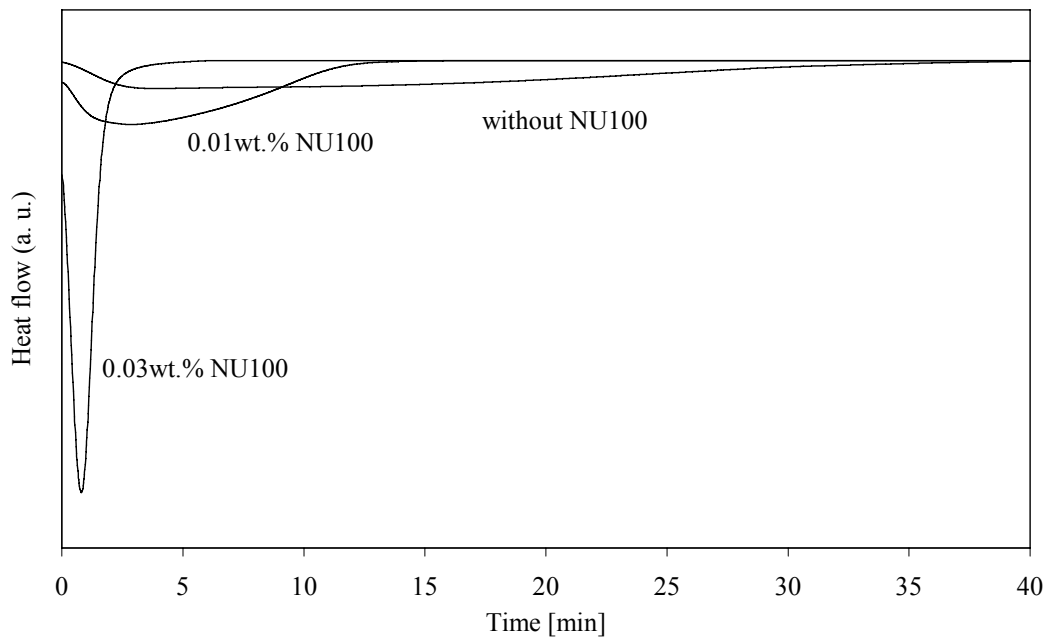

Figure 10.17 Crystallization exotherms of the samples with MFI 20.0 g/10 min with different content of NU 100
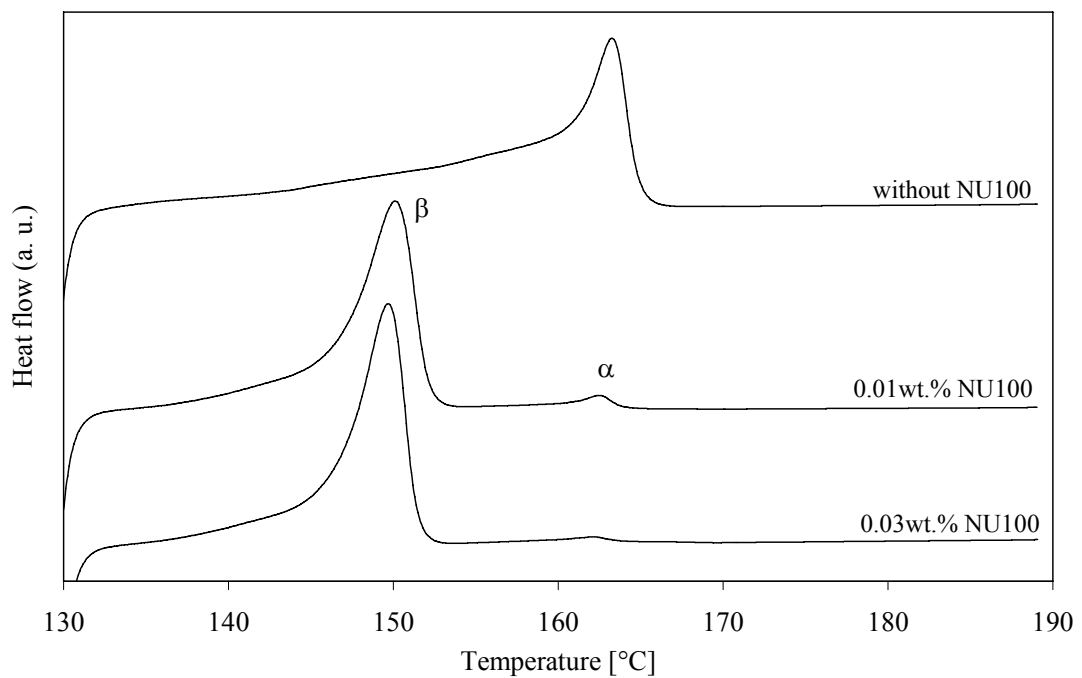

Figure 10.18 Melting thermograms of the samples with MFI 20.0 g/10 min with different content of NU 100

10.2.6 MFI 27.0 g/10 min

Figure 10.19 shows crystallization exotherms of the samples with MFI 27.0 g/10 min with different content of NU 100. The exotherm of neat material shows asymmetry, however, the nucleated ones are symmetric. Melting thermograms of the samples with MFI 27.0 g/10 min with different content of NU 100 are shown in Figure 10.20.
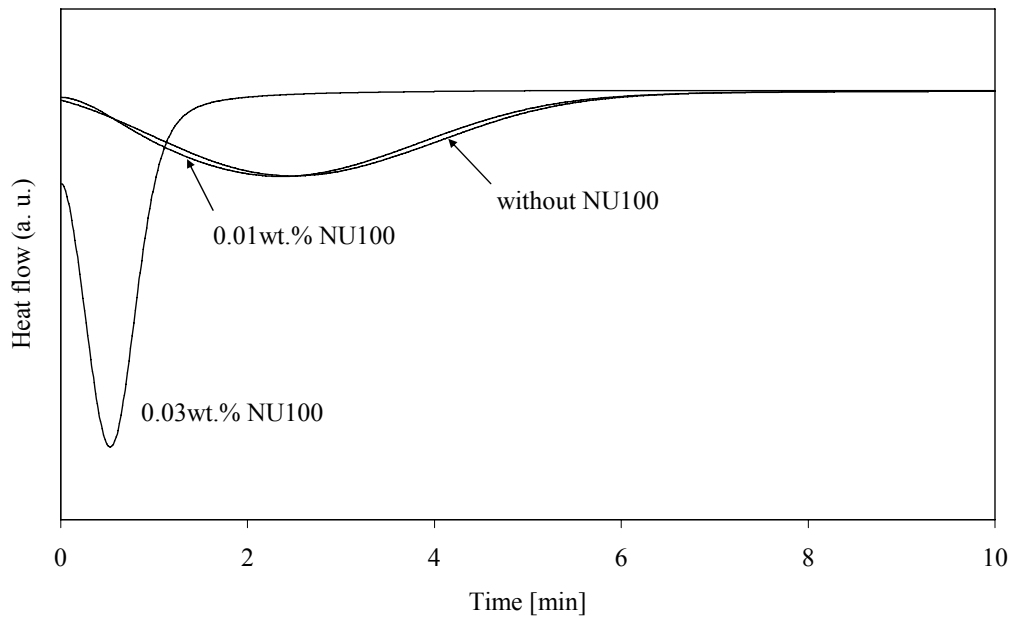

Figure 10.19 Crystallization exotherms of the samples with MFI 27.0 g/10 min with different content of NU 100

Figure 10.20 Melting thermograms of the samples with MFI 27.0 g/10 min with different content of NU 100

10.2.7 MFI 37.0 g/10 min

Figure 10.21 shows crystallization exotherms of the samples with MFI 37.0 g/10 min with different content of NU 100. All the crystallization peaks are significantly assymetric. The nucleation only decreases the crystallization time and narrows the peaks. Melting thermograms of the samples with MFI 37.0 g/10 min with different content of NU 100 are shown in Figure 10.22.

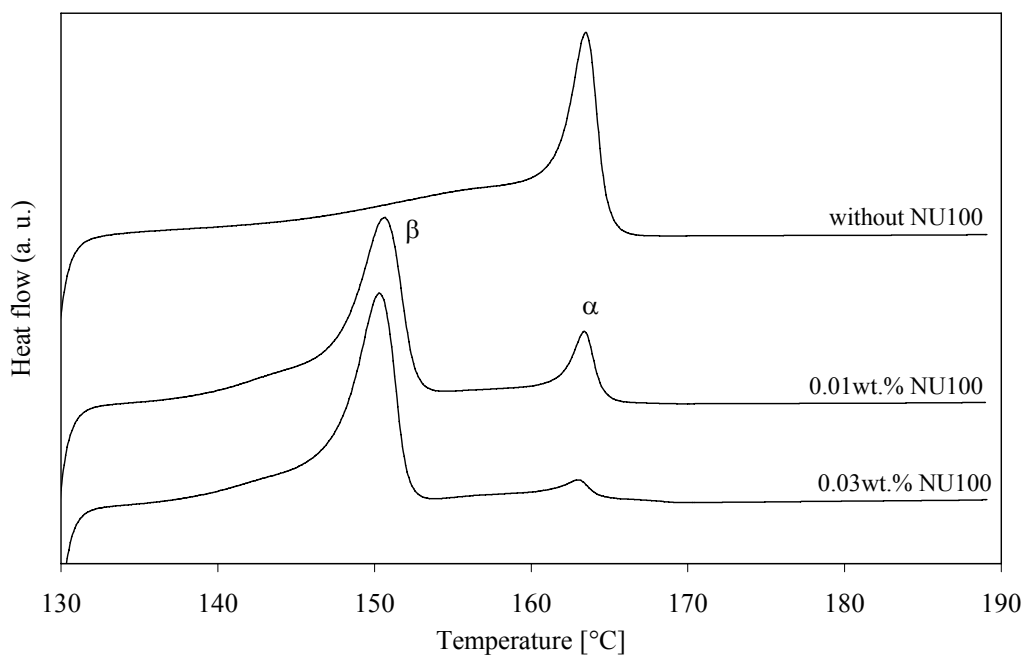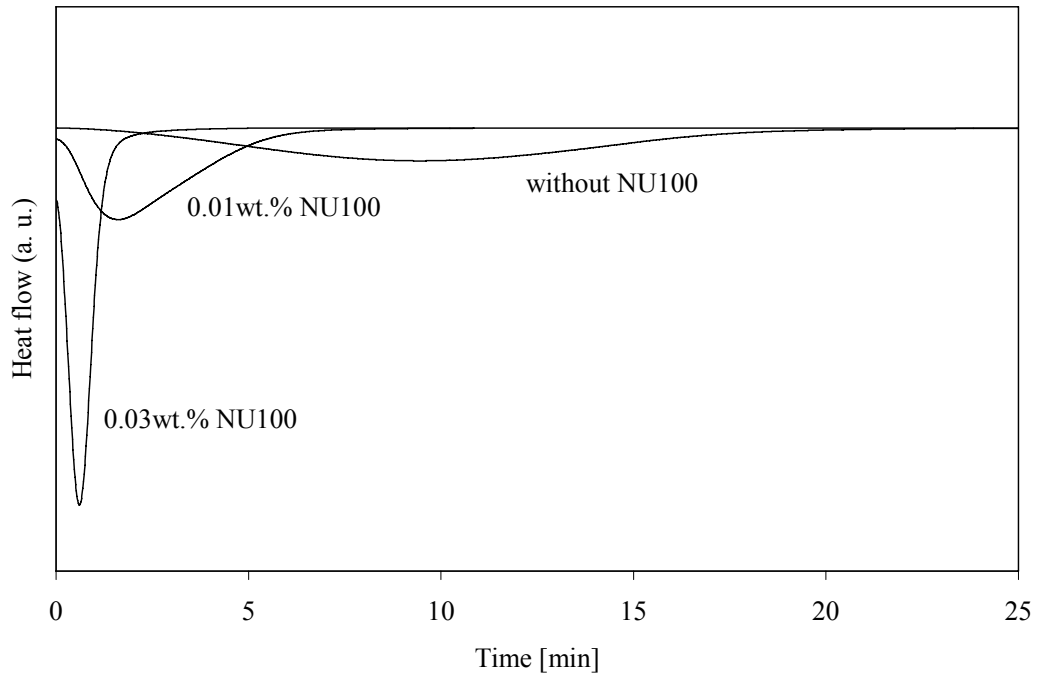Figure 10.21 Crystallization exotherms of the samples with MFI 37.0 g/10 min with different content of NU 100

Figure 10.22 Melting thermograms of the samples with MFI 37.0 g/10 min with different content of NU 100

10.2.8 MFI 125.0 g/10 min

Figure 10.23 shows crystallization exotherms of the samples with MFI 125.0 g/10 min with different content of NU 100. As is seen in the figure the exotherms of neat and low-nucleated samples overlap each other. Only the addition of 0.03 wt. % NU 100 leads to the decrease of crystallization time and narrowing of the peak. Melting thermograms of the samples with MFI 125.0 g/10 min with different content of NU 100 are shown in Figure 10.24.

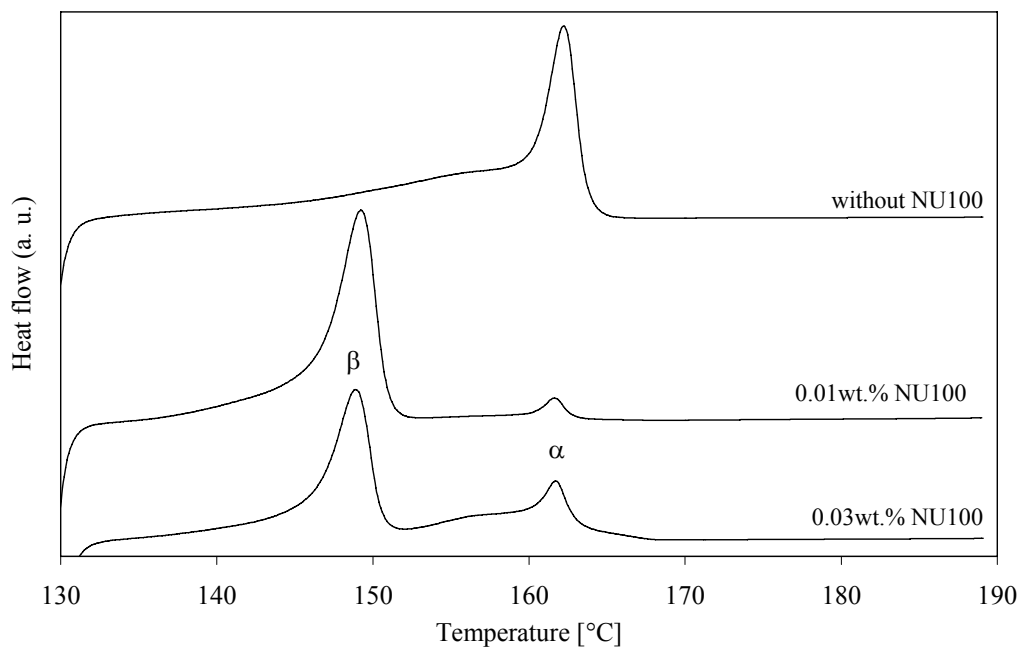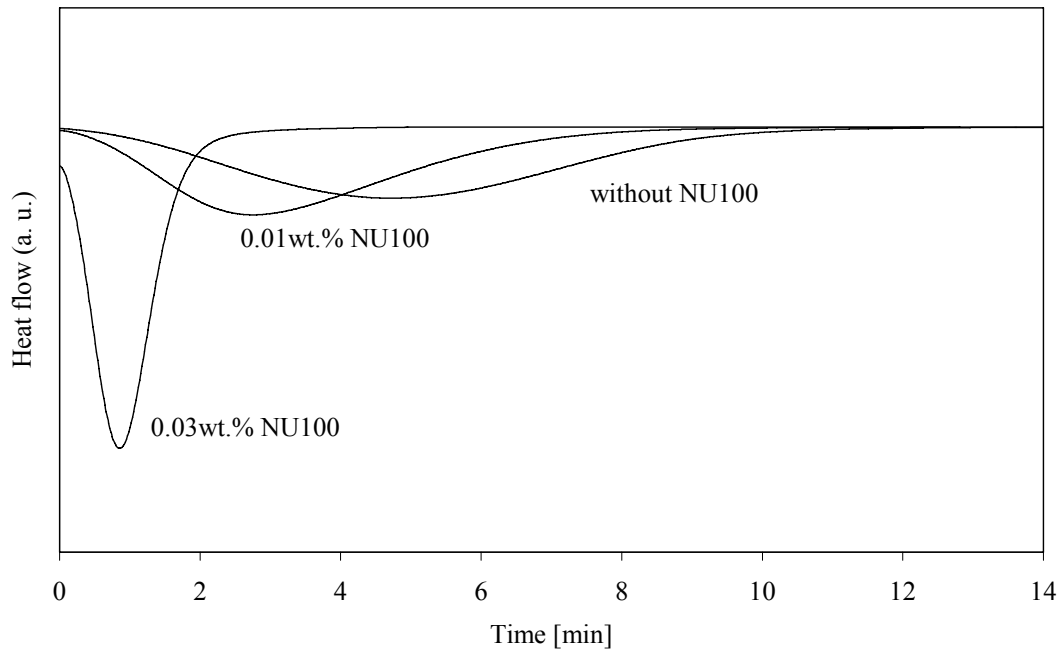Figure 10.23 Crystallization exotherms of the samples with MFI 125.0 g/10 min with different content of NU 100

Figure 10.24 Melting thermograms of the samples with MFI 125.0 g/10 min with different content of NU 100

10.2.9 MFI 450.0 g/10 min

Figure 10.25 shows crystallization exotherms of the samples with MFI 450.0 g/10 min with different content of NU 100. Only the material with low amount of nucleator embodies the asymmetry of the exotherm. The neat and high-nucleated material show symmetric peaks. Melting thermograms of the samples with MFI 450.0 g/10 min with different content of NU 100 are shown in Figure 10.26.

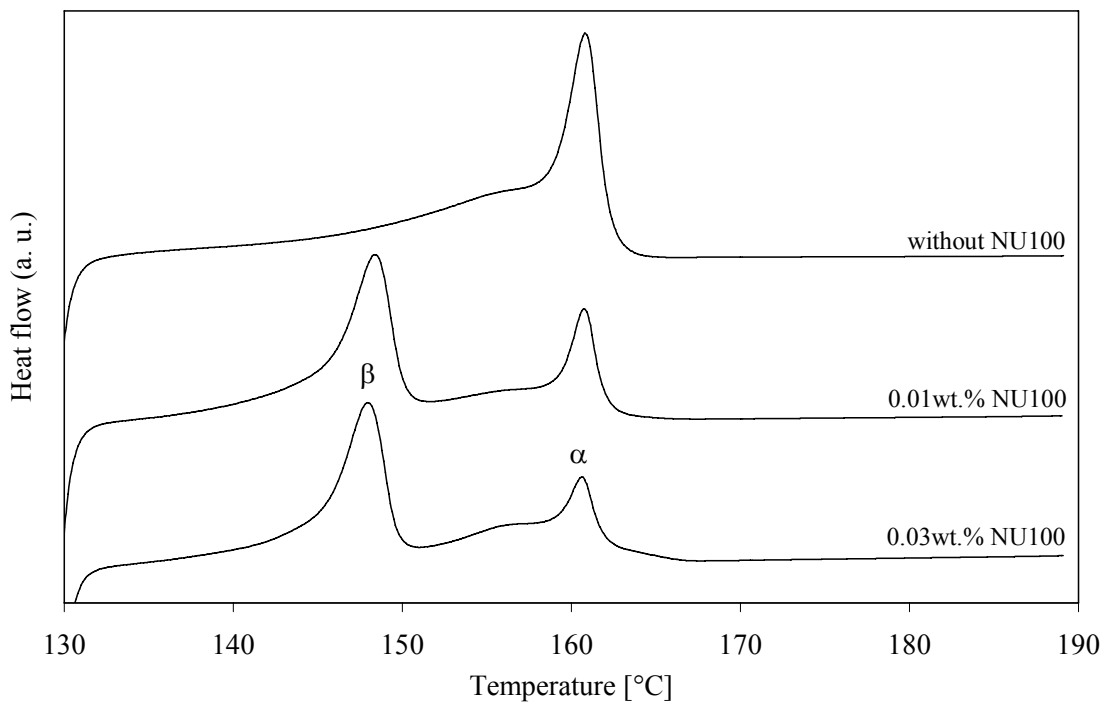Figure 10.25 Crystallization exotherms of the samples with MFI 450.0 g/10 min with different content of NU 100

Figure 10.26 Melting thermograms of the samples with MFI 450.0 g/10 min with different content of NU 100

10.2.10 MFI 800.0 g/10 min

Figure 10.27 shows crystallization exotherms of the samples with MFI 800.0 g/10 min with different content of NU 100. All crystallization peaks are symmetric and well recognized. Melting thermograms of the samples with MFI 800.0 g/10 min with different content of NU 100 are shown in Figure 10.28.

Figure 10.27 Crystallization exotherms of the samples with MFI 800.0 g/10 min with different content of NU 100

Figure 10.28 Melting thermograms of the samples with MFI 800.0 g/10 min with different content of NU 100

10.2.11 MFI 1200.0 g/10 min

Figure 10.29 shows crystallization exotherms of the samples with MFI 1200.0 g/10 min with different content of NU 100. As is seen in the figure, only crystallization peak of material with 0.01 wt. % NU 100 is asymmetric. Melting thermograms of the samples with MFI 1200.0 g/10 min with different content of NU 100 are shown in Figure 10.30.
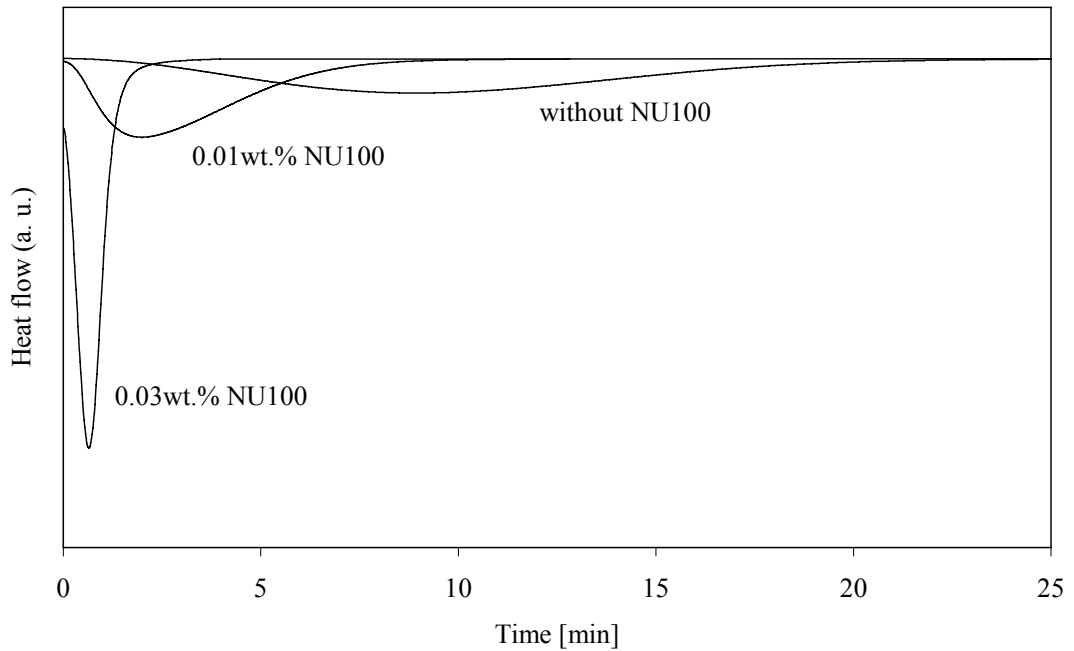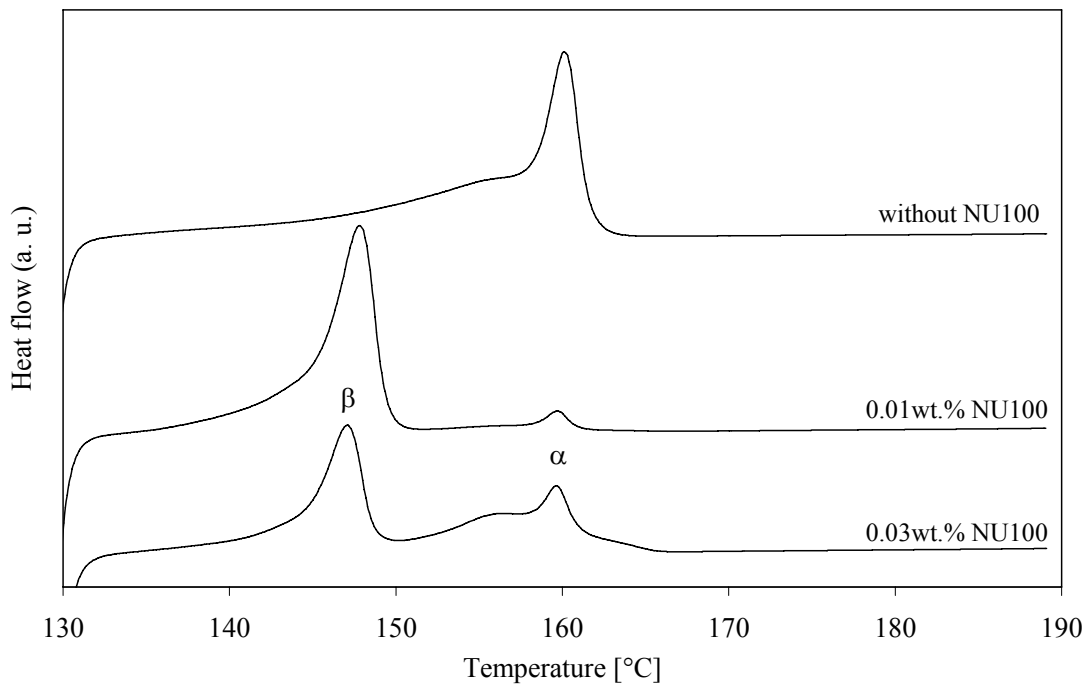

Figure 10.29 Crystallization exotherms of the samples with MFI 1200.0 g/10 min with different content of NU 100

Figure 10.30 Melting thermograms of the samples with MFI 1200.0 g/10 min with different content of NU 100

CONCLUSIONS

This thesis deals with efficiency of the commercially available β-specific nucleating agent NJ Star NU 100 in isotactic polypropylenes Borealis differing in melt flow indexes. Crystallization of neat and β-nucleated samples under different conditions was carried out using a differential scanning calorimeter. The structure of iPP samples was studied using wide-angle X-ray scattering, differential scanning calorimetry and light microscopy.

The influence of MFI on efficiency of nucleating agent was found only in case of samples containing 0.01 wt. % NU 100 crystallized in hydraulic press. The step change of β-form content (*k-value*) occurred between materials with very low MFI (0.3 and 1.0 g/10 min) and materials with MFI 12 g/10 min and higher (from *k-value* 0.04 to 0.91). No influence of MFI on nucleator efficiency of high-nucleated (0.03 wt. %) samples was noted.

As for samples crystallized in DSC under controlled conditions at two different cooling rates, the versatile content of β-form depending on the MFI in the samples with 0.01 wt. % NU 100 was observed. Such nucleated samples with MFI 37.0 g/10 min and higher possessed nearly the same β-form content as that of α-form. However, some materials (with MFI 1.0 and 27.0 g/10 min crystallized at 10°C/min and materials with MFI 0.3, 1.0 and 27.0 g/10 min crystallized at 50°C/min) crystallized only into α-form although they were β-nucleated. The samples containing 0.03 wt. % NU 100 showed the prevailing formation of β-form, while the pure material crystallized only into α-form.

Regarding the isothermal crystallization, some neat materials (with MFI 8.0, 12.0, 27.0 and 37.0 g/10 min) showed doubled crystallization exotherms. It can be caused by the presence of the additives in the plastic (these additives are used by producer of the material and the information of them are not available).

The crystallization time decreased with rising amount of the nucleating agent, of both isothermally and non-isothermally crystallized samples.

The heating scans of isothermally crystallized samples were very similar to that of non-isothermally crystallized samples at cooling rate 10°C/min. In most cases of samples containing 0.01 wt. % NU 100, the β-peak was dominant indicating the majority content of β-form in the material. However, in some materials (with MFI 1.0, 20.0 and 27.0 g/10 min) dominating α-form was detected. As for materials with MFI 1.0 and 27.0 g/10 min even only α-melting peak was observed. To evaluate the influence of isothermal crystallization on nucleator efficiency in detail, it would be proper to carry out the crystallization at several different temperatures.

It should be also noted, that the samples with high MFI are more sensitive to recrystallization, which is ascribed to the perfection of the structure within the same crystal form during heating (αα-recrystallization and ββ-recrystallization) and also to inter-phase βα-recrystallization.

REFERENCES

[1]   THANOMKIAT. P.; SUPAPHOL, P.; PHILLIP, P., R.: Influence of Different Molecular Characteristics of Synd. Polypropylene on Equil. Melting Temperature and Crystall. Behavior. Chulalongkorn University, Thailand

[2]   GROENINCKX, G., VANNESTE M., EVERAERT V.: Crystallization, morfological structure, and melting of polymers blends. Catholic University of Leuven, Belgium

[3]   WUNDERLICH, B.: Macromolecular physics. by Academic Press, INC, 1976, ISBN 0-12-765602-2.

[4]   SHANKS, R. A., TIGANIS B. E: Nucleating agents for thermoplastics, Plastics aditived: An A-Z Reference, Chapman & Hall, London, 1998, ISBN 0 412 72720 X

[5]   MAIER, C.; CALAFUT, T.: Polypropylene – The Definitive User's Guideand Datebook, Plastics design Library, 1998

[6]   RAM, A.: Fundamentals of Polymer Engineering, Plenum Press, 1997

[7]   ELIAS, H. G.: An introduction to plastics - 2nd completely rev. ed.: Wiley-VCH, 2003, 387 s. ISBN 3-527-29602-6

[8]   WOODWARD, A. E.: Understanding polymer morphology, Hanser/Gardner, 1995, ISBN 3-449-17434-1

[9]   SPERLING, L. H.: Introduction to Physical Polymer Science. 3rd. edition, Wiley-Interscience, 2001. 671 p. ISBN 0-471-32921-5

[10]   HOFFMAN, J. D.; DAVIS, G. T.; LAURITZEN Jr., J. I.; in Treatise on Solid State Chemisíi Vol. 3, Crystalline and Noncrystalline Solids, N. B. Hannay, ed., Plenum, New York, 1976 Chap. 7.

[11]   BAILEY, M.S., BRAUER, D., Polypropylene: New Array of Polymer Variations Expand End- use Applications, Modern Plastics Encyclopedia 1995, reference book (M603.1.5) – McGraw-Hill, 1994.

[12]   ELBER, G., Back to Basics: Polypropylene, Plastics Design Forum, Trade Journal (Vol. 18, No. 5) – Advanstar Communications, 1993.

[13]   MONASSE, B.; HAUDIN, J. M.: Polypropylene: Structure, blends and composites, Vol. 1. Crystalline structures of polypropylene homo- and copolymers, Chapman&Hall, London, 1995

[14]   KARGER-KOCSIS, J.: Polypropylene – An A-Z Reference, Kluwer Publishers, Dordrecht.1999

[15]   http://pslc.ws/macrogcss/pp.html

[16]   CAPSHEW, C., Polypropylene: A Commodity Plastic Reaches Record Highs in 1995 Production, Modern Plastics Encyclopedia 1997, reference book (Vol. 73, No. 12) – McGraw-Hill, 1997.

[17]   GRAVES, V., Polypropylene: A Commodity Plastic Reaches Record Highs in 1994 Production, Modern Plastics Encyclopedia 1996

[18]   Metallolcene Catalysis: Polymers by Design, Rapra Abstracts Database on CD-ROM, computer database (CD9602) – Rapra Technology LTD., 1996.

[19]   LANGHAUSER, F., Metallocenes as Catalysts in Industrial Olefin Polymerization Processes, ANTEC 1995

[20]   CHENG, C.Y, Extrusion Behavior of Exxpol Metallocene Polypropylene, ANTEC 1996, conference proceedings – Society of Plastics Engineers, 1996.

[21]   MLEZIVA, J. – ŠŇUPÁREK, J.: Polymery – Výroba, struktura, vlastnosti a použití. 2. vyd., Sobotáles, 2000. 544 p. ISBN: 80-85920-72-7

[22]   BRYDSON, J.: Plastics Materials (7th Edition), Butterworth-Heinemann, 1999

[23] PHILLIPS, P. J.; MEZGHANI, K.: Polypropylene, Isotactic (Polymorphism), University of Tennessee, 1996

[24] NATTA, G.; CORRADINI, P.: Nuovo Cimento, Suppl., 15, 40

[25] TURNER-JONES, A.; AIZLEWOOD, J.M. and BECKETT, D.R. (1964) Crystalline forms of isotactic polypropylene. Makromolekulare Chemie, 75,

[26] CHENG, D. Z. S.; JANIMAK, J. J.; RODRIGUEZ, J.: Polypropylene: Structure, blends and composites, Vol. 2. Crystalline structures of polypropylene homo- and copolymers, Chapman&Hall, London, 1995

[27] PHILLIPS, R.A., WOLKOWICZ, M.D., Structure and Morphology, Polypropylene Handbook, reference book (ISBN 3-446-18176-8) – Carl Hanser Verlag, 1996.

[28] CHEUNG, T., TJONG, S.C., Li, R.K.Y., Mechanical Behavior of Calcium Carbonate Filled Beta-Crystalline Form Polypropylene Composite,ANTEC 1996, conference proceedings – Society of Plastics Engineers, 1996.

[29] MEZGHANI, K., PHILLIPS, P.J., The Morphology of the Gamma Form of Isotactic Polypropylene at 200 MPA, ANTEC 1996, conference proceedings – Society of Plastics Engineers, 1996.

[30] VARGA, J.: Polypropylene: Structure, blends and composites, Vol. 3, Crystallization, melting and supermolecular structure of isotactic polypropylene, Chapman&Hall, London, 1995

[31] ADDINK, E. J. – BIENTEMA, J.: Polymer, 2, 185, 1961

[32] VARGA, J.; β-modification of isotactic polypropylene: preparation, structure, processing, properties, and application; Journal of Macromolecular Science, vol. 41, pp. 1121-1171, 2002.

[33] OBADAL, M., ČERMÁK, R., BARAN, N., STOKLASA, K., ŠIMONÍK, J.: J. Int. Polym. Process., 19 (2004) 35

[34] VARGA, J. (1995) Crystallization, melting and supermolecular structure of isotactic polypropylene, in Polypropylene: Structure, Blends and Composites, Vol.1, Structure and Morphology (ed. J. Karger-Kocsis), Chapman & Hall, London, pp. 56-115.

[35] VARGA, J. (1989) β-Modification of polypropylene and its two-component systems. J. Thermal Analysis, 35, 1891-1912.

[36] VARGA, J.; ANGEW. Makromol. Chem., 104 (1982) 79.

[37] LOTZ, B.: Polymer, 39, 19 (1998) 4561.

[38] LOTZ, B., FILLON, B., SHERRY A., WITTMANN, J.C.: Polymer Bull., 25 (1991) 101

[39] DUSWALT, A., COX, W. Thermal Study of β-form polypropylene. Am. Chem. Soc. Div. Org. Coat. 1970, 30, 93-96

[40] DUSWALT, A., COX, W.: Thermal Study of β-form polypropylene. In Polymer Characterization, Interdisciplinary Approaches,; Craver, D.D., Ed.; Plenum Press: New York, 1971; 147-155

[41] JACOBY, P.; BERSTED, B.H.; KISSEL, W.J.; SMITH C.E. (1986) Studies on β-crystalline form of isotactic polypropylene. J. Polymer Sci.: Polymer Phys., 24.

[42] KARGER-KOCSIS, J. and VARGA, J. (1996) Effects of β-α transformation on the static and dynamic tensile behavior of isotactic polypropylene. J. Appl. Polymer Sci., 62, 291-300.

[43] MEILLE. S.V.; BRUCKNER, S.; PORZIO, W. (1990) γ-isotactic polypropylene. A structure with nonparallel chain axes. Macromolecules, 23, 4114-21.

[44] LOTZ, B.; WITTMANN, J.C.; LOVINGER, A.J. (1996) Structure and morphology of poly(propy1enes): a molecular analysis. Polymer, 37,4979-92.

[45]   ČERMÁK, R.: Beta polypropylene: Interrelations between structure, properties and processing (Doctoral thesis), UTB Zlín, 2005

[46]   HATAKEYAMA, T.; QUINN, F. X.: Thermal analysis, Wiley & Sons, New York, 1994

[47]   SCHEIRS, J.: Compositional And Failure Analysis Of Polymers – A practical Approach. John Wiley & Sons, Ltd, 2000. 766 p. ISBN 0-471-62572-8

[48]   DEAN, John A. The Analytical Chemistry Handbook. New York. McGraw Hill, Inc. 1995. p15.1-15.5

[49]   http://en.wikipedia.org/wiki/Differential_scanning_calorimetry

[50]   CHEREMISINOFF, N. P.: Polymer Characterization – Laboratory Techniques and Analysis. Notes Publications in 1996, ISBN 0-8155-1403-4

[51]   SKOOG, D. A.; HOLLER F. J.; NIEMAN, T.: Principles of Instrumental Analysis. Fith Edition. New York. 1998. p905-908.

[52]   CAMPBELL, D.; WHITE, J. R. Polymer characterization. New York (United States of America): Chapman and Hall, 1989.

[53]   LEROY, E., A.: X-Ray diffraction in Polymer Science, Wiley-Interscience, New York, 1969

[54]   www.matter.org.uk/diffraction/x-ray/default.htm

[55]   www.opticsplanet.netlompolquantr.html

LIST OF SYMBOLS AND SHORTCUTS

iPP	isotactic polypropylene
α	monoclinic crystallic form of polypropylene
β	trigonal crystallic form of polypropylene
γ	orthorhombic crystallic form of polypropylene
α-iPP	polypropylene with predominant α-form
β-iPP	polypropylene with predominant β-form
MFI [g/10 min]	melt flow index
TA	thermal analysis
DSC	differential scanning calorimetry
WAXS	wide angle X-ray scattering
PLM	polarized light microscopy
ΔG [J]	change of Gibbs free energy
ΔH [J]	change of enthalpy
ΔS	change of entropy
T [°C]	temperature
T_m [°C]	melting temperature
T_m^0 [°C]	equilibrium melting temperature
T_c [°C]	crystallization temperature
T_g [°C]	glass transition temperature
T_R^* [°C]	critical recooling temperature
$T(\alpha\beta)$ [°C]	low limit temperature of growth transition
$T(\beta\alpha)$ [°C]	upper limit temperature of growth transition
t [min]	time
$t_{1/2}$ [min]	halftime of primary crystallization
wt. % [%]	weight percent
X_C	percentage of crystallinity
λ [nm]	wavelength
2θ [°]	angle of diffraction
d [nm]	interplanar distance
$h_{\alpha 1}$	intensity of α-diffraction peak corresponding to angle $2\theta = 14.2°$
$h_{\alpha 2}$	intensity of α-diffraction peak corresponding to angle $2\theta = 17.0°$
$h_{\alpha 3}$	intensity of α-diffraction peak corresponding to angle $2\theta = 18.8°$
h_β	intensity of β-diffraction peak corresponding to angle $2\theta = 16.2°$
h_γ	intensity of γ-diffraction peak corresponding to angle $2\theta = 19.9°$
tg δ	loss angle

LIST OF FIGURES

I. Theoretical background

II. Experimental

III. Results and discussion

LIST OF TABLES

LIST OF APPENDICES

A Table 1 Characteristics of iPP Borealis

Materials	Melt flow index (230/2.16) [g/10min] ISO 1133	Density [kg/m^3] ISO 1183	Characteristics	Melting temperature [°C] ISO 3146
BE50	0.3	905	high molecular weight low melt flow high stiffness high heat distortion temperature high resistance to thermal ageing	unlisted by producer
HB205TF	1.0	905	low melt flow very good processability and melt stability very good stiffness and impact balance very good organoleptic properties	162-165
HD601CF	8.0	900-910	high gloss, low haze excellent processability/gauge control good mechanical properties heat sterilisable	162-166
HE125MO	12.0	908	good flow properties high stiffness very good organoleptic properties	unlisted by producer
HF136MO	20.0	908	good combination of mechanical and flow properties narrow molecular weight distribution	unlisted by producer
HG455FB	27.0	unlisted by producer	narrow molecular weight distribution controlled rheology easy processability anti-gasfading version optical product consistency very good flow	161-165

HH450FB	37.0	unlisted by producer	very high flow narrow molecular weight distribution controlled rheology easy processability anti-gasfading formulated optical product consistency and resin purity very neutral colour appearance	161-165
HK060AE	125.0	905	low viscosity	unlisted by producer
HL504FB	450.0	unlisted by producer	narrow molecular weight distribution easy processability optical product consistency very high flow	161-165
HL508FB	800.0	unlisted by producer	narrow molecular weight distribution easy processability optical product consistency very high flow perfect suitable for electrostatic charging	156-160
HL612FB	1200.0	unlisted by producer	narrow molecular weight distribution easy processability optical product consistency very high flow	156-160

A Table 2 Melting characteristics of samples crystallized in hydraulic press

Material	MFI [g/10min]	0.00 wt. % NU 100						0.01 wt. % NU 100						0.03 wt. % NU 100					
		X_c [%]	k-value [-]	$T_{m\alpha}$ [°C]		$T_{m\beta}$ [°C]	ΔH_m [J/g]	X_c [%]	k-value [-]	$T_{m\alpha}$ [°C]	$T_{m\beta}$ [°C]		ΔH_m [J/g]	X_c [%]	k-vaule [-]	$T_{m\alpha}$ [°C]	$T_{m\beta}$ [°C]		ΔH_m [J/g]
BE50	0.3	46	0.01	-	163.3	-	81.9	45	0.03	162.3	-	-	89.2	42	0.93	165.6	146.1	-	*
HB205TF	1.0	45	0.00	-	162.7	-	79.8	47	0.04	160.5	-	-	86.5	46	0.96	166.3	145.8	-	*
HD601CF	8.0	46	0.00	-	164.1	-	76.1	41	0.51	163.5	141.9	150.1	87.3	41	0.93	165.9	145.6	151.3	*
HE125MO	12.0	47	0.01	-	158.4	-	88.7	42	0.91	164.9	144.9	150.0	*	43	0.93	164.6	145.5	149.8	*
HF136MO	20.0	47	0.00	-	158.3	-	93.0	43	0.94	164.7	143.6	150.0	*	44	0.95	165.3	146.1	-	*
HG455FB	27.0	47	0.00	-	160.8	-	95.4	42	0.92	164.7	144.6	150.1	*	44	0.92	165.3	145.5	150.0	*
HH450FB	37.0	43	0.01	156.8	163.6	-	82.0	41	0.95	164.4	142.3	149.6	*	41	0.95	164.8	145.5	150.9	*
HK060AE	125.0	47	0.01	-	158.3	-	95.3	47	0.94	166.4	145.8	152.3	*	42	0.84	166.1	145.8	151.9	*
HL504FB	450.0	48	0.01	155.8	164.3	-	93.9	42	0.91	164.4	144.4	150.7	*	48	0.95	164.6	144.8	150.7	*
HL508FB	800.0	53	0.00	154.8	164.0	-	93.9	44	0.92	163.6	143.6	150.0	*	47	0.92	163.6	144.0	149.7	*
HL612FB	1200.0	46	0.01	153.4	162.9	-	77.5	45	0.93	162.7	142.9	148.8	*	45	0.92	162.6	143.3	149.0	*

* undershoot

A Table 3 Crystallization and melting characteristics of the samples crystallized in DSC under controlled conditions

Cooling rate 10°C/min

Material	MFI [g/10 min]	0.00 wt.% NU 100									0.01 wt.% NU 100									0.03 wt.% NU 100								
		T_c [°C]	ΔH_c [J/g]	$t_{1/2}$ [min]	$T_{m\alpha}$ [°C]	$T_{m\alpha}$ [°C]	$T_{m\beta}$ [°C]	$T_{m\beta}$ [°C]	$\Delta H_{m\alpha}$ [J/g]	$\Delta H_{m\beta}$ [J/g]	T_c [°C]	ΔH_c [J/g]	$t_{1/2}$ [min]	$T_{m\alpha}$ [°C]	$T_{m\alpha}$ [°C]	$T_{m\beta}$ [°C]	$T_{m\beta}$ [°C]	$\Delta H_{m\alpha}$ [J/g]	$\Delta H_{m\beta}$ [J/g]	T_c [°C]	ΔH_c [J/g]	$t_{1/2}$ [min]	$T_{m\alpha}$ [°C]	$T_{m\alpha}$ [°C]	$T_{m\beta}$ [°C]	$T_{m\beta}$ [°C]	$\Delta H_{m\alpha}$ [J/g]	$\Delta H_{m\beta}$ [J/g]
BE50	0.3	113.2	94.3	10.7	-	161.5	-	-	87.6	-	114.0	87.2	10.6	161.3	*	146.5	-	36.3	11.2	121.8	83.9	9.9	-	167.1	148.4	-	undershoot	
HB205TF	1.0	112.0	94.6	10.8	-	161.0	-	-	85.0	-	116.9	89.9	10.3	160.8	-	-	-	50.6	0.1	122.1	82.2	9.8	-	167.3	148.7	-	undershoot	
HD601CF	8.0	111.9	98.1	10.8	158.8	-	-	-	84.8	-	117.6	99.1	10.2	159.4	*	146.0	151.9	34.6	24.4	120.9	87.6	9.9	159.9	167.0	147.1	151.6	25.9	48.8
HE125MO	12.0	116.4	103.7	10.4	159.4	-	-	-	96.6	-	117.8	109.8	10.2	159.8	*	146.3	-	42.2	12.1	122.5	90.7	9.7	160.8	165.5	147.9	-	19.7	78.1
HF136MO	20.0	113.6	101.9	10.7	158.7	-	-	-	87.2	-	116.8	104.3	10.3	159.6	-	145.5	-	43.2	2.6	122.5	93.9	9.7	160.8	165.7	147.6	-	undershoot	
HG455FB	27.0	113.9	100.0	10.6	159.0	-	-	-	91.0	-	116.5	104.9	10.3	158.8	-	-	-	59.4	0.1	122.5	94.8	9.8	160.8	165.7	147.4	-	undershoot	
HH450FB	37.0	110.7	94.3	10.8	157.4	-	-	-	85.7	-	115.5	82.2	10.3	157.5	164.9	143.9	150.2	27.6	51.5	123.2	81.4	9.7	-	165.9	147.3	-	undershoot	
HK060AE	125.0	118.9	112.9	10.2	159.7	-	-	-	98.8	-	118.4	106.2	10.1	159.2	-	145.9	152.1	33.8	34.1	125.4	94.3	9.5	161.8	166.4	148.8	-	undershoot	
HL504FB	450.0	114.1	107.9	10.6	156.9	163.7	-	-	96.9	-	118.4	96.3	10.1	157.7	164.4	144.9	150.8	37.4	33.4	124.9	97.4	9.5	160.1	164.3	147.1	-	34.6	56.0
HL508FB	800.0	116.6	102.5	10.4	156.4	162.6	-	-	97.3	-	118.1	105.9	10.2	156.8	163.2	143.7	149.9	43.3	15.0	123.9	95.0	9.6	158.8	163.5	145.9	150.0	36.4	41.1
HL612FB	1200.0	114.6	101.1	10.6	155.0	162.8	-	-	94.9	-	117.9	89.7	10.2	155.7	162.6	142.9	149.1	40.8	41.6	124.5	91.9	9.5	158.3	162.7	145.6	149.2	37.8	49.3

Cooling rate 50°C/min

Material	MFI [g/10 min]	0.00 wt.% NU 100									0.01 wt.% NU 100									0.03 wt.% NU 100								
		T_c [°C]	ΔH_c [J/g]	$t_{1/2}$ [min]	$T_{m\alpha}$ [°C]	$T_{m\alpha}$ [°C]	$T_{m\beta}$ [°C]	$T_{m\beta}$ [°C]	$\Delta H_{m\alpha}$ [J/g]	$\Delta H_{m\beta}$ [J/g]	T_c [°C]	ΔH_c [J/g]	$t_{1/2}$ [min]	$T_{m\alpha}$ [°C]	$T_{m\alpha}$ [°C]	$T_{m\beta}$ [°C]	$T_{m\beta}$ [°C]	$\Delta H_{m\alpha}$ [J/g]	$\Delta H_{m\beta}$ [J/g]	T_c [°C]	ΔH_c [J/g]	$t_{1/2}$ [min]	$T_{m\alpha}$ [°C]	$T_{m\alpha}$ [°C]	$T_{m\beta}$ [°C]	$T_{m\beta}$ [°C]	$\Delta H_{m\alpha}$ [J/g]	$\Delta H_{m\beta}$ [J/g]
BE50	0.3	107.3	57.1	2.4	161.6	-	-	-	82.1	-	105.3	50.2	2.4	161.0	-	-	-	54.2	0.8	112.1	80.0	2.3	159.4	166.0	145.4	150.7	35.7	34.3
HB205TF	1.0	105.5	68.2	2.4	159.7	-	-	-	85.8	-	108.6	85.6	2.3	159.5	-	-	-	85.7	1.2	112.9	74.8	2.2	-	167.0	145.9	151.2	undershoot	
HD601CF	8.0	107.6	53.5	2.4	157.2	163.7	-	-	87.7	-	108.0	90.0	2.4	157.4	163.7	142.6	150.4	39.4	19.8	112.9	82.9	2.2	157.4	164.7	143.9	151.0	29.1	36.9
HE125MO	12.0	111.0	63.7	2.4	157.6	*	-	-	95.2	-	109.3	72.8	2.3	157.6	-	143.3	150.5	43.4	4.9	113.8	60.9	2.2	158.9	165.3	145.1	150.0	undershoot	
HF136MO	20.0	108.0	47.2	2.4	157.2	*	-	-	86.2	-	108.1	81.5	2.3	157.6	-	142.8	150.2	47.9	1.3	114.5	61.3	2.2	158.8	165.4	144.7	150.2	undershoot	
HG455FB	27.0	102.6	54.2	2.4	157.0	162.8	-	-	90.5	-	110.5	97.3	2.3	157.3	-	-	-	96.2	0.8	114.4	76.0	2.2	158.6	165.5	144.7	150.3	undershoot	
HH450FB	37.0	100.9	66.8	2.5	155.1	163.2	-	-	78.7	-	105.4	78.0	2.4	154.8	163.8	140.1	148.9	31.9	40.5	115.7	76.6	2.2	-	165.4	144.3	150.8	undershoot	
HK060AE	125.0	107.6	50.7	2.3	157.6	164.1	-	-	87.8	-	110.7	58.1	2.3	157.4	163.8	143.4	151.0	45.1	21.7	117.2	67.6	2.1	159.8	166.4	146.1	152.0	undershoot	
HL504FB	450.0	105.3	52.6	2.4	155.4	164.0	-	-	87.5	-	109.3	83.4	2.3	155.5	164.0	141.5	149.1	46.4	32.8	117.2	79.6	2.1	158.1	164.5	144.6	150.7	undershoot	
HL508FB	800.0	107.0	49.3	2.4	154.4	163.4	-	-	97.6	-	109.4	88.9	2.3	154.5	163.0	141.0	143.4	51.3	11.2	115.7	73.5	2.2	156.9	163.5	143.4	149.6	undershoot	
HL612FB	1200.0	105.3	55.5	2.4	153.5	162.8	-	-	91.7	-	110.0	90.8	2.3	153.5	162.3	140.2	147.6	undershoot		117.8	89.2	2.1	156.2	162.3	143.8	148.8	undershoot	

* undetermined

A Table 4 Crystallization and melting characteristics of the samples isothermally crystallized in DSC

Material	MFI [g/10 min]	0.00 wt. % NU 100						0.01 wt. % NU 100						0.03 wt. % NU 100					
		ΔH_c [J/g]	$t_{1/2}$ [min]	$T_{m\alpha}$ [°C]	$T_{m\beta}$ [°C]	$\Delta H_{m\alpha}$ [J/g]	$\Delta H_{m\beta}$ [J/g]	ΔH_c [J/g]	$t_{1/2}$ [min]	$T_{m\alpha}$ [°C]	$T_{m\beta}$ [°C]	$\Delta H_{m\alpha}$ [J/g]	$\Delta H_{m\beta}$ [J/g]	ΔH_c [J/g]	$t_{1/2}$ [min]	$T_{m\alpha}$ [°C]	$T_{m\beta}$ [°C]	$\Delta H_{m\alpha}$ [J/g]	$\Delta H_{m\beta}$ [J/g]
BE50	0.3	94.0	11.1	165.5	-	92.1	-	88.0	9.1	165.2	152.6	15.8	30.4	53.7	2.4	164.3	151.9	3.9	59.1
HB205TF	1.0	91.2	11.5	165.1	-	96.9	-	87.7	4.2	164.3	-	94.0	-	63.2	2.5	164.2	151.8	2.8	70.8
HD601CF	8.0	100.1	17.4	164.3	-	94.8	-	94.1	4.1	163.7	151.1	10.1	62.4	73.4	2.7	163.5	150.9	13.3	45.3
HE125MO	12.0	101.6	11.5	164.1	-	104.8	-	92.4	6.1	163.5	150.5	14.4	48.4	73.4	2.2	163.0	150.4	11.1	51.1
HF136MO	20.0	105.9	20.5	164.3	-	99.9	-	97.1	5.0	163.7	150.2	9.6	35.0	76.7	2.3	163.2	150.3	10.2	59.1
HG455FB	27.0	104.7	14.6	164.3	-	102.6	-	70.3	4.3	163.2	-	73.4	-	78.9	2.3	163.2	150.1	10.3	54.6
HH450FB	37.0	96.4	15	163.3	-	99.1	-	53.9	5.8	162.5	150.1	2.6	60.9	52.6	1.9	162.0	149.6	1.6	74.0
HK060AE	125.0	104.8	4.6	163.5	-	108.8	-	90.5	3.7	163.4	150.7	14.3	62.9	60.3	1.5	163.0	150.3	8.1	75.1
HL504FB	450.0	108.1	11.7	162.1	-	108.4	-	77.9	3.3	161.6	149.2	2.9	77.8	70.0	1.6	161.7	148.9	23.2	50.4
HL508FB	800.0	106.3	6.9	160.8	-	106.0	-	90.3	4.5	160.8	148.4	23.7	39.0	76.7	1.9	160.7	147.9	26.5	40.8
HL612FB	1200.0	104.1	11.7	160.2	-	105.9	-	83.4	3.7	159.6	147.9	3.4	71.9	68.0	1.7	159.7	147.1	29.7	36.2